

Discovery of K-Ras Inhibitors for the Treatment of Cancer

By

Qi Sun

Dissertation

Submitted to the Faculty of the
Graduate School of Vanderbilt University
in partial fulfillment of the requirements

for the degree of

DOCTOR OF PHILOSOPHY

in

Biochemistry

May, 2015

Nashville, Tennessee

Approved:

Stephen W. Fesik, Ph.D.

Walter J. Chazin, Ph.D.

Robert J. Coffey, M.D.

Lawrence J. Marnett, Ph.D.

Charles R. Sanders, Ph.D.

ACKNOWLEDGEMENTS

I would like to express my deep appreciation and gratitude to my advisor, Dr. Stephen Fesik, for the patient guidance, mentorship as well as intellectual and financial support he provided to me. I am truly fortunate to have had the opportunity to work with him. I also thank his assistant, Natalia Smothers, for always having a kind and encouraging word for me. Additionally, I would like to thank the members of my dissertation committee, Drs. Walter Chazin, Lawrence Marnett, Charles Sanders, and Robert Coffey, for their collective advice, critical review, and friendly guidance during the course of my graduate career.

In a similar vein, I'd like to recognize Drs. Jason Phan, Edward Olejniczak, Alex Waterson, Taekyu Lee and Olivia Rossanese for the contributions that each of them made to my intellectual growth during my years of study at the Vanderbilt University. They have provided me with much useful scientific advice, acted as models of scientific ability and thinking. I am grateful to all of those with whom I have had the pleasure to work during my graduate studies. My fellow graduate students Michael Burns, Craig Goodwin, and Laura Keigher have provided much needed camaraderie throughout this process. And I wish to thank DeMarco Camper for providing excellent technical support.

This work would not have been possible without the financial support of the Vanderbilt International Scholars Award, NCI SPORE grant for GI cancers or the Lustgarten Foundation for Pancreatic Cancer Research.

Nobody has been more important to me in the pursuit of this project than the members of my family. I would like to thank my parents, whose love and guidance are with me in whatever I pursue. Most importantly, I wish to thank my loving and supportive wife, Fei, and my wonderful daughter, Mia, who provide unending inspiration.

TABLE OF CONTENTS

	Page
Acknowledgements.....	ii
List of Tables.....	v
List of Figures.....	vi
Chapter	
I. Introduction.....	1
Biochemical and Cell Biology of Ras	
The Binary Aspect of Ras.....	3
Structural Basis of GEF-catalyzed Nucleotide Exchange.....	5
GAP-catalyzed GTP hydrolysis and the structural basis of oncogenic mutations...8	
Ras isoforms and Ras prenylation.....	10
Ras Signaling Pathway.....	12
EGFR-Ras-MAPK pathway.....	13
PI3K-AKT pathway.....	13
Ras is a Well-Validated Cancer Target.....	14
Previous Attempts to Target Ras.....	16
Targeting Ras signaling.....	23
Fragment-Based Drug Discovery.....	26
Scope of the Dissertation.....	30
II. Identification of Small Molecules that Bind to Ras.....	32
Introduction.....	32
Results	
Protein Purification.....	33
Fragment Screening by NMR.....	35
Crystal Structures of Small Molecules Bound to K-Ras.....	36
Compound Optimization and Structure-based Design.....	39
Compounds Block Nucleotide Exchange.....	41
Discussion and Conclusion.....	44
Materials and Methods.....	46
III. Second-site Screening of K-Ras in the Presence of a Covalently Attached First-site Ligand.....	51
Introduction.....	51
Results	
Cysteine Tethering Strategy.....	53

Fragment Screening for the Second-site Ligand.....	58
Crystal Structures of the Second-site Ligands Bound to a New Pocket.....	59
Discussion and Conclusion.....	61
Opportunities to Specifically Target K-Ras G12C.....	65
Materials and Methods.....	67
IV. Targeting Ras Signaling with Nucleotide Exchange Activators.....	70
Introduction.....	70
Results	
Discovery of Activators from the Nucleotide Exchange Assay.....	71
Crystal Structure of Activator-bound Ternary Complexes.....	76
Functional Relevance of the New Pocket.....	80
Co-crystal Structures of the Different Classes of Activators.....	82
Design and Optimization of HTS activators.....	84
Compounds Increase Ras-GTP and Perturb Ras Signaling in Cells.....	87
Discussion and Conclusion.....	92
Materials and Methods.....	95
V. Discussion and Perspective	101
Significance.....	101
Issues and Challenges.....	103
Novel Approaches.....	108
Hybrid Peptide.....	109
Interfacial Inhibitor.....	110
Closing.....	115
APPENDIX	
A. Hits from the Fragment Screening of GDP-bound K-Ras (G12D).....	116
B. Fragment Hits or Analogs co-crystalized with GDP-bound K-Ras (WT/G12V).....	121
C. Nucleotide Exchange Activators Co-crystalized with Ras:SOS:Ras Ternary Complex, Ras:SOS Binary Complex, or SOS-CDC25 Domain.....	122
REFERENCES.....	124

LIST OF TABLES

Table	Page
1. Compound binding affinity with GDP K-Ras (G12D) measured by HSQC titration and functional activity in a Sos-catalyzed nucleotide exchange assays.....	40
2. Examples of the hits identified from the second-site screen	59
3. The Structure-Activity Relationship of activator compounds 1-5	72

LIST OF FIGURES

Figure	Page
1. Cancer is caused by a series of genetic mutations.	2
2. Ras is cycling between GTP-bound form and GDP-bound form.....	4
3. Conformational switches between GDP-bound and GTP-bound Ras.....	5
4. Molecular mechanism of the SOS-mediated nucleotide exchange of Ras.....	6
5. Allosteric activation of SOS by GTP-bound Ras.....	7
6. Structural mechanism of GAP catalyzed GTP hydrolysis of Ras.....	9
7. Ras isoforms and Ras prenylation.....	10
8. Ras signaling pathway is a highly complex system.....	12
9. Potential binding pockets predicted by in silico methods.....	18
10. Small molecules that directly bind to Ras.....	19
11. Targeting K-Ras (G12C) by covalently attach a compound to the Cys-12.....	22
12. Inhibitors affect Ras post-translational modifications and localization.....	25
13. Linking strategy in the fragment-based drug discovery.....	27
14. SAR by NMR.....	28
15. Expression of K-Ras as a MBP fusion protein.....	33
16. $^1\text{H}/^{15}\text{N}$ HSQC spectrum of GDP-bound K-Ras (G12D).....	34
17. Multiple chemotypes were identified in the fragment-based screen.....	35
18. Chemical shift perturbation by a fragment hit and K_D measurement.....	36
19. Co-crystal structures of GDP-K-Ras complexed to small molecules.....	38
20. Conformational changes between ligand-free and ligand-bound K-Ras.....	39

21. Co-crystal structure of GDP-bound K-Ras complexed to compound 13	41
22. Effect of compound 12 on SOS-mediated K-Ras activation.....	42
23. K-Ras/ 13 structure overlaid with Ras-SOS complex crystal structure.....	42
24. HSQC spectra of GDP-K-Ras (G12D) w/ and w/o SOS and compound 13	43
25. Ras ligand binding revealed in co-crystal structures.....	45
26. Six residues around the primary binding pocket were mutated to cysteine.....	54
27. Crystal structures of K-Ras mutants covalently attached to a thiol-reactive probe.....	55
28. The thiol-reactive compounds used to identify the preferred mutant/compound combination for the second site screen.....	56
29. Strategy to identify thiol-reactive compound that blocks the first-site binding pocket.....	57
30. Crystal structures of GDP-bound K-Ras S39C that was reacted with thiol-reactive compounds.....	58
31. Crystal structures revealed small-molecules bind at the S3 pocket of K-Ras.....	60
32. Crystal structures of optimized analogs bind in the S3 pocket.....	60
33. Crystal structure of K-Ras G75C showed a disordered switch II.....	63
34. Molecular modeling to determine how to connect the first-site ligands and the second-site ligands.....	64
35. Covalently attach S3 ligands to Cys-12.....	66
36. Nucleotide exchange activators were detected.....	71
37. API compounds increase SOS-catalyzed nucleotide exchange on Ras.....	73
38. Compounds that activate the SOS-catalyzed nucleotide exchange of K-Ras were identified from a High-throughput screen.....	74
39. Nucleotide exchange activation by API compounds is SOS-dependent and does not require the allosteric Ras binding site.....	75
40. API compounds bind to the HRas ^{WT} :SOS ^{cat} :HRas ^{Y64A} ternary complex.....	78

41. Saturation and competition binding experiments conducted using FITC-conjugated compounds.....	80
42. Mutation of the activator binding site on SOS prevents activation of nucleotide exchange by amino-piperidine indole.....	82
43. Crystal structures of activators from High-throughput screen when bound to SOS...	83
44. A ligand bound co-crystal structure of SOS-CDC25 domain	84
45. Strategies to design compounds to fill the pocket optimally.....	85
46. Mix-and-match strategy in designing improved ligands.....	86
47. Compounds are cell-permeable and inhibit cell proliferation and anchorage-independent growth.....	88
48. Amino-piperidine indole compounds perturb Ras signaling by acting at the level of the Ras-SOS interaction.....	90
49. Compounds designed from the molecular modeling.....	94
50. Molecular docking model of inhibitor binding to GDP-bound RalA.....	105
51. Connecting site 2 and site 3 by modeling.....	106
52. Design a hybrid peptide to inhibit Ras.....	110
53. Identify interfacial inhibitors of Ras.....	111
54. Linking the activators to an indole on Ras with flexible linkers.....	112
55. Using molecular modeling to design interfacial inhibitors against Ras:SOS complex.....	114

CHAPTER I

INTRODUCTION

Cancer remains one of the leading causes of death worldwide. According to the WHO, 7.6 million patients died of cancers in 2008, and in 2013, 1.6 million new cases of cancers were diagnosed in the United States. Effective therapies for the treatment of cancer are one of the most critical unmet medical needs today [1, 2].

Cancer is a group of diseases in which abnormal cells divide without control and are able to invade other tissues. One of the major causes of cancer are gene mutations. For example, certain mutations that impair DNA damage repair and programmed cell death can lead to the activation of oncogenes and the inactivation of tumor suppressors. The overall process is similar to a chain reaction initiated by one or more mutations, which lead to more severe errors, each progressively allowing the cell to escape from normal cell regulation (Figure 1). Typically, changes in several genes are required to transform a normal cell into a cancer cell [3]. The transition from proto-oncogenes to oncogenes is a key event in the malignant transformation.

Developing an effective therapy against cancer is extremely difficult due to the heterogeneous nature of the disease. However, despite the heterogeneity of tumors, there are a few important traits that are common in most, if not all, cancers. These have been called “the hallmarks of cancer” [4]. As one of the most notorious oncogenes, Rat Sarcoma (Ras), affects many important pathways that contribute to these critical cellular events [5]. While the important discoveries about the basic aspects of Ras biology and how the dysregulation of Ras contributes to disease continue to emerge, Ras has always been considered an important target for cancer

treatment. Thus, major pharmaceutical companies as well as academic labs have spent a great deal of effort to target this important protein. However, to date, no effective treatment against Ras has been found.

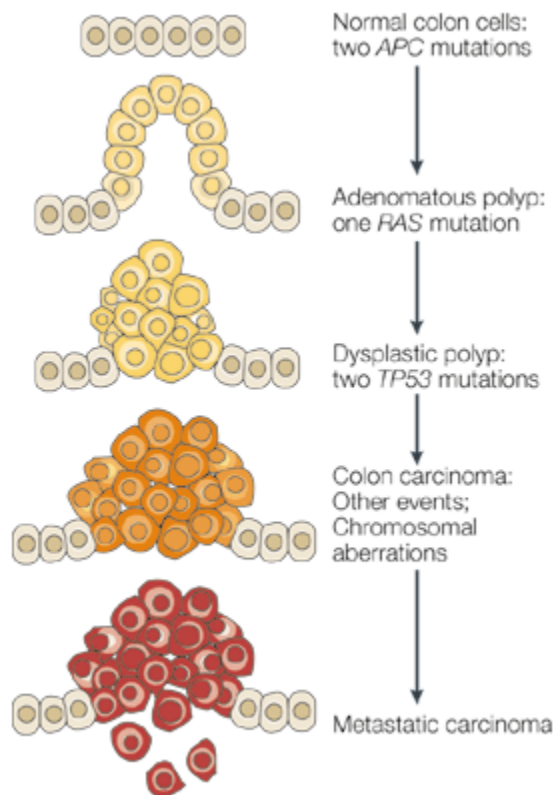


Figure 1. Cancer is caused by a series of genetic mutations. Each mutation alters the behavior of the cell and initiates the next stage of the malignant transformation. For instance, in colorectal cancers, multiple mutational events correlate with each step in the initiation and progression of cancer. (This figure is adapted from Knudson et al. [3])

Biochemical and cell biology of Ras

The Binary Aspect of Ras

Ras is an enzyme that controls cell proliferation, differentiation and survival.[6] It serves as a bridge to connect upstream signals to downstream effectors. A key feature of the Ras protein is that it cycles between the active (GTP-bound) state and inactive (GDP-bound) state. (Figure 2) In resting cells, Ras is bound to GDP (Guanosine Diphosphate), which is exchanged for GTP (Guanosine Triphosphate) upon receiving extracellular stimuli. When bound to GTP, Ras interacts specifically with effector proteins, thereby initiating cascades of signals downstream that may finally lead to cell proliferation and other important cellular events. To return to the inactive state, Ras cleaves off the terminal phosphate moiety (Gamma-Phosphate) of GTP via hydrolysis and turning Ras back to the GDP-bound form. The cycling between the GTP-bound state and GDP-bound state induces a conformational change of Ras that is mainly restricted to two highly mobile regions of the protein designated as switch I (residues 30–40) and switch II (residues 60–76) [7, 8]. The two switch regions are shown in Figure 3. The switch I region is critical for the binding to the downstream effectors. Both switches are near the γ -phosphate of GTP and subject to conformational changes. The conformational changes of the switch regions control the interaction with regulatory proteins and downstream effectors [9, 10]. When GTP binds to Ras, it forms an accessible loop on the surface of the protein that exhibits high-affinity binding to downstream effector proteins [11].

The binary aspect of the Ras protein enables it to function as a molecular switch in a broad range of signaling functions, often in the transduction of extracellular signals to the interior of cells.

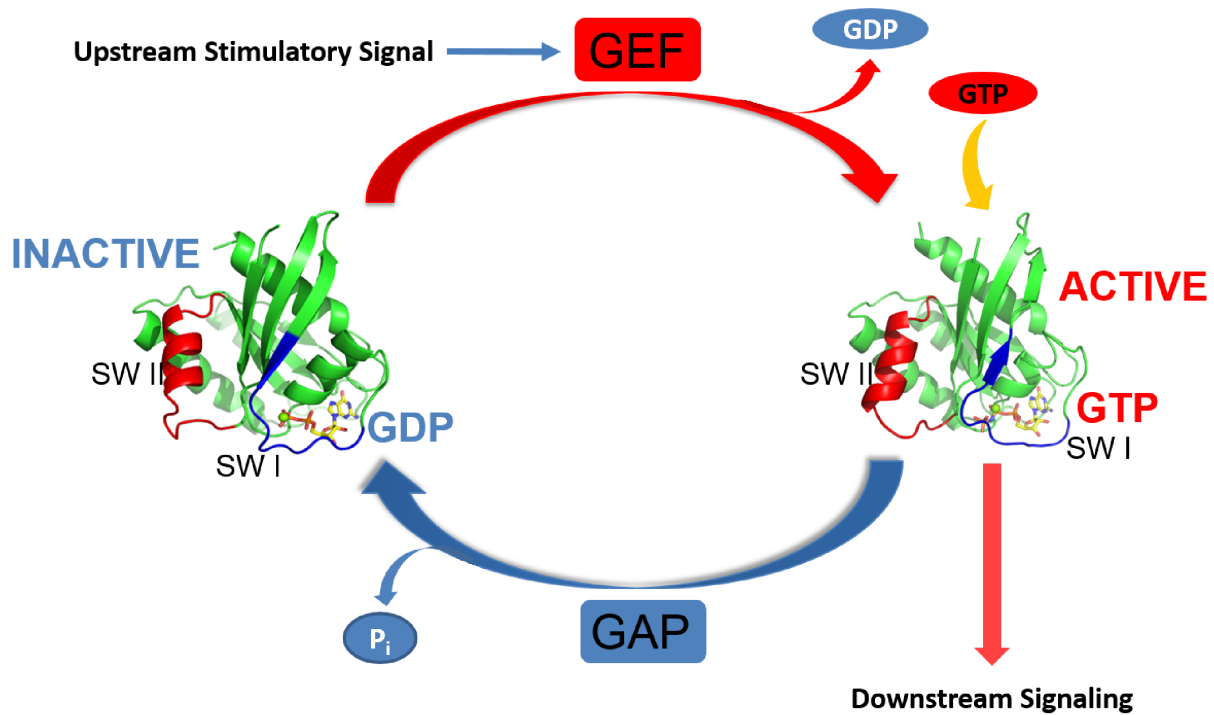


Figure 2. Ras is cycling between GTP-bound form and GDP-bound form.

GTP/GDP exchange and the hydrolysis of GTP are tightly regulated in the cell. For Ras, the intrinsic nucleotide exchange rate and nucleotide hydrolysis rate are very low. In order to quickly respond to the stimuli, two regulatory proteins, GTPase activating proteins (GAPs) [12], and guanine nucleotide exchange factors (GEFs), are needed to accelerate and regulate both processes.

SOS (son of sevenless) is the GEF for the Ras protein. When SOS binds to the Ras GTPase, the bound GDP is released, cellular GTP, which is ~10 times more concentrated than cellular GDP, binds to Ras to form active Ras [13]. To turn off the switch, GAPs bind to Ras and accelerate the hydrolysis of GTP and promote the formation of inactive Ras.

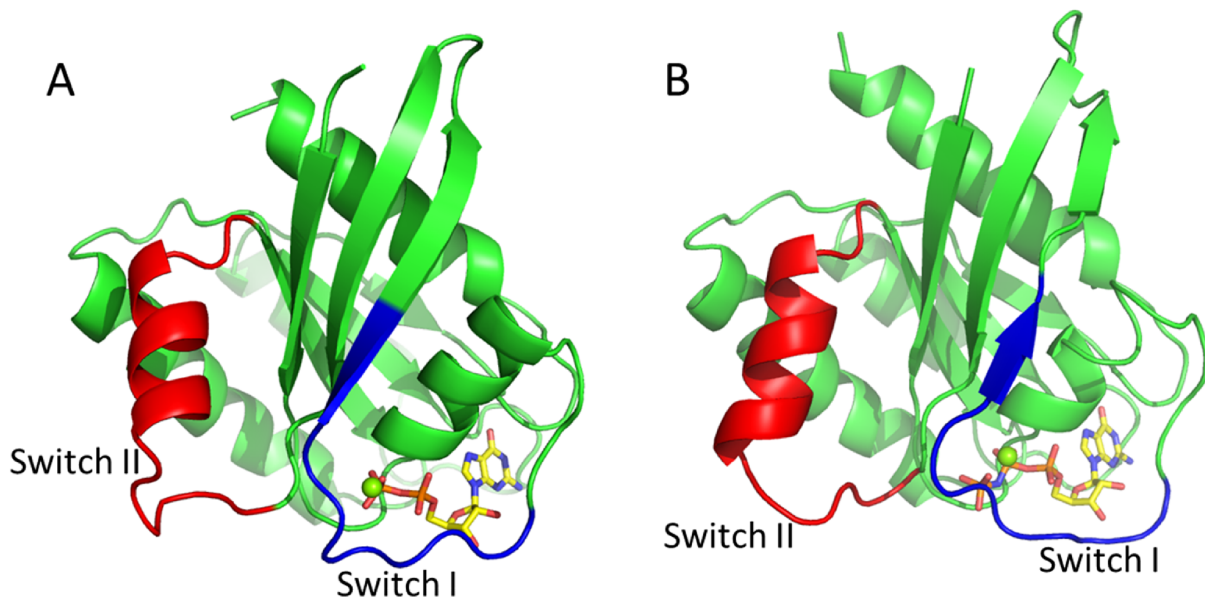


Figure 3. Conformational switches in the GDP-bound (A) and GTP-bound (B) Ras. Switch I consists of residues 30–40 (blue) and switch II consists of residues 60–76 (red).

Structural basis of GEF-catalyzed nucleotide exchange

The molecular mechanism of the SOS-mediated nucleotide exchange process has been well studied. SOS binds to Ras and facilitates the release of the nucleotide. Biochemical studies of Ras exchange factors have shown that Ras forms a stable complex with SOS and dissociates by rebinding to either GTP or GDP without preference. Since the cytoplasmic GTP concentration is about 10-fold higher than GDP, binding to SOS is usually considered to accelerate the formation of GTP-bound Ras. The crystal structure of the Ras-SOS complex revealed the molecular mechanism of how SOS catalyzes nucleotide exchange [14]. (Figure 4) By comparing the nucleotide-bound (Figure 4A,C) and nucleotide-free (Figure 4B, D) forms of Ras, SOS-mediated nucleotide exchange can be dissected into several key events. The

cell division cycle-25 (CDC25) domain of SOS interacts with Ras to initiate the nucleotide exchange, while the helical Ras exchanger motif (REM) region plays a structural role in this process.

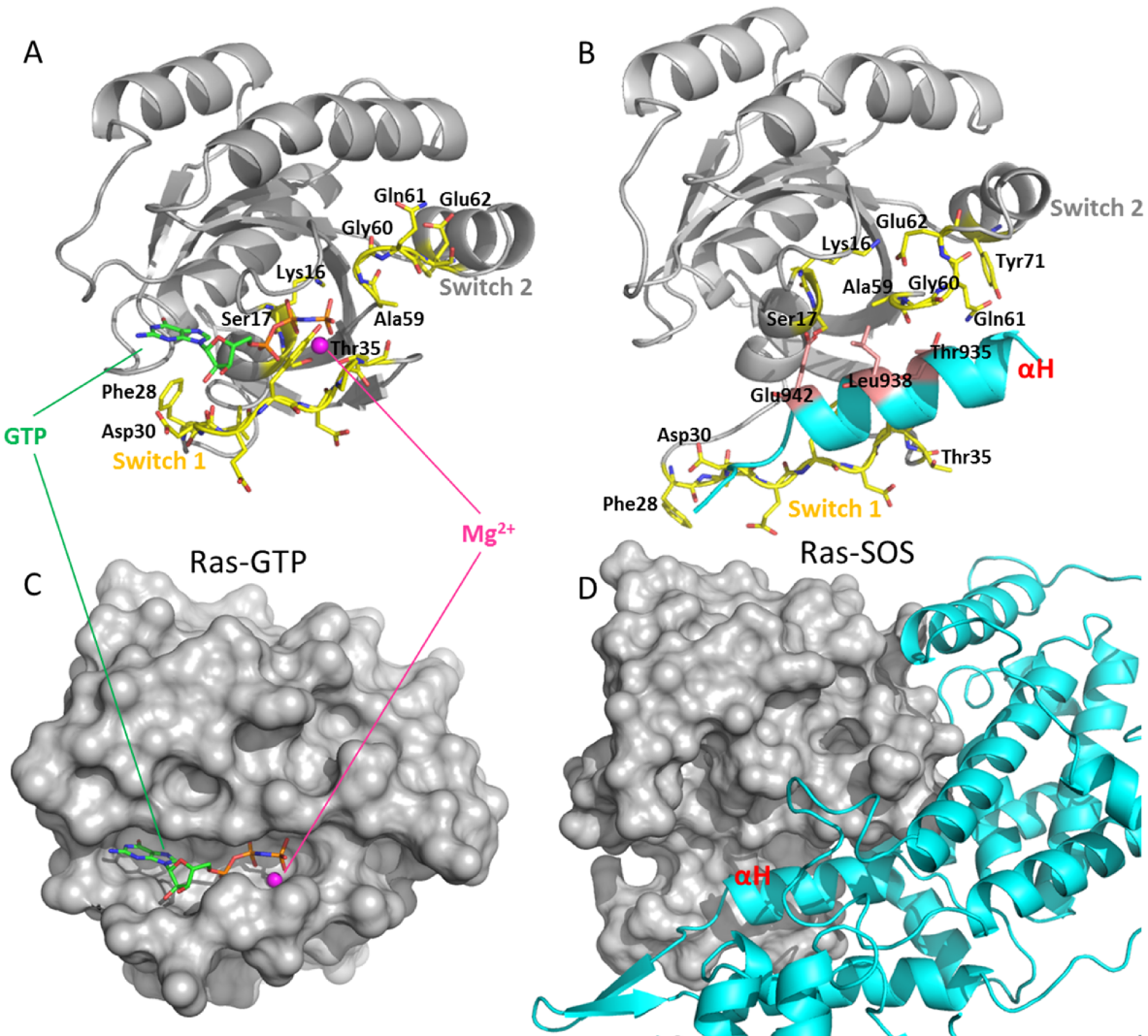


Figure 4. Molecular mechanism of the SOS-mediated nucleotide exchange of Ras.

Three critical residues on Ras, Tyr-64, Met-67 and Tyr-71, insert into the hydrophobic core of SOS at the center of the binding interface. (Figure 4B) This hydrophobic anchor is surrounded by other residues of the switch II region mainly through charge-charge interactions.

The helical hairpin α H- α I of SOS protrudes from the core and inserts into the Ras nucleotide-binding site. As a result, switch I is removed from the nucleotide binding site, breaking up its interaction with the nucleotide. (Figure 4D) Residues of α H impede the binding of Mg^{2+} and the α phosphate. In addition, the GTP interacting residues, Gly-60 and Lys-16, form new interactions with Glu-62 and Ala-59, which acts to occlude the Mg^{2+} binding site. (Figure 4B)

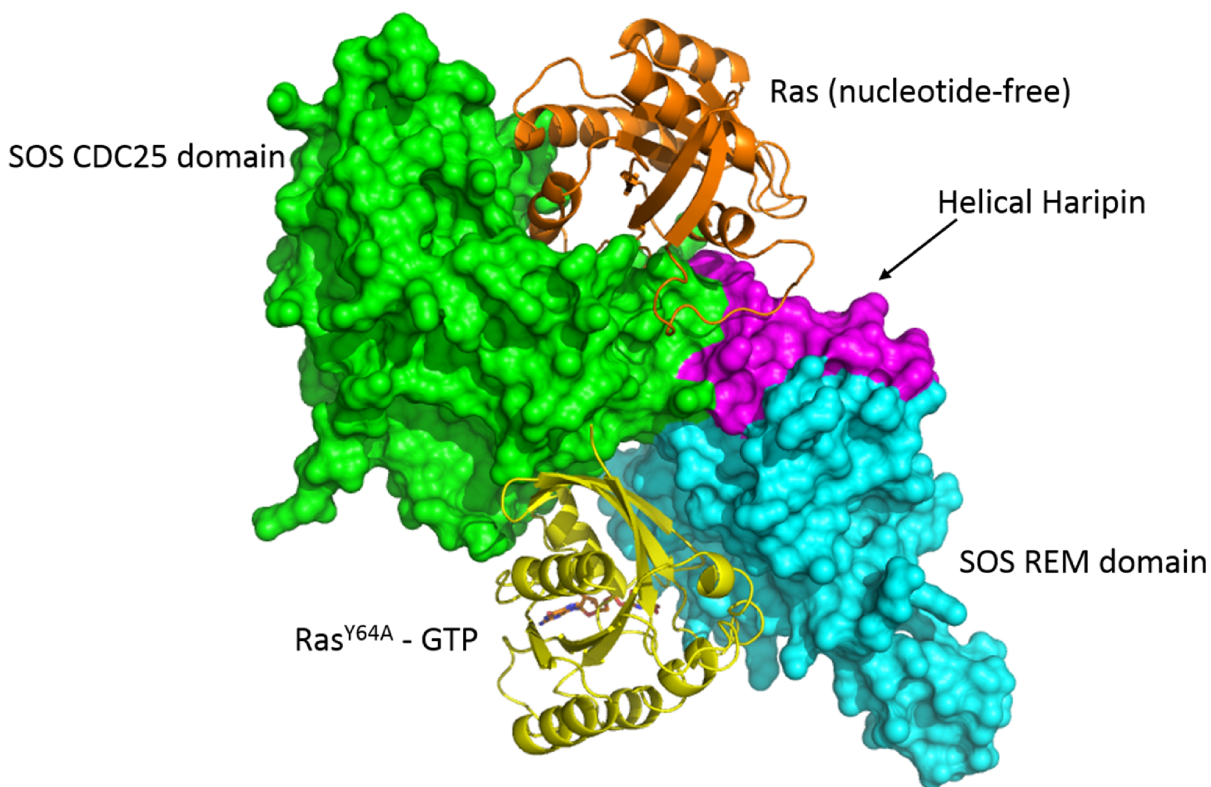


Figure 5. Allosteric activation of SOS by GTP-bound Ras. During the SOS-mediated nucleotide exchange of Ras, two Ras molecules and one SOS molecule form a ternary complex. A Ras molecule (brown) binds to SOS at the catalytic site causing the dissociation of the bound nucleotide. Another GTP-bound Ras molecule (yellow) binds to an allosteric site of SOS located between CDC25 (green) and REM (cyan) domains and induces a conformational change of the helical hairpin (magenta) of SOS, leading to the activation of the nucleotide exchange activity of SOS.

An interesting feature of SOS-mediated nucleotide exchange is the allosteric activation caused by a GTP-bound Ras molecule [15]. A second GTP-bound Ras molecule binds at a cleft

between the REM and CDC25 domains, allosterically activating the nucleotide exchange activity of SOS. As shown in Figure 5, a second Ras molecule interacts with the base of the α H- α I helical hairpin, which is responsible for guanine nucleotide exchange of the first Ras molecule at the catalytic site. Binding of a second Ras shifts the REM domain to a position that it can now reach the switch I region of the catalytic Ras molecule, causing an increase in the nucleotide exchange activity of SOS. Notably, in full-length SOS, the N-terminal DH and PH domains occupy this allosteric binding site and auto-inhibit the allosteric activation of SOS [16].

GAP-catalyzed GTP hydrolysis and the structural basis of oncogenic mutations

Despite the relative abundance of GTP relative to GDP in the cytoplasm, the majority of Ras proteins exist in the GDP-bound state under normal cellular conditions, due to the dramatic increase in hydrolytic activity enabled by GAPs. The intrinsic GTPase activity for Ras is usually quite low. GAP binds to the switch I region of Ras and greatly accelerates this process. The molecular mechanism of GAP accelerated GTP hydrolysis was uncovered by the crystal structure of the Ras-RasGAP complex [17]. Ras and GAP interact through both hydrophobic and polar interactions. (Figure 6C) Specifically, switch I of Ras interacts predominantly with the central helices, α 6c and α 7c. Pro-34, Ile-36, Tyr-32 and Tyr-64 of Ras directly interact with Leu-902 and Leu-910 of α 6c of GAP. The acidic residues on the Ras switch I region create a negatively charged surface which interacts with GAP. Asp-33 on Ras forms a direct hydrogen bond to Asn-942. The positively charged guanidine group of Arg-789 on the loop L1c inserts its “arginine finger” into the active site, which introduces a positive charge into this area and neutralizes the developing charges in the transition state of phosphoryl transfer reactions [18]. (Figure 6A) Binding of GAP also stabilizes the switch II region of Ras and allows the amide

group of the Ras Gln-61 side chain to form a hydrogen bond with the backbone carbonyl of Arg-789 and positions a nucleophilic water molecule. This structure was useful for understanding the structural basis of how oncogenic mutations of Ras could impede the GTP hydrolysis process. As demonstrated in Figure 6D, mutations of Gly-12, Gly-13 or Gln-61 could either block the binding of the “Arginine finger” or disturb the positioning of the nucleophilic water, thus preventing the hydrolysis of GTP.

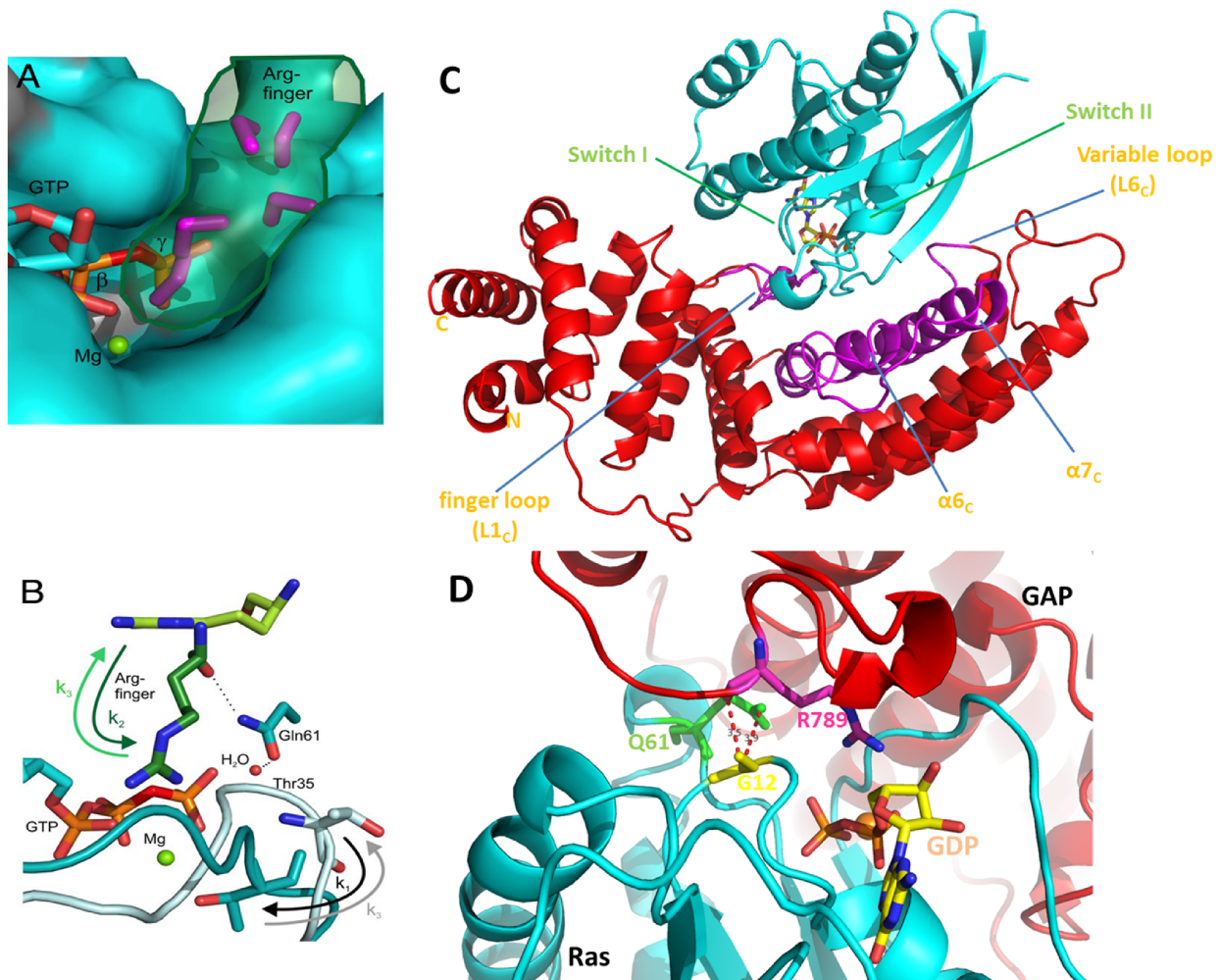


Figure 6. Structural mechanism of GAP catalyzed GTP hydrolysis of Ras. (A) Modeling suggests that several structured water molecules (purple stick) would be replaced if we move the arginine (green shading) into the binding pocket of Ras-GTP [19], which would increase the entropy for the GTPase reaction. (B) The conformational changes in this process include: The conformation of switch I of Ras is changed from “off” to “on” (k_1); the arginine finger is moved into the binding pocket. The carbonyl group of the arginine-finger coordinates Gln-61 of the

switch II, which positions the nucleophilic water (k2). Both processes can be reversed (k3). (C) Ribbon representation of the Ras-GAP complex. The catalytic domains of GAP are shown in red, regions of GAP contacting Ras in magenta, Ras in cyan. (D) Close approach of the Arg finger loop of GAP to the P-loop of Ras. The crystal structure of H-Ras and GAP (PDB entry: 1WQ1) suggests that a bulky residue replacement at the 12 position of Ras will clash with the finger loop and interfere GAP from catalyzing the GTPase reaction. The C α of Gly-12 (yellow) is in proximity to the side chain of Gln-61 (green) and Arg-789 (magenta). (This figure is adapted from Kotting et al. [18])

Ras isoforms and Ras prenylation

There are three canonical members of the Ras family, H-RAS, N-RAS, and K-RAS (including two exon splice variants: K-Ras4A and K-Ras4B). They are highly conserved in the catalytic domain and mainly differ in their C-terminal hypervariable regions. (Residue 169-189) (Figure 7)

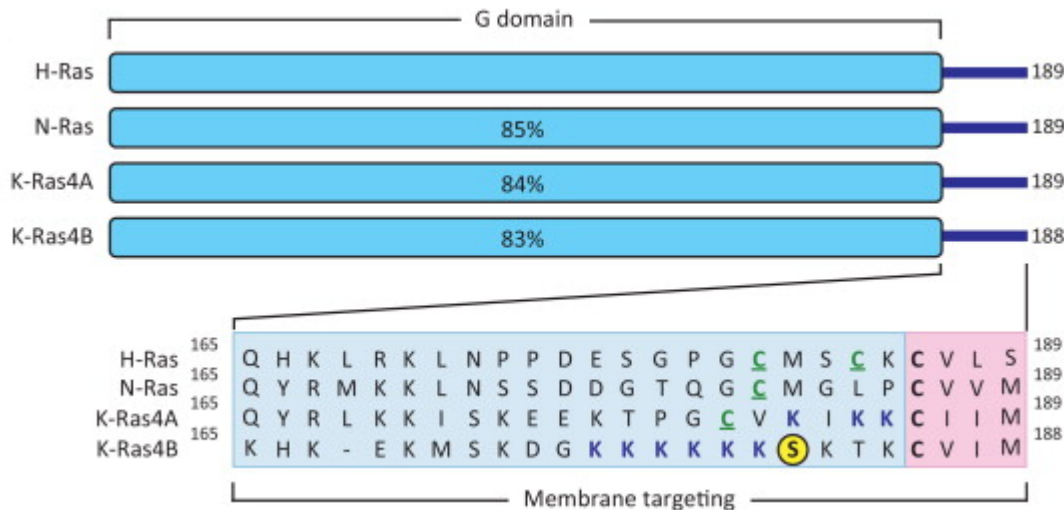


Figure 7. Ras isoforms and Ras prenylation. The human RAS genes encode 188 or 189 amino acid proteins that have high sequence similarity (82–90% overall). Residues 1–164 contain the G domain that binds and hydrolyzes GTP (93–99% sequence identity). The C-terminal hypervariable region (shown in the inset) comprise the cell membrane targeting sequence (16–40% identity), and the C-terminal four residues comprise the CAAX motif that signals the

farnesyltransferase-catalyzed covalent addition of a farnesyl group to the cysteine residue. (This figure is adapted from Bryant. et al. [20])

The most important function of the hypervariable region is to target Ras for membrane attachment. Specifically, a CAAX (C = cysteine, A = aliphatic; X = terminal amino acid) tetrapeptide sequence at the Ras C-terminus can be recognized by farnesyltransferase or geranylgeranyltransferase, which catalyzes the covalent attachment of a farnesyl or geranylgeranyl isoprenoid to the cysteine residue of the CAAX sequence. The prenylation targets Ras proteins to specific membrane compartments and subcellular locations and is critical for the biological activity of Ras [21]. Differences in the hypervariable region of the primary sequence of Ras isoforms determine the differences in post-translational modification, trafficking, localization, and ultimately biological functions.

Ras Signaling Pathway

The Ras signaling pathway is a highly complex system. As indicated in Figure 8. Ras proteins were found to interact with hundreds of factors.

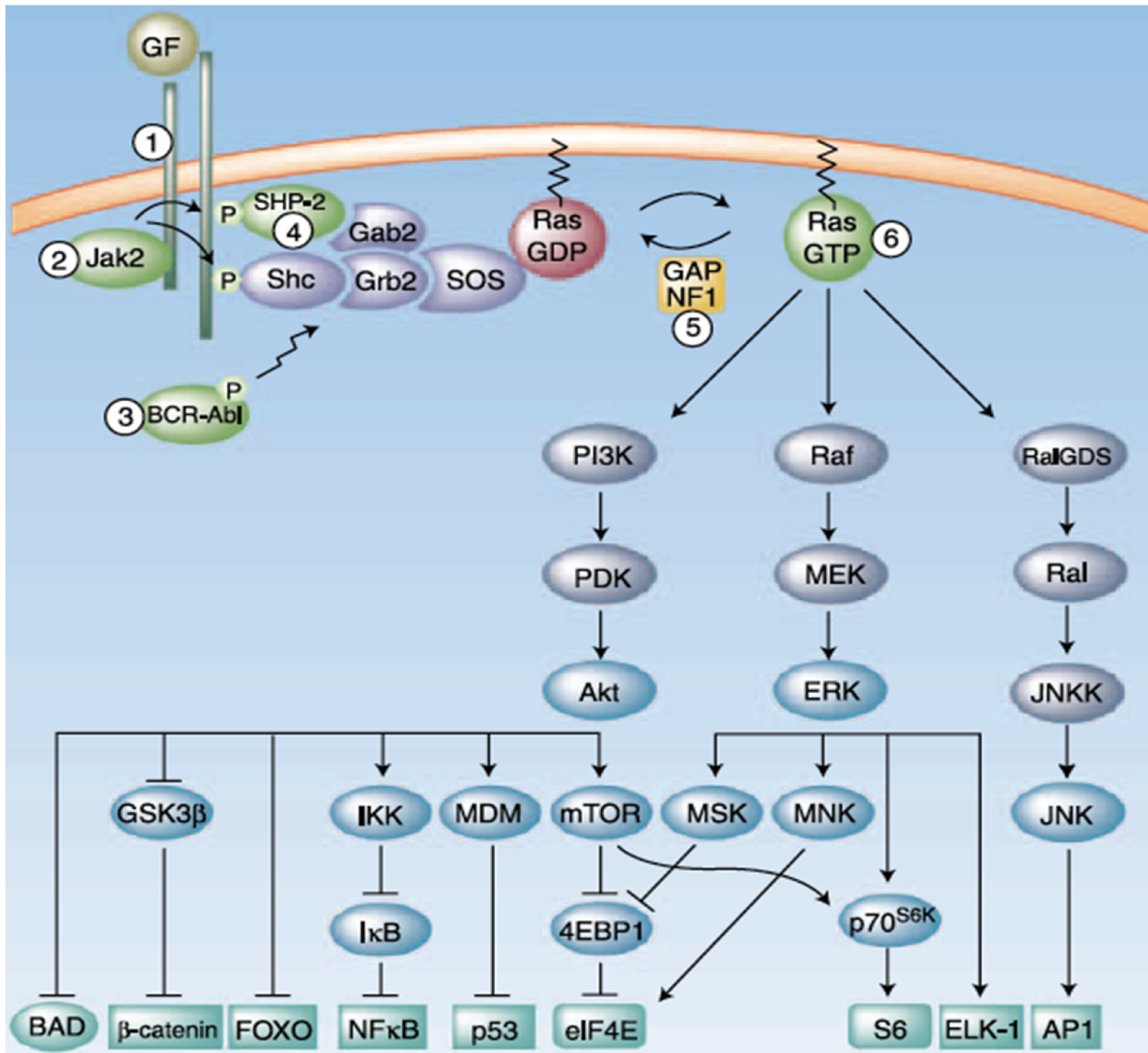


Figure 8. Ras signaling pathway is a highly complex system. (This figure is adapted from Braun et al. [22])

In normal cells, Ras is activated in response to extracellular signals, and GTP-bound Ras activates a number of signaling pathways. Here two important pathways are described:

Ras/Raf/MEK/MAPK and Ras/PI3K/Akt.

EGFR-Ras-MAPK pathway

The EGFR-Ras-MAPK pathway is the best characterized Ras signaling pathway [23]. When epidermal growth factor receptor (EGFR) tyrosine kinase receives extracellular stimuli, it undergoes autophosphorylation. Phosphorylated EGFR activates and recruits SOS to the cytoplasm membrane through the adapter protein Grb2 (Growth Factor Receptor-Bound Protein-2). When Ras is activated by SOS, it recruits Raf serine/threonine kinase to the plasma membrane, where additional phosphorylation occurs on Raf and promotes full activation of Raf kinase, which initiates a series of signaling cascades. The Raf kinase controls the activation of the MAPK (mitogen-activated protein kinases) pathway and plays a significant role in controlling proliferation and differentiation. Raf phosphorylates and activates the MEK1/2 kinase, which then phosphorylates the mitogen-activated protein (MAP) kinase. Phosphorylated MAPK translocates from the cytoplasm into the nucleus where it subsequently activates a number of transcription factors, including the transcription factor Elk1 and c-myc. Activated transcription factors turn on the transcription of particular sets of target gene, promote cell proliferation, growth and survival.

PI3K-AKT pathway

Another well-characterized pathway is the PI3K-AKT pathway. PI3K (phosphatidylinositol 3-kinases) is a major effector downstream of Ras [24, 25]. It has important

roles in mediating the pro-survival and proliferative functions of Ras [26]. Ras activation is responsible for Ras-induced transformation, which occurs through PI3K-dependent and -independent pathways [27, 28]. PI3K is recruited by the active Ras to the membrane docking site and become activated. The activation of PI3K results in the generation of the second messenger, phosphatidylinositol 3,4,5-triphosphate (PIP3) from phosphatidylinositol 4,5-bisphosphate (PIP2). Activation of PI3K leads to the activation of the lipid kinase as a result of its translocation to the membrane and conformational changes. PIP3 facilitates the activation of the Akt serine/threonine kinase by inducing the phosphorylation of Akt at Thr-308 and Ser-473. AKT/PKB (Protein Kinase-B) has a strong anti-apoptotic function by phosphorylating various targets [29] and plays an important role in Ras-mediated cell survival [30].

Ras is a well-validated cancer target

Ras is a well-validated anticancer target based on the known functions of Ras, the importance of Ras in oncogenesis, the prevalence of Ras mutations in human tumors, and the dramatic effect of Ras inhibition in tumor models.

As one of the most notorious oncoproteins that has been identified, RAS was first identified as a transforming gene delivered by retroviruses. Further investigation revealed cellular homologues present in bladder and lung carcinoma cell lines that corresponded to the Harvey and Kirtsten rat sarcoma viruses [31] as well as the BALB murine sarcoma virus that, like their retroviral counterparts, could transform fibroblasts upon transfection [32, 33].

Ras interacts with a great number of signaling molecules, which makes Ras proteins a key component of many cellular processes. Activating mutations in RAS genes are the most common genetic lesions in human tumors [34]. Mutations of Ras residues 12, 13, and 61 are the most common mutations in human cancer due to their greatest impairment in GTPase activity [35, 36]. Ras proteins carrying such mutations are not effective in hydrolyzing GTP and are locked in the active state, endowing cells with capabilities that represent the hallmarks of cancer [37]. These include the ability to proliferate, evade apoptosis, reprogram cell metabolism, induce angiogenesis, activate invasion and metastasis, and escape immune destruction [5]. Indeed, aberrant K-Ras signaling is found in 30% of all human cancers, with the highest incidence of activating mutations found in pancreatic (70-90%), colon (30-50%), and lung (20-30%) carcinomas [38-41]. In addition, activating mutations on H-Ras are found in approximately 10% of bladder carcinomas and 10% of renal cancers; and mutations on N-Ras are found in 30% of melanomas, 30% of liver cancers, and 30% of acute myelogenous leukemias [42]. K-Ras mutations are also associated with resistance to chemotherapy and radiotherapy, which contribute to a poor prognosis [43]. Other than oncogenic mutations, Ras proteins may promote oncogenesis *via* gene amplification, overexpression or upstream activation of the pathway. Wild-type K-Ras gene amplification has been found in 40% of esophageal adenocarcinomas [44]. Elevated Ras activity has also been observed in 50% of breast cancers, which is associated with overexpression of the epidermal growth factor receptor (EGFR) and human epidermal growth factor receptor-2 (HER-2) [45].

The importance of Ras signaling in tumor initiation and maintenance is also emphasized by the indirect dysregulation of Ras activity as well. For example, loss of the tumor suppressor NF1, which encodes a protein with similarities to the catalytic domain of GAP family members,

results in elevated levels of GTP-bound Ras and is associated with malignant transformation [46-48].

Thus, Ras represents a highly validated and important target for a wide variety of cancers. Therefore, inhibiting Ras would be expected to produce a clinical benefit. Indeed, a dominant negative H-Ras with an N116Y mutation in a site critical for GTP binding can revert the malignant phenotype of NIH3T3 cells transformed by oncogenic Ras [49, 50] and is also capable of inhibiting the growth of esophageal and pancreatic tumors in mouse models [51, 52]. Silencing K-Ras by siRNA has shown to result in the reversal of the transformed phenotype and suppression of tumorigenicity of human cancer cells [53-55]. Inhibition of K-Ras activity by a mutant GEF, which forms a more stable Ras:SOS complex, also reverted the oncogenic K-Ras transformed mouse fibroblasts to wild-type phenotypes [56]. Furthermore, downregulation of activated Ras reverses the transformed phenotype of cells and results in the dramatic regression of tumors in murine xenograft models [57, 58].

As above, deregulation of Ras signaling has been proven to cause cancers. Inhibition of Ras activity in established tumors or tumor cell lines results in cell death or reversal of the malignant phenotype. Therefore, effectively inhibiting Ras remains a very attractive goal for the treatment of cancer for the past two decades. However, to date, this goal has not led to any effective solutions.

Previous attempts to directly target Ras

To date, attempts to develop small molecules that directly target Ras have only met with minimal success. One of the major challenges is that Ras is an “undruggable” target. Such proteins typically lack well-defined binding pockets making them difficult to target with small

molecules [59]. In analogy to ATP-competitive kinase inhibitors, exploring GTP-competitive inhibitors of Ras has been attempted [60, 61]. However, the affinity of kinases for ATP are usually in the micromolar range [62], picomolar guanosine nucleotide affinities of Ras combined with millimolar intracellular nucleotide pools hinder the success of GTP-competitive inhibitors [63].

To identify binding pockets on Ras, potential small molecule binding sites were evaluated using *in silico* prediction methods, such as a fast Fourier transform correlation mapping algorithm (FTmap) [64] and molecular dynamics simulations. Several groups [65-67] have mapped the surface of Ras and identified several potential binding pockets. By clustering all these predictions, several “hot spots” on the Ras surface have been identified which are highlighted in Figure 9. Other than the guanosine nucleotide binding site, several predicted ligand binding pockets include: site 1 (switch I region), site 2 (region between switch II and central β sheet), site 3 (region between switch II and helix 3), site 4 (region between switch II, the phosphate-binding loop (P-loop), and the back-side of loop 8), and site 5 located between loop 7, loop 9, and helix 5. Some of these pockets have also been identified experimentally using multiple solvent crystal structures (MSCS), an X-ray crystallographic technique pioneered by Mattos et al. [68]. Basically, gluteraldehyde cross-linked protein crystals are transferred into solutions containing high concentration of multiple organic solvents. If a ligand binding pocket is present, solvent molecules, such as dimethylformamide or isopropanol, may bind to this pocket in the crystal structure. By clustering the protein-bound solvent molecules, the “hot-spots” on the protein surface can be identified.

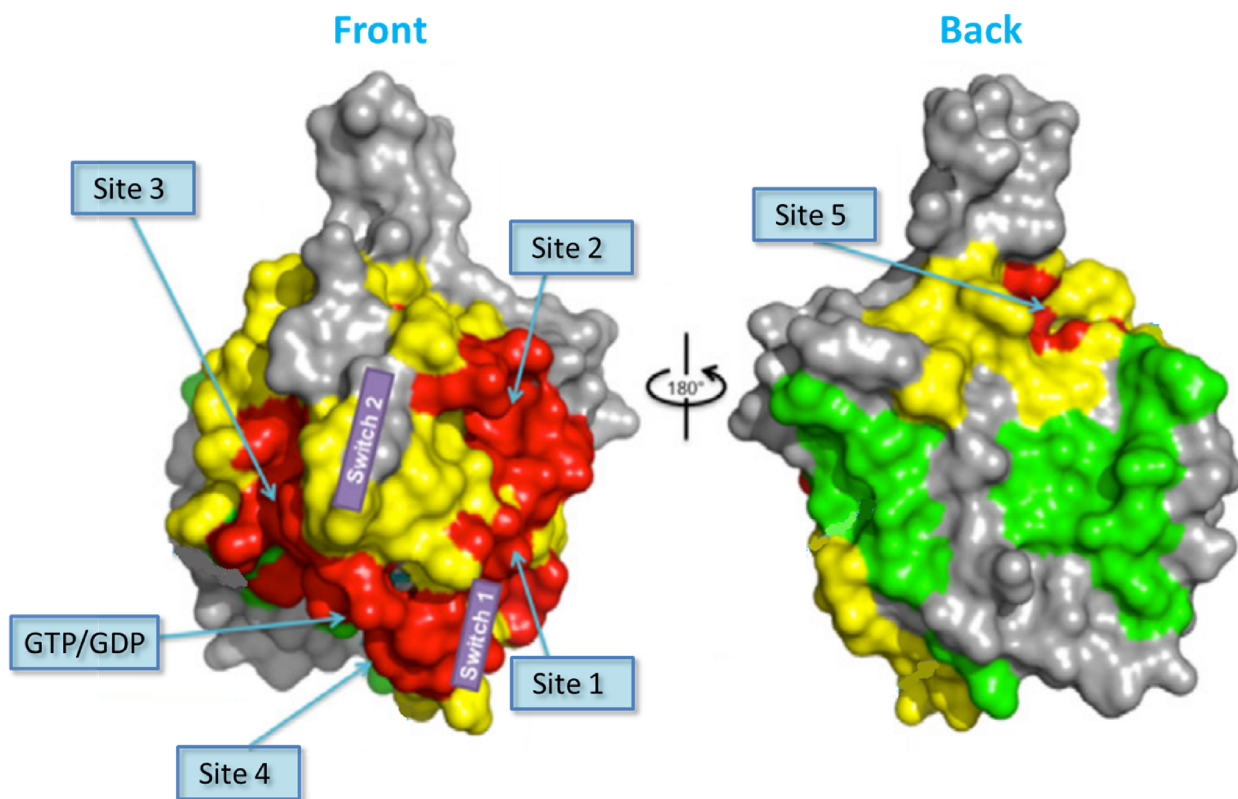


Figure 9. Potential binding pockets predicted by *in silico* methods. (This figure is adapted from Wang et al. [69]) Predicted ligand binding sites are mapped onto K-Ras crystal structure (shown in two views, front and back). The areas of the K-Ras surface involved in ligand binding are color-coded. The sites are classified based on the level of consensus among different predictions. (Green: low; Yellow: medium; Red: high)

Although K-Ras is an extremely challenging target, several small molecules have been reported to bind to Ras directly. Some of these ligand binding sites correspond to the sites of highest prediction consensus, and many of the binding sites appear to be functionally relevant. For example, SCH54292 (Figure 10, compound **1**) and SCH53870 (Figure 10, compound **2**) bind to GDP-bound H-Ras and inhibit intrinsic nucleotide exchange of Ras with IC₅₀'s of 0.5-0.7 μ M [70]. Their inhibitory activities were found to be non-competitive with GDP binding, and the formation of tertiary complexes was observed by electrospray ionization mass spectrometry analysis [71]. ¹H/¹⁵N Heteronuclear Single Quantum Coherence (HSQC) NMR analysis of H-

Ras-GDP bound to SCH54292 revealed that the compound binds to a hydrophobic pocket in the vicinity of the switch II region (site3) [72]. The docking model of the complex predicted that the hydroxylamine is located near the Mg^{2+} and the β -phosphate of GDP in the active site.

Interestingly, SCH53870 exhibited efficacy in PC12 cells by blocking NGF (nerve growth factor) induced neurite outgrowth mediated by Ras activation [70].

Peri and coworkers discovered a series of sugar-derived Ras inhibitors [73-76]. In a cell-based assay, compound (**3**) delayed the growth of K-Ras transformed NIH3T3 mouse fibroblasts at 100 μ M and showed selective toxicity toward cells expressing oncogenic mutant K-Ras G13D over wild-type cells [77]. Another sugar-derived compound (**4**) binds to GDP-bound H-Ras at the Switch II region with an affinity of 37 μ M [78]. It inhibits SOS-mediated nucleotide exchange of H-Ras with an IC_{50} of 100 μ M and also suppressed cell proliferation in NIH3T3 mouse fibroblasts (IC_{50} = 150 μ M).

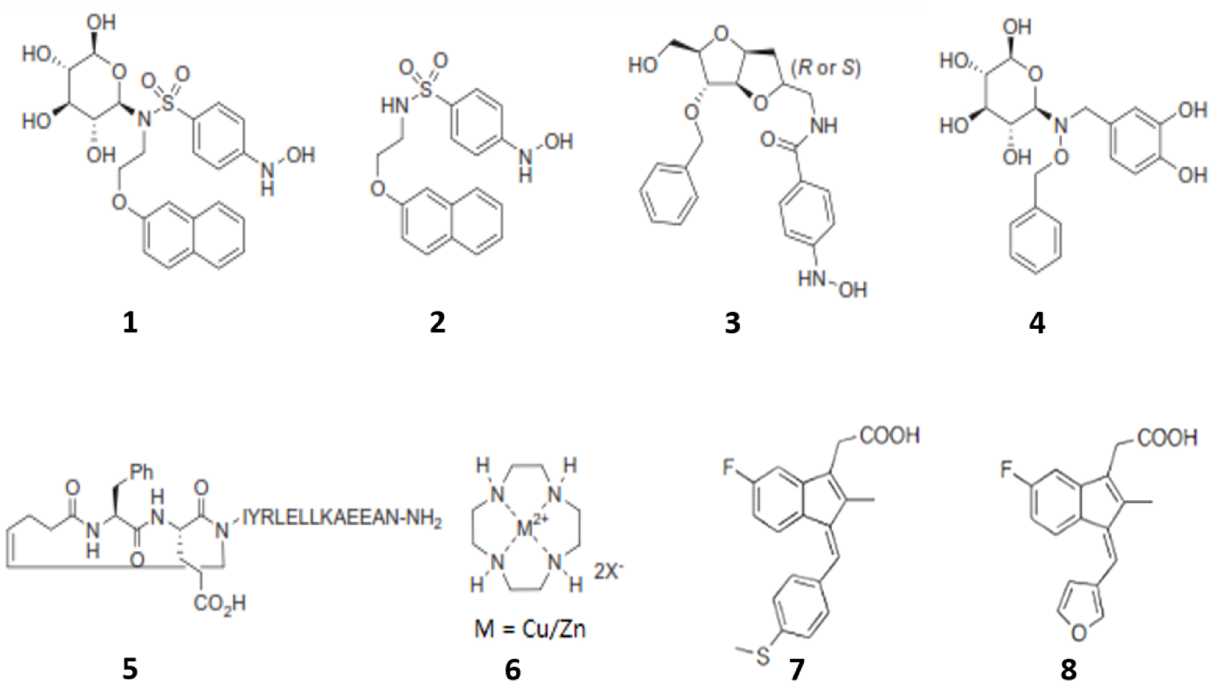


Figure 10. Small molecules that directly bind to Ras.

Other than inhibiting GDP-bound Ras, compounds also have been found that bind to the GTP-bound form of Ras. Using $^1\text{H}/^{15}\text{N}$ - HSQC NMR, Muller et al. showed that sulindac sulfide (Figure 10, compound **7**) bound to Ras-GTP near the switch I region, resulting in resonance shifts of residues K16, V29, and Y40 [75]. These compounds were shown to inhibit Ras-dependent activation of Raf kinase in a dose-dependent manner by blocking the Ras-Raf interaction in the potency range of 100-200 μM . A more potent inhibitor (Figure 10, compound **8**, $\text{IC}_{50} = 30 \mu\text{M}$) was identified by synthesizing a series of analogs [79]. However, their poor potency, promiscuous pharmacological effects, and lack of detailed structural information, precluded them from being investigated further.

The cyclen derivatives represent another series of compounds that directly inhibit Ras. Spoerner and co-workers used ^{31}P NMR to monitor the Ras conformations in solution and showed that multiple Ras conformations co-exist in equilibrium [80]. They found that binding to Ras by Zn^{2+} -cyclen (Figure 10, compound **6**) shifted the equilibrium of GTP-bound Ras towards a less active conformation. Rosnizeck et al. later confirmed that both Zn^{2+} and Cu^{2+} -cyclen stabilize a conformational state of GTP-bound Ras that has low affinity for the effector proteins. In their most recent studies, it was found that the Zn^{2+} -cyclen can stabilize a less-active form of GTP-bound K-Ras and perturbs the equilibrium of the system, producing a better potency that far beyond the K_D of the compounds [81]. Co-crystal structures revealed that one of the cyclen binding sites is located between loop 7, loop 9, and helix 5 (site 4) [82]. Although interesting, metal-bound cyclen is not a drug-like molecule and not a good starting point for the discovery of a useful pharmaceutical agent.

In addition to small molecules, peptide-based compounds have also been discovered that bind to Ras. For example, Patgiri and co-workers designed a synthetic HBS3 peptide (Figure 10,

compound **5**) as an orthosteric inhibitor that disrupts the SOS-Ras interaction and inhibits SOS-mediated nucleotide exchange [83]. The α H helix of SOS is known to be a key structural element in the SOS-mediated nucleotide exchange of Ras. Compound **5**, a peptidyl mimetic of SOS α H, binds to nucleotide-free Ras with a K_D of 28 μ M and to GDP-bound Ras with a K_D of 158 μ M. An NMR mapping study indicated that this peptide binds between site 1 and site 2, which is close to the nucleotide-binding pocket, supporting the prediction that this peptide can act as a direct mimic of the α H helix in SOS.

Efforts to target K-Ras directly at the nucleotide binding site have faced difficulties owing to its picomolar affinity for GTP/GDP [84] and the absence of known allosteric regulatory sites. However, a special oncogenic Ras mutant, G12C, which is the most prevalent (25%) K-Ras mutation in lung cancers [85], has been targeted using irreversible inhibitors due to the reactivity of the Cys-12. As shown in Figure 11A, an electrophile was attached to the GDP to react with Cys-12 [86]. Biochemical and biophysical measurements suggest that the Ras protein covalently modified by this compound was locked in the inactive state and no longer functional [87].

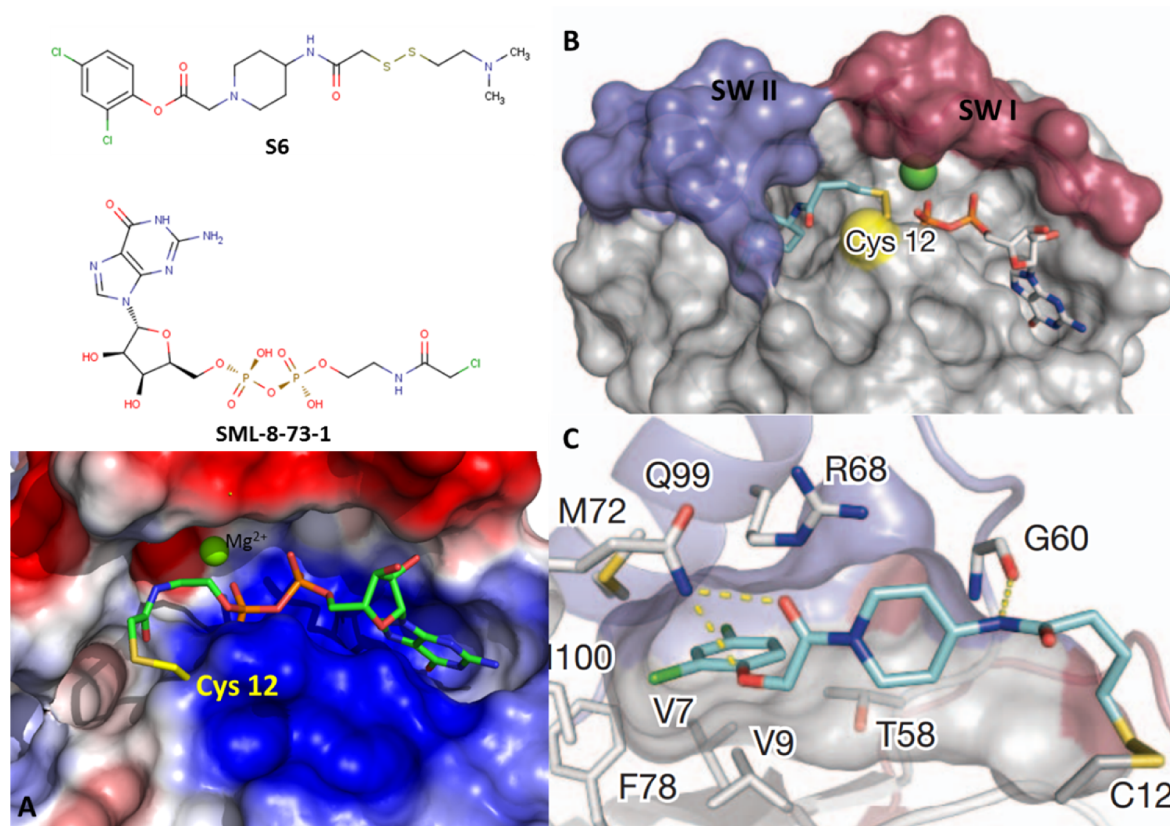


Figure 11. Targeting K-Ras (G12C) by covalently attach a compound to the Cys-12. (A) An electrophile was added on GDP (**SML-8-73-1**) to covalently react with Cys-12. (B) Co-crystal structure of compound **S6** (cyan) and K-Ras (G12C) with GDP (grey). **S6** binds under a flexible loop of switch II (blue), interferes the nucleotide binding. (C) Surface representation of switch II around compound **S6** showing hydrogen bonds (yellow lines). Indicated residues make hydrophobic contacts with **S6**.

Although compound **SML-8-73-1** is able to prevent Ras activation, a nucleotide-like molecule will not easily penetrate the cell membrane. Recently, Ostrem et al. reported the discovery of small molecules that irreversibly bind to K-Ras (G12C) without competing with the nucleotides. In their report, they screened a library of cysteine-reactive compounds against K-Ras G12C and identified compounds that covalently attached to Cys-12 and interfere with the binding of GTP [88]. (Figure 12B, C) Different from the previous work, these compounds bind to a pocket under the switch II loop (site 3). Binding of these inhibitors to K-Ras (G12C) disrupts both switch-I and switch-II, subverting the native nucleotide preference to favor GDP over GTP.

Cancer cells that carry a K-Ras G12C mutation showed a decrease in signals downstream of Ras and an increase in apoptosis upon treatment with these compounds.

The discovery of small molecule Ras ligands that modulate Ras signaling is encouraging and suggests that it may be possible to obtain therapeutic agents that directly targeting the Ras protein. However, most of these compounds are weak inhibitors with only micromolar to millimolar affinities. The absence of structural information limits their ability from being further improved. In addition, most of them do not possess the drug-like properties necessary to serve as a useful *in vivo* tool or a potential therapeutic agent. The most promising study so far is the discovery of the irreversible inhibitor against G12C mutant of Ras. However, the G12C mutation only occurs in 2% of human cancers, which significantly limits the application of this strategy [89]. In addition, irreversible inhibitors usually suffer from low specificity and high toxicity [90]. Clearly, a significant amount of work will be necessary to optimize these lead compounds for *in vivo* efficacy and other pharmaceutical properties.

Targeting Ras signaling

Because of the pivotal role of K-Ras in oncogenesis, various approaches have been developed to target Ras signaling. These approaches include targeting upstream regulators, downstream effectors, and post-translational modifications of Ras.

Efforts in targeting proteins upstream and downstream of Ras have been mainly focused on the Raf-MEK-MAPK and PI3K-Akt-mTOR pathways. The Ras-Raf-MEK-MAPK pathway features several oncogenes and is deregulated in approximately 30% of all human cancers. It has emerged as a prime target for anti-cancer therapy [91]. Inhibitors targeting upstream of Ras including EGFR, VEGFR, Her-2 and bcr-abl have been successful in clinical trials and many of

them are already in the market [92]. Targeting the downstream effectors including the kinases C-Raf, B-Raf, MEK and mTOR has also been an active area of high interest with demonstrated efficacy in clinical trials [93-96].

Although inhibitors of Raf kinase have shown clinical benefit for the treatment of B-Raf mutant metastatic melanoma, they only have limited efficacy in Ras mutant tumors [97]. Resistance has been observed upon prolonged treatment with B-Raf inhibitors, which would be the outcome of N-Ras activating mutations [98]. In addition, Raf kinase inhibitors can lead to paradoxical activation of the MAPK pathway in Ras mutant tumor cells [99, 100]. All these pitfalls may limit the use of Raf inhibitors in the treatment of Ras-driven cancers. MEK inhibitors effectively block the Ras-MAPK pathway, but often activate the PI3K pathway, and have shown little clinical benefit in Ras mutant tumors as single agents. This activation is mediated by receptor tyrosine kinases through relief of a negative feedback loop from MAPK to SOS [101, 102]. Similarly, targeting the PI3K pathway also has problems, particularly against cancers with Ras mutations. Current data suggest that Ras mutant tumors are insensitive to single-agent PI3K inhibitors [97].

While all these approaches show promising anti-tumor activity, none of the therapeutic agents has shown convincing efficacy against oncogenic K-Ras signaling. Therefore, other strategies are focused on directly interfering with Ras functions.

Ras is recruited to the cytoplasmic membrane where it exerts signaling activity. A cascade of post-translational modifications on Ras, including the linkage of a farnesyl group to the C-terminal CAAX sequence, regulates the membrane localization of Ras. Inhibition of the K-Ras activity has been attempted by blocking this process with farnesyltransferase inhibitors (FTIs, Figure 12, compound **9** and **10**) or geranylgeranyltransferase inhibitors (GGTIs).

However, treatment with FTIs alone was ineffective against Ras-induced cancers [103, 104] due to the compensatory mechanism of geranylgeranylation [105, 106]. Moreover, the combination treatment of FTIs and GGTIs resulted in very high toxicity. Developing inhibitors against “post-prenylation” processing enzymes, such as RCE1 and ICMT [107] has also been attempted. However, like farnesyl transferases, these enzymes have many substrates besides Ras and are expected to provide low safety margins. Most of these inhibitors displayed low efficacy and high toxicity, and eventually failed in clinical trials.

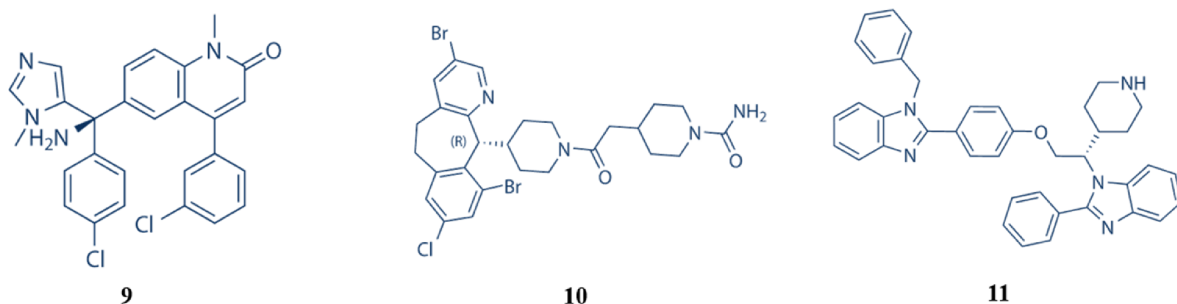


Figure 12. Inhibitors affect Ras post-translational modifications and localization. **9.** Tipifarnib, **10.** Lonafarnib, **11.** Deltarasin

Recently, a new way to interfere with the membrane localization of Ras was attempted by inhibiting the K-Ras/PDE δ interaction [108]. PDE δ is the chaperone that regulates trafficking of farnesylated and non-palmitoylatable K-Ras in cells, maintains the spatial organization and activity of K-Ras, and facilitates selective K-Ras localization at the plasma membrane [109-111]. Zimmermann and co-workers identified small molecules that bind to the farnesyl-binding pocket of PDE δ in a high-throughput Alpha screen. Guided by crystal structures, they linked two compounds together to produce the inhibitor Deltarasin that has low nanomolar affinity to the PDE δ . (Figure 12, compound **11**) The lead compounds inhibited Ras signaling *in vitro* and *in vivo* and suppressed K-Ras-dependent tumor cell growth. However, although this compound is

very potent, it also suffers from potential side effects, since PDE δ is responsible for shuttling other GTPases [110, 112, 113].

Fragment-based drug discovery

Proteins that exert their functions through protein-protein interactions are generally considered to be “undruggable” or at least very challenging to drug. The surface of such interactions are relatively flat and do not contain binding pockets for small molecules. A perfect example of such a protein is Ras. Although Ras falls into this “undruggable” category, Ras, along with many other “undruggable” proteins, are critical in human diseases and represents an attractive drug target.

The emerging application of fragment-based methods and structure-based design provide a very promising way to discover small molecules that can inhibit such protein-protein interactions. For the past 20 years, fragment-based drug design (FBDD) has been shown to be an attractive and productive route for *de novo* drug discovery. Two successful applications of FBDD are represented by the discovery of Bcl-2 family inhibitors such as ABT-737 [114] and B-Raf inhibitor Vemurafenib [115].

“Fragments” are defined as small molecules with molecular weight under 300 Daltons. Fragment-based screens typically employ a library containing hundreds or thousands of small molecules to screen a biological target. The basic strategy of this approach is to identify small chemical fragments, which may only bind weakly to the target, and then grow or link them to produce a lead compound with higher affinity. The binding affinity of a linked compound is, in

principle, the product of the binding constants of the individual fragments plus a term that accounts for the changes in binding affinity that are due to linking [116]. (Figure 13)

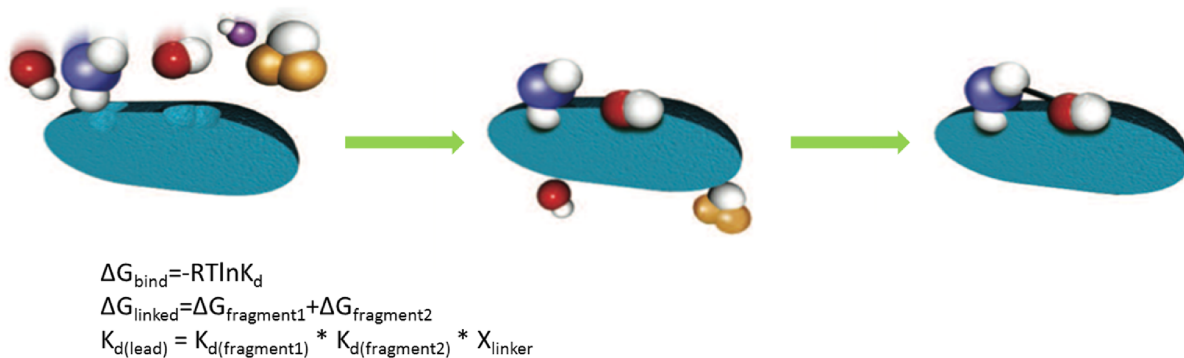


Figure 13. Linking strategy in the fragment-based drug discovery.

Compared to traditional high-throughput screening, FBDD has several advantages. Fragment-based screening can cover a large chemical space with a relatively small library [116-118]. In theory, for a protein with two independent binding sites, a compound collection containing 10^4 fragments represents a virtual library of more than 10^8 “full-size” molecules.

The hits from the fragment-based screen usually have more chemical diversity and better ligand efficiency than the molecules identified through conventional methods. These advantages may be useful in discovering lead compounds with higher potency and better pharmaceutical properties (Lower molecular weight, better pharmacokinetics, lower toxicity). Furthermore, FBDD can be much more efficient than other approaches because a certain group of fragment hits can be selected that target only a specific binding site (eg. the binding site for a critical ligand) rather than a distribution across the entire protein.

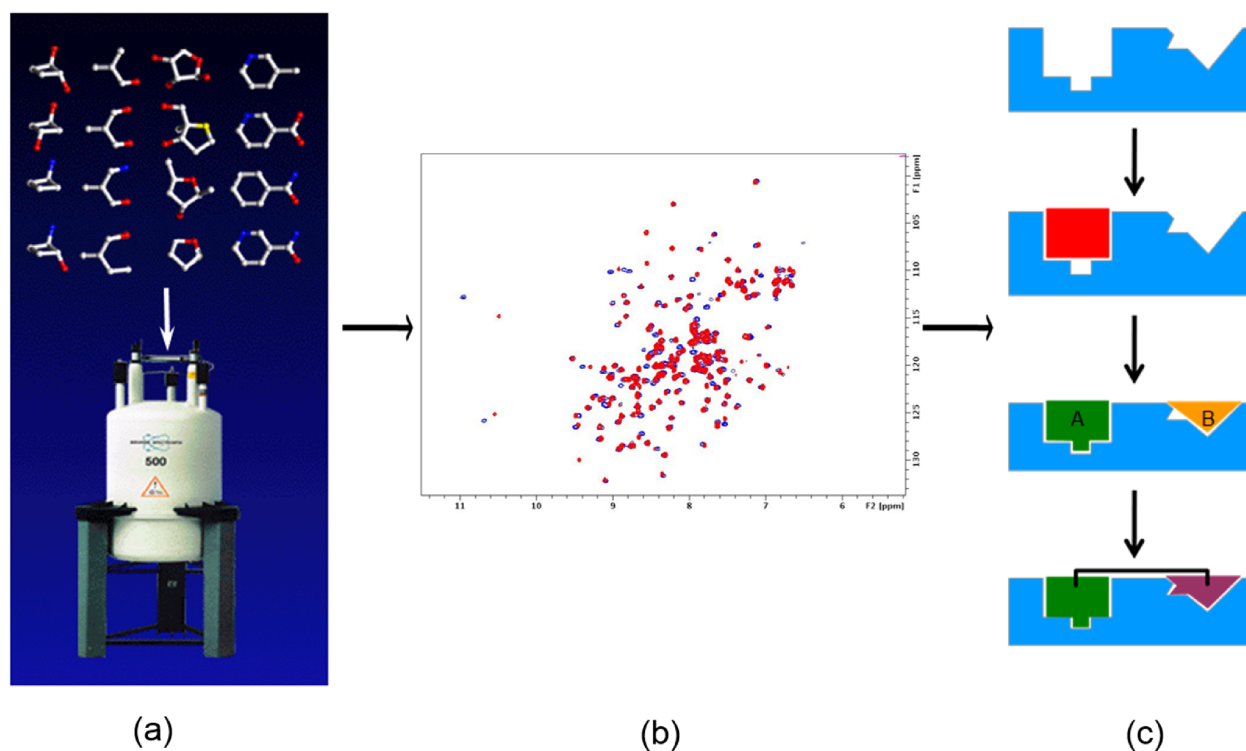


Figure 14. SAR by NMR. NMR spectroscopy is used to reliably measure the weakly bound compound (a). The target protein is expressed in uniformly ^{15}N labeled form to produce an HSQC spectrum (b, blue), and then we can follow chemical shift changes of protein signals upon addition of a potential ligand (b, red). Once we identified ligands that binds to one site, we will then screen in the present of this first-site ligand for potential second-site ligands that bind nearby, with the ideas that we would ultimately like to link them together (c).

NMR-based fragment screening methodologies were pioneered by Fesik and coworkers at Abbott [116]. The method has been widely used in the identification of lead small molecules for a number of protein targets, including those previously considered to be undruggable. Among all other approaches, NMR spectroscopy appears to be the best method for detecting weakly bound compounds reliably. In addition, the NMR technique usually does not suffer as much from false-positives, which is common using other screening techniques. Furthermore, protein-based NMR screening also provides valuable information about the location of the binding sites, which could be advantageous for structure-guided ligand design. For small proteins, two-dimensional heteronuclear single quantum correlation (HSQC) experiments performed on uniformly ^{15}N -

labeled protein generates a two-dimensional spectrum consisting of a unique peak for each proton connected to a nitrogen atom to create a characteristic pattern of signals for each protein. (Figure 14) Consequently, $^1\text{H}/^{15}\text{N}$ HSQC spectra sensitively monitors the ligand binding, and the ligand-induced changes in chemical shift that occur yield information on the probable binding site. This method requires no prior knowledge of protein function and can robustly detect low affinity (millimolar range) ligand-protein interactions. Adaptation to an automated format allows the screening of large numbers of small molecules in a relatively short time. Previous studies have also shown that using NMR to detect the binding of small molecules (Molecular Weight ≤ 300 Da) using a “fragment library” provides a reliable method to determine a target’s druggability. Indeed, a high correlation was observed between the hit rate obtained in NMR-based screens and the ability to identify high-affinity protein inhibitors [119]. Thus, NMR-based experimental screening data can be used to assess druggability, and proteins with hit rates $>0.1\%$ using this approach can be considered to be druggable targets.

Scope of the Dissertation

In the following chapters of my dissertation, I describe my effort to target Ras with the ultimate goal of discovering a small molecule that is useful for treating Ras-driven tumors.

In chapter II, I describe a fragment-based screen which was used to identify small molecules that bind directly to Ras [120]. As a first step for the screen, I expressed and purified a large amount of K-Ras. Then, using GDP-bound K-Ras (G12D), I screened a fragment library of 11,000 compounds by NMR and identified approximately 140 hits. Several structures of K-Ras/ligand complexes were obtained and revealed a new binding pocket located between the $\alpha 2$ helix of switch II and the central β sheet. This new binding pocket is created by a conformational change in the switch II region. This binding site has not been previously observed in the ligand-free Ras structures. Based on the structures of protein-ligand complexes, new analogs were designed and synthesized. Some of these fragment analogs had improved binding affinities and were found to inhibit SOS-mediated nucleotide exchange of K-Ras in a nucleotide exchange assay.

In chapter III, I describe our attempts to conduct a second-site screen to obtain better affinity ligands [121]. In our first attempt, we used conventional methods to identify second-site ligands. However, we experienced difficulties due to our inability to saturate the first site. To solve this problem, we developed an approach that involves covalently attaching a first-site ligand to a cysteine residue near the binding pocket to saturate the primary binding pocket. Using this approach, we obtained a K-Ras mutant (S39C) with its first-site pocket blocked by a covalently attached molecule, which is suitable for the second-site screen. Using this mutant, we conducted the second-site screen and identified several hits. Crystal structures of some of these

hits complexed to K-Ras S39C were obtained and revealed a new binding pocket near the guanine nucleotide. Unfortunately, the newly identified hits were too far to link to our first site ligands. Using molecular modeling, we pursued several alternative strategies, which include developing a covalent inhibitor by extending the new ligands to reach Cys-12 in an oncogenic K-Ras (G12C) mutant.

In chapter IV, I describe an alternative approach to target Ras using nucleotide exchange activators [122]. During the fragment-based screen of K-Ras, we found that some of the hits activate SOS-mediated nucleotide exchange rather than inhibiting it. By conducting an HTS screen using a nucleotide exchange assay, we identified additional compounds that had this activity. Although structurally distinct from the fragment hits, they are also able to activate SOS-mediated nucleotide exchange. To determine the molecular mechanism of this interesting phenomena, I, along with another graduate student, Michael Burns, followed up on these molecules. I determined ligand-bound Ras:SOS:Ras ternary complex structures using X-ray crystallography, which revealed that the activators bind to a novel pocket on the CDC25 domain of SOS near the Ras-SOS binding interface. Experiments using mutations of the residues inside this pocket confirmed the functional relevance of this binding site. Guided by the crystal structures, we were able to improve the potency of these compounds using a mix and match strategy. Interestingly, these activators paradoxically downregulate Ras downstream pathways, including the Raf-MEK-MAPK and PI3K-AKT pathways. The cellular mechanism of this paradoxical inhibition is currently under investigation. These activators may serve as a new approach to target the Ras pathway.

Finally, in the last chapter, I summarize all my results and discuss the potential limitations of this work, as well as offer new thoughts on how our mission might be achieved.

CHAPTER II

IDENTIFICATION OF SMALL MOLECULES THAT BIND TO RAS

Introduction

K-Ras inhibition represents an attractive therapeutic strategy for many cancers. The primary objective of my work was to discover potent small molecule inhibitors that bind to GDP-bound K-Ras that could prevent Ras from binding to SOS. This could stabilize the K-Ras protein in the GDP-bound form. An important concern is that Ras activation and signaling is accomplished primarily through protein-protein interactions. Such protein interfaces typically lack well-defined binding pockets and have been difficult to target with small molecules.[59] Although the detailed structural information is missing, previous reports identified small molecules that bind to K-Ras and block its functions. In addition, computational approaches have predicted a number of hydrophobic binding pockets.

Using state-of-the-art fragment-based methods, I have identified inhibitors against K-Ras and successfully improved their affinities by structure-based design. These inhibitors disrupt the Ras-SOS interaction and inhibit SOS-mediated nucleotide exchange of K-Ras.

(This Chapter is adapted from Sun et al. [120])

Results

Protein Purification

To conduct a fragment-based screen, a large amount of ^{15}N -labeled protein is needed. Although H-Ras can be easily expressed as described in previous studies, H-Ras is not a good cancer target. As a first attempt to express K-Ras alone, we obtained insoluble protein. To solve this problem, we expressed K-Ras as a His₆-MBP (Maltose-binding protein)-tagged fusion protein to increase its solubility. We engineered a linker between MBP and Ras that contains a TEV (tobacco etch virus) protease cleavage sequence. After the first nickel column, MBP was cleaved off by TEV protease, and the cleaved products were subjected to a second, subtractive nickel column with K-Ras protein collected in the flowthrough. (Figure 15) The $^1\text{H}/^{15}\text{N}$ HSQC spectrum confirmed that the protein was folded, and the sample prepared in this way was suitable for NMR-based screening. (Figure 16)

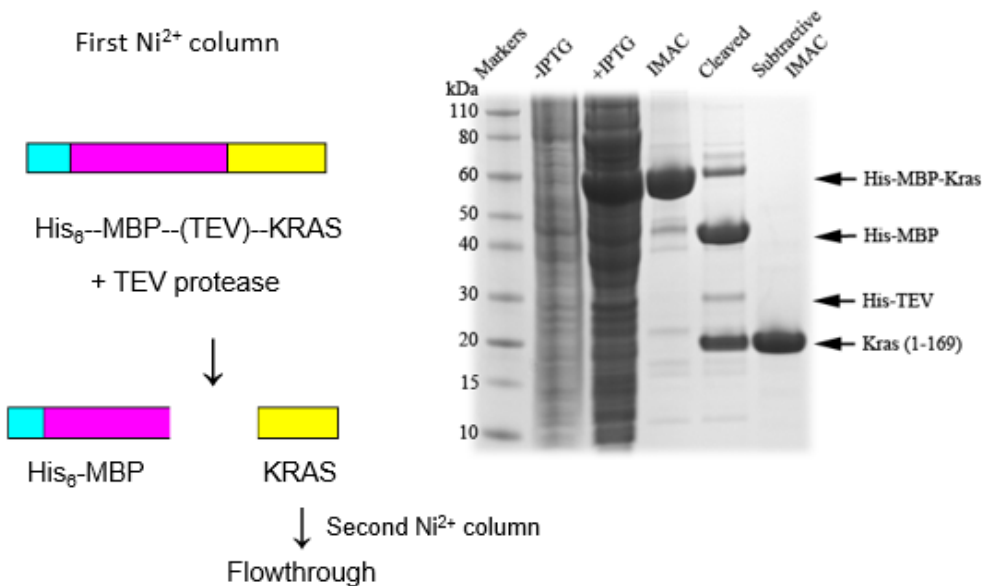


Figure 15. Expression of K-Ras as an MBP fusion protein.

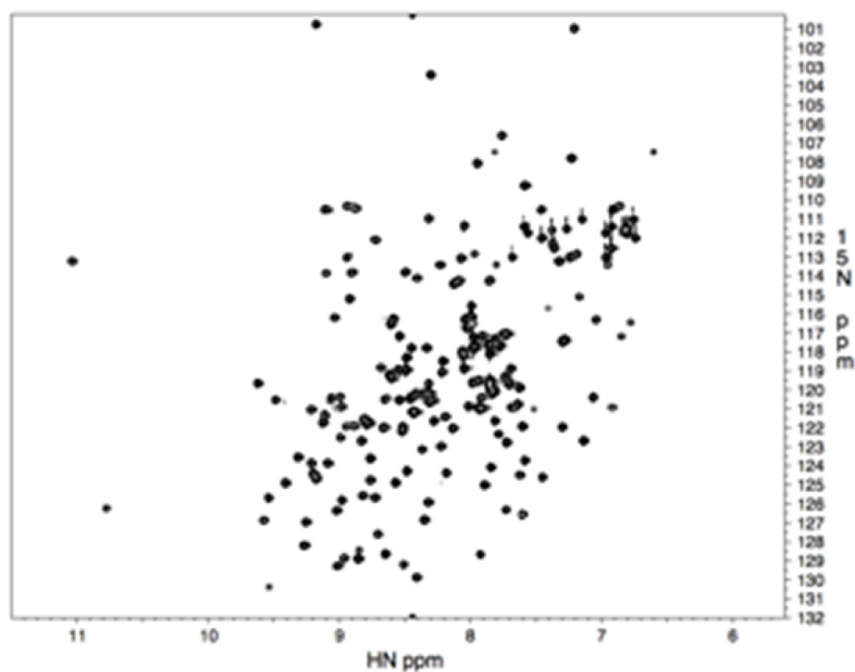


Figure 16. $^1\text{H}/^{15}\text{N}$ HSQC spectrum of GDP-bound K-Ras (G12D).

The Ras proteins purified from *E. coli* are primarily in the GDP-bound form due to its intrinsic GTPase activity. To produce Ras-GTP, an excess amount of non-hydrolyzable GTP analogs, 5'-Guanylyl imidodiphosphate (GppNHp) or Guanosine 5'-O-[gamma-thio]triphosphate ($\text{GTP}\gamma\text{S}$) are added to the Ras protein in the present of EDTA and apyrase. There are dramatic differences in $^1\text{H}/^{15}\text{N}$ HSQC spectra between GDP- and GppNHp-bound K-Ras, indicating major conformational changes upon nucleotide exchange.

Fragment Screening by NMR

We decided to use the K-Ras G12D mutant because of its high prevalence in pancreatic cancer. I screened a fragment library containing 11,000 compounds and followed the chemical shift changes of uniformly ^{15}N -labeled protein upon the addition of the compounds. Top-rated hits were titrated, and binding constants were obtained. By adding an increasing amount of the compound to the protein, we can fit the chemical shift changes into a titration curve to calculate the binding affinities [123]. (Figure 18B). From the initial screen, we identified over 140 fragments that bind to GDP-K-Ras with K_{d} s from $\sim 300\ \mu\text{M}$ to 2 mM. (hit rate=1.3%) Multiple chemotypes were discovered. (Figure 17) A complete list of the hits identified is attached in Appendix A.

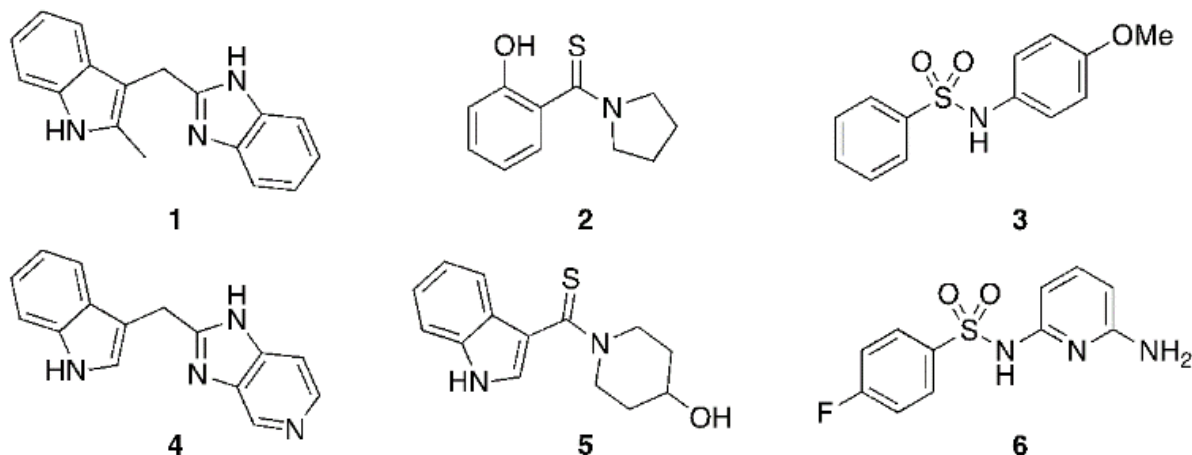


Figure 17. Multiple chemotypes were identified in the fragment-based screen, including indoles (1), phenols (2), and sulfonamides (3). Analogs of these compounds (4, 5, 6) were synthesized to increase their water solubility and binding affinity.

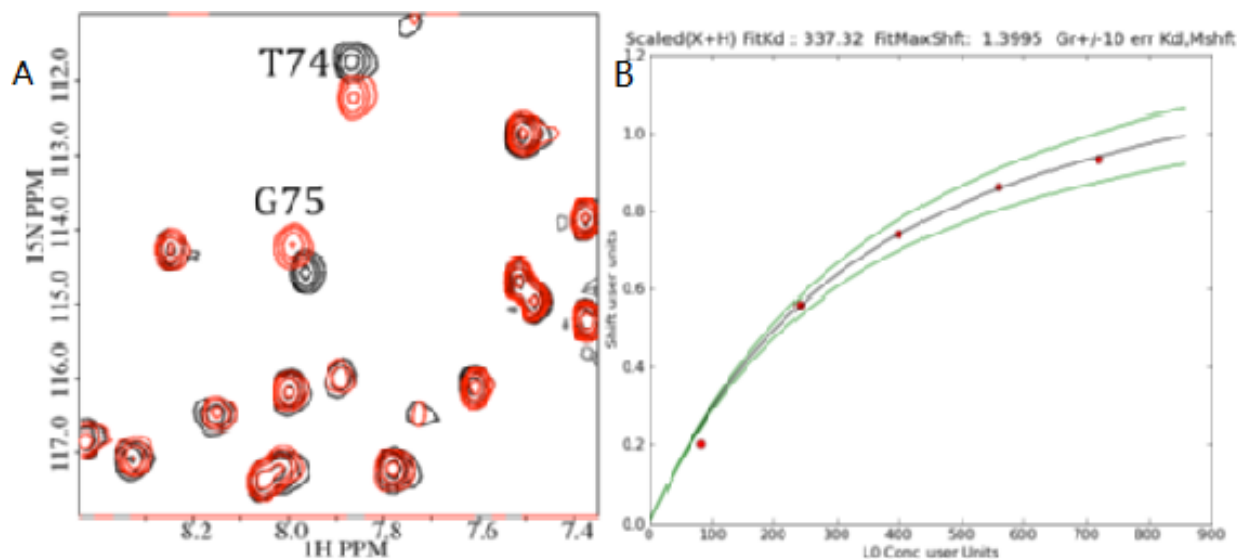


Figure 18. Chemical shift perturbation by a fragment hit and K_D measurement. (A) $^1\text{H}/^{15}\text{N}$ resonance shift for T74 and G75 of GDP-bound K-Ras G12D. (B) Titration curve of one fragment hit for binding to K-Ras.

Crystal structures of small molecules bound to K-Ras

To determine how the fragment hits and analogs bind to K-Ras, we obtained X-ray co-crystal structures. Initial attempts to co-crystallize K-Ras (G12D) with these compounds failed to produce suitable crystals due to the limited number of space groups available to this mutant form of the protein. To solve this problem, we performed crystallization screens of both wild-type and G12V mutant K-Ras. Both proteins crystallized across a broad range of conditions in multiple space groups and yielded high-resolution co-crystal structures. In all, 25 co-crystal structures (A complete list of compounds co-crystallized with GDP-bound K-Ras is attached in Appendix B) were obtained thus far. The compounds occupy a hydrophobic pocket located between the $\alpha 2$ helix of switch II (60-74) and the central β sheet of the protein. This site was described as site 2 in the previous chapter. Figure 19A depicts a high-resolution structure of **4**, an analog of a screening hit (**1**), complexed to the GDP-bound form of wild-type K-Ras. The indole of **4** binds into a hydrophobic pocket formed by Val-7, Leu-56, and Tyr-71, as well as the aliphatic portion

of the side chains of Lys-5 and Thr-74. The imidazopyridine portion of the molecule lies flat in an adjacent binding cleft formed on one side by the side-chain of Tyr-71. The nitrogen at the 1-position of the imidazopyridine is involved in a water-mediated interaction with Ser-39, and the indole NH group forms a hydrogen bond with Asp-54. Another member of the indole series (**5**) uses a thiocarbonyl instead of a methylene linker to access the secondary binding cleft. The binding mode of the indole moiety in this instance is rotated towards the $\alpha 2$ helix and the switch II loop region, forming a hydrogen bond with Ser-39 instead of Asp-54 which positions the piperidine ring closer to the helix (Figure 19B). In addition to an indole, a phenol moiety is also able to bind into this hydrophobic pocket, as demonstrated by the X-ray structure of compound 2 bound to K-Ras (Figure 19C). The hydroxyl group of the phenol forms a hydrogen bond with Asp-54 while the pyrrolidine moiety forms stacking interactions with Tyr-71. The binding mode of a member of the sulfonamides series is shown in Figure 19D. The pyridine nitrogen of **6** forms three water-mediated hydrogen bonds to Asp-54, Arg-41 and Ser-39, and the ortho amino group interacts with the Asp-54 side chain and a backbone carbonyl. From these structures, it appears that a hydrogen bond donor, such as the -NH on the indole or the -OH on the phenol is necessary for binding. This is supported by the lack of binding of analogs containing substituents at these positions that occlude hydrogen bond formation.

Analysis of the ligand-protein co-crystal structures reveal that all the compounds bind to a pocket that is not readily observed in the ligand-free form (Figure 20A) but in an "open" form of the protein (Figure 20B). The pocket is created by a conformational change (Figure 20C) in which the $\alpha 2$ helix moves away from the central β sheet, and the side chain of Tyr-71 breaks the hydrogen bond network present in the ligand-free form. In addition, the side chain of Met-67 rotates out of the way to form a secondary binding cleft. This conformational change creates a

new binding site for small molecules that is not present in the “closed” form. In subsequent X-ray structures obtained of ligand free K-Ras under different experimental conditions as well as recently published molecular dynamics simulations, the “open” form has been observed, suggesting that the “open” and “closed” conformations are present in equilibrium.

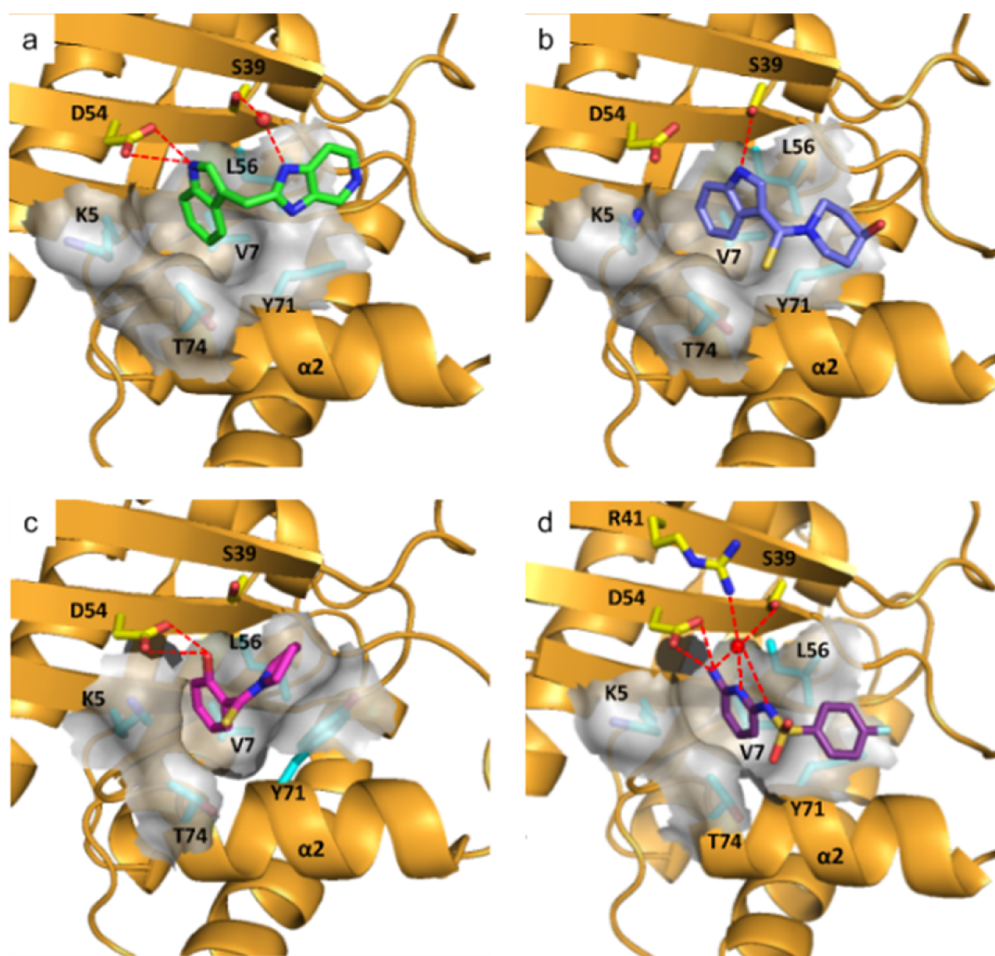


Figure 19. Co-crystal structures of GDP-K-Ras complexed to small molecules. Ribbon and molecular surface representations of the X-ray co-crystal structures of GDP-K-Ras complexed to: a) 4,(PDB 4EPV) b) 5, (PDB 4EPW) c) 2, (PDB 4EPT) and d) 6. (PDB 4EPX)

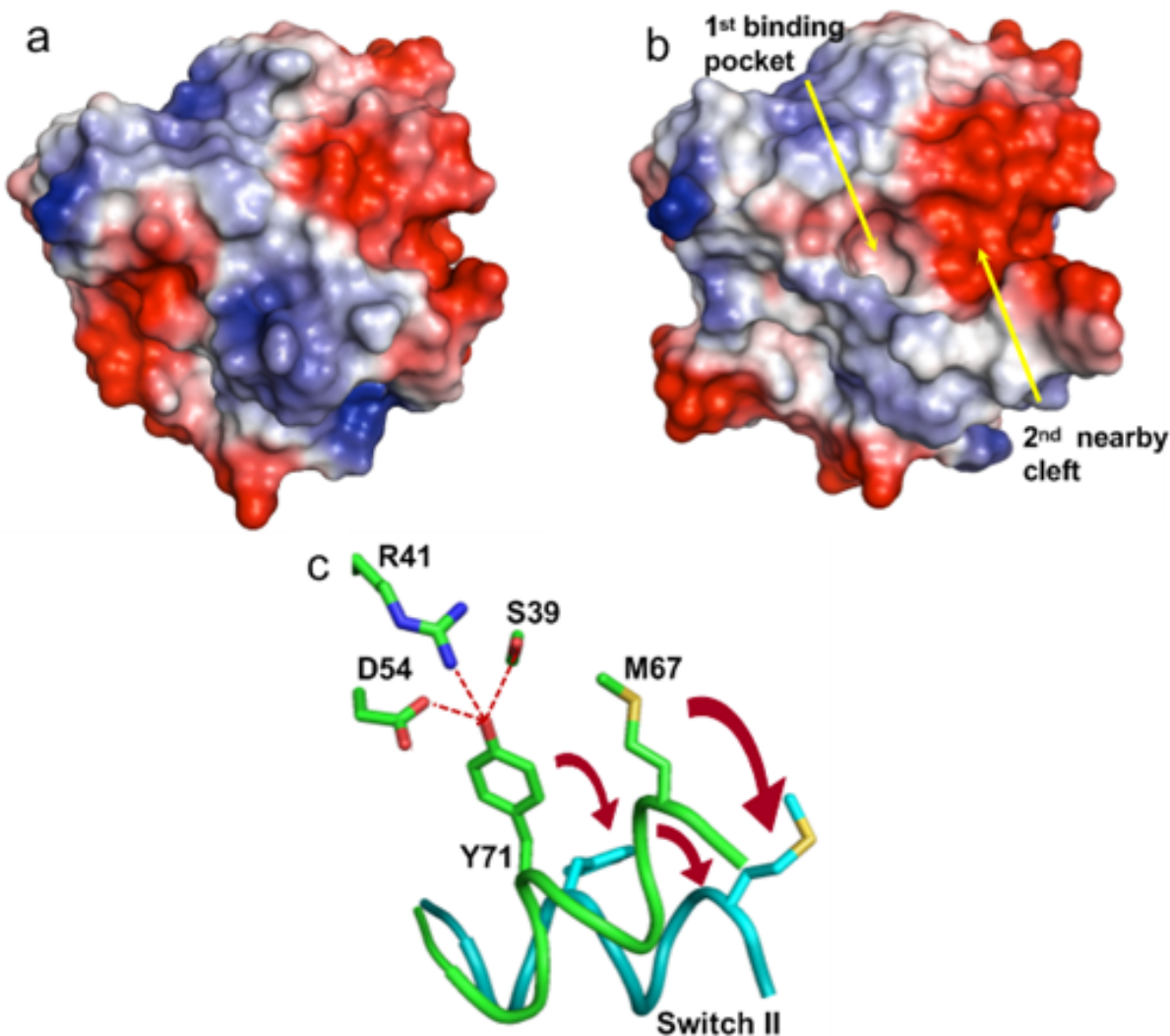
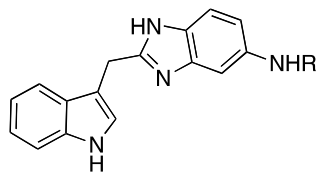


Figure 20. Conformational changes between ligand-free and ligand-bound K-Ras. Electrostatic surface representations of GDP-bound K-Ras a) in the absence of a ligand and b) in the “open” form showing the primary hydrophobic binding pocket and the adjacent electronegative cleft. c) Schematic representation of the transition of GDP-bound K-Ras from the “closed” form (green) to the “open” form (cyan).

Compound optimization and structure-based design

The secondary binding cleft is electronegative in character (Figure 20B) and contains two acidic residues, Glu-37 and Asp-38. To bind to this region of the protein, we synthesized amide-linked amino acid analogs of the indole-benzimidazole fragment containing positively charged amines (Table 1). Improved binding to K-Ras was observed for several of these analogs. The

best compound in this series contains an isoleucine (**12**) which binds to K-Ras with an affinity of 190 μM , an improvement of roughly 10 fold over the unsubstituted compound **7**.



Cmpd	R	K_D (μM)	%Inh.
7	-H	~ 1300	no inh.
8	-Gly	420	27 ± 9
9	-Ala	350	51 ± 4
10	$-\beta$ -Ala	340	32 ± 10
11	-Val	240	73 ± 12
12	-Ile	190	78 ± 8
13	-Pro	340	58 ± 8

Table 1. Compound binding affinity with GDP K-Ras (G12D) measured by HSQC titration and functional activity in a SOS-mediated nucleotide exchange assay.

We were able to obtain a high-resolution X-ray co-crystal structure of one of these analogs (**13**) complexed to GDP-bound K-Ras (G12V). (Figure 21) As designed, the indole is located in the primary binding pocket, and the positively charged amino group of the amino acid interacts with the carboxylic acid side chain of Asp-38 in the secondary binding cleft.

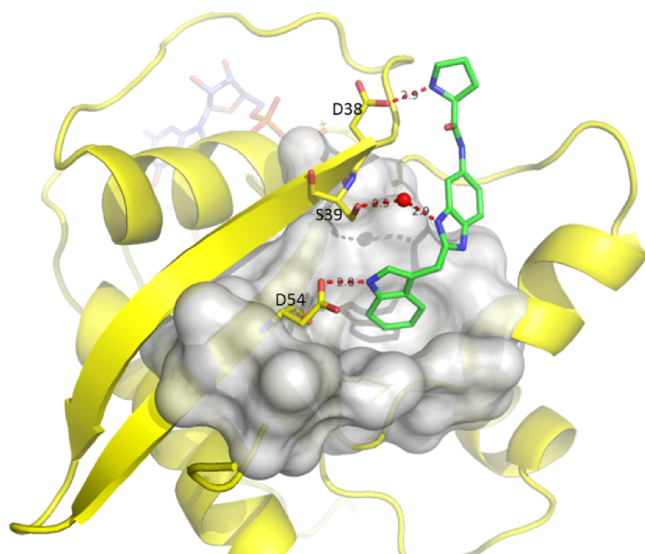


Figure 21. Ribbon and molecular surface representations of GDP-bound K-Ras complexed to **13**. Interactions are labeled in red dashed lines.

Compounds block nucleotide exchange

To examine the functional consequences of binding to K-Ras, compounds were tested for their ability to inhibit Sos-mediated nucleotide exchange. (Figure 22) In this assay, unlabeled GDP is exchanged for BODIPY-GTP which is catalyzed by Sos and results in an increase in fluorescence [83]. As shown in Table 1, the extended analogs with binding affinity $<500 \mu\text{M}$ inhibited the nucleotide exchange process at a concentration of 1 mM. For example, an analog containing an isoleucine (**12**) inhibited nucleotide exchange at 78% (Table 1)

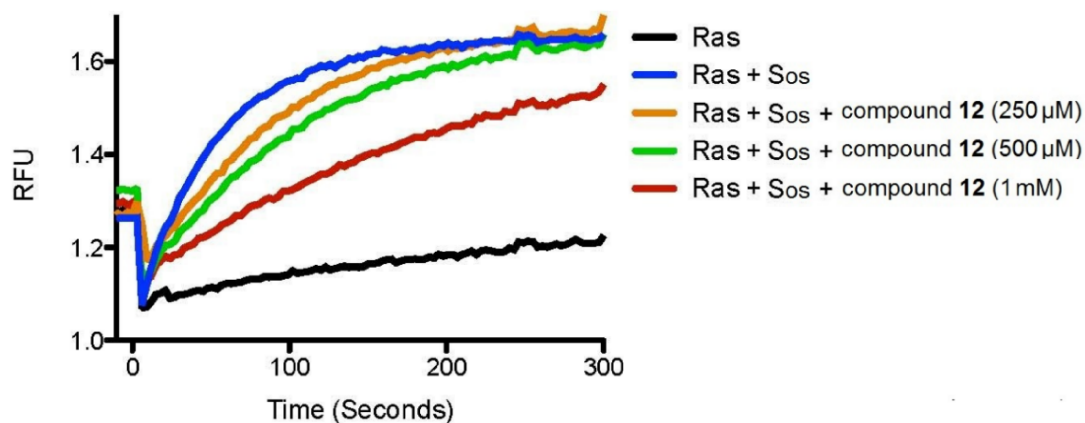


Figure 22. Effect of compound **12** on SOS-mediated K-Ras activation. Comparison of intrinsic (black) and SOS-mediated nucleotide exchange in the absence (blue) or presence of increasing concentration of compound **12**. Exchange assays were performed by addition 1 μM K-Ras (G12D) to a mixture containing 1 μM Sos, 1 μM BODIPY-GTP, and 250 μM (orange), 500 μM (green), or 1 mM (red), respectively.

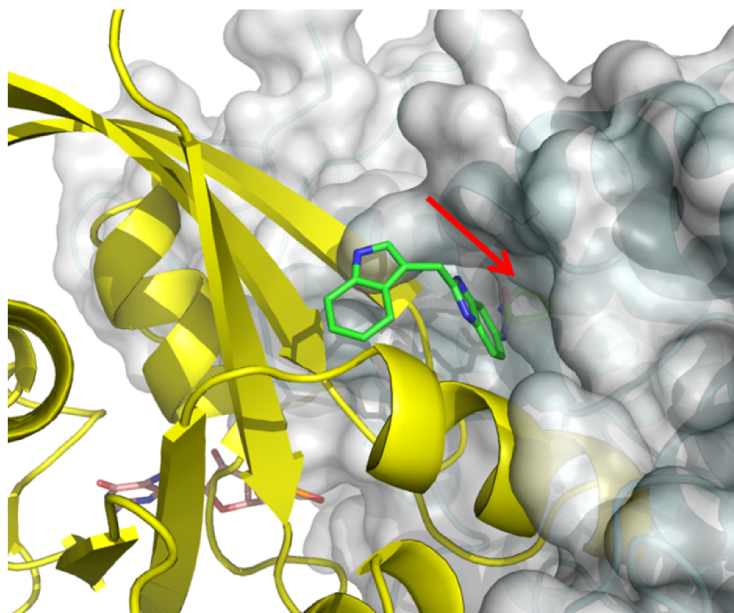
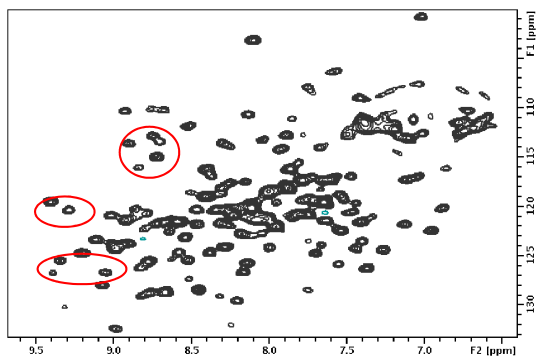


Figure 23. K-Ras/**13** X-ray structure overlaid with a previously reported Ras-Sos complex crystal structure (PDB entry: 1BKD). The proline moiety (red arrow) of the compound **13** is clashing with SOS (grey surface).

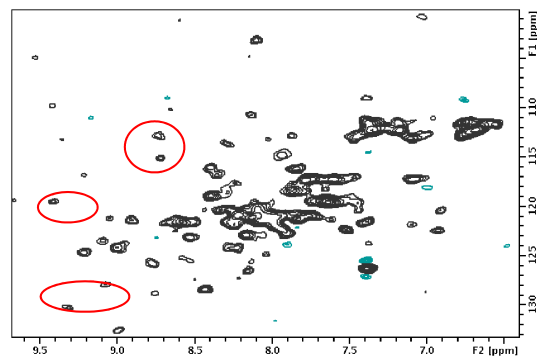
The inhibition of Sos-mediated nucleotide exchange that we observe can be rationalized from a model prepared by overlaying the X-ray structure of the K-Ras/**13** complex (Figure 23)

onto a previously reported structure of H-Ras complexed with Sos [14]. The amino acid portion of **13** clashes with α H of Sos. The model predicts that Sos would not be able to bind to K-Ras when complexed to a small molecule that extends into this space (e.g., **8-13**).

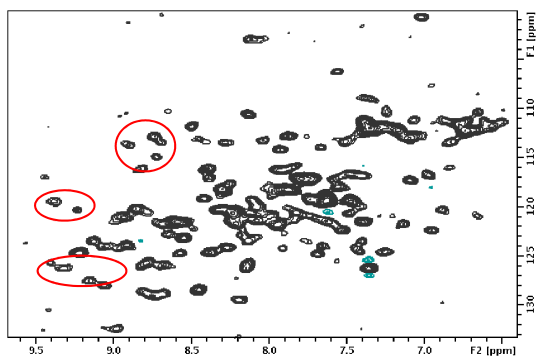
A. [U-¹⁵N] K-Ras



B. [U-¹⁵N] K-Ras / SOS



C. [U-¹⁵N] K-Ras / SOS / Compound **13**



D. [U-¹⁵N] K-Ras / Compound **13**

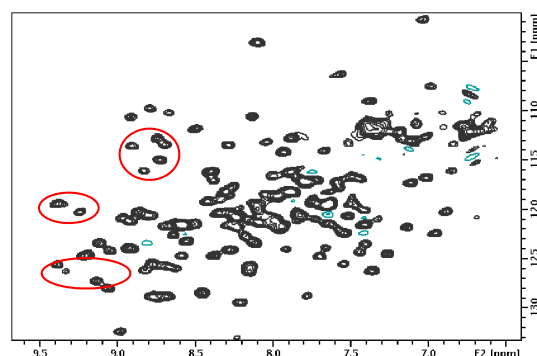


Figure 24. HSQC spectra of GDP-K-Ras (G12D) w/ and w/o SOS and compound **13**. ¹H-¹⁵N HSQC spectra of uniformly ¹⁵N-labeled GDP-bound K-Ras (G12D) with and without SOS and compound **13**. A). [U-¹⁵N] K-Ras (50 μM). B). [U-¹⁵N] K-Ras (50 μM) / SOS (200 μM). C). [U-¹⁵N] K-Ras (50 μM) / SOS (200 μM) / Compound **13** (4 mM). D). [U-¹⁵N] K-Ras (50 μM) / Compound **13** (1 mM). Addition of an excess of SOS causes K-Ras resonance peaks to shift, broaden, and disappear when compared to K-Ras alone (A vs. B). Addition of compound **13** to the K-Ras/SOS complex causes peaks to reappear (C) which results in a spectrum similar to that obtained for the K-Ras/Compound **13** complex (D).

This model is supported by NMR experiments in which the $^1\text{H}/^{15}\text{N}$ HSQC spectrum of ^{15}N -labeled K-Ras (G12D) when complexed to unlabeled Sos dramatically changes upon the addition of compound **13**. This new spectrum resembles that of the K-Ras/**13** complex without SOS. (Figure 24) Furthermore, in the absence of K-Ras, compound **13** does not bind to SOS, and an analog of **13** with the indole moiety N-methylated does not bind to K-Ras and does not inhibit Sos-mediated nucleotide exchange.

Discussion and Conclusion

Using a fragment-based screen, we have identified small molecules that bind to K-Ras in a hydrophobic pocket that is occupied by Tyr-71 in ligand-free Ras. A total of 25 compounds from several different chemical series have been co-crystallized with K-Ras. Guided by crystal structures, we obtained analogs of the fragment hits with improved binding affinity. The optimized analogs extend into the interface between Ras and SOS, which explains how the compounds inhibit SOS-mediated nucleotide exchange.

At the same time, a research group in Genentech published small molecules that bind to K-Ras [124]. They have identified a binding pocket on K-Ras located between α -helix 2 and β -strand 3, which is the same one as we found. (Figure 25A) Although the overall outcome is very similar, several interesting observations are worthy of discussion.

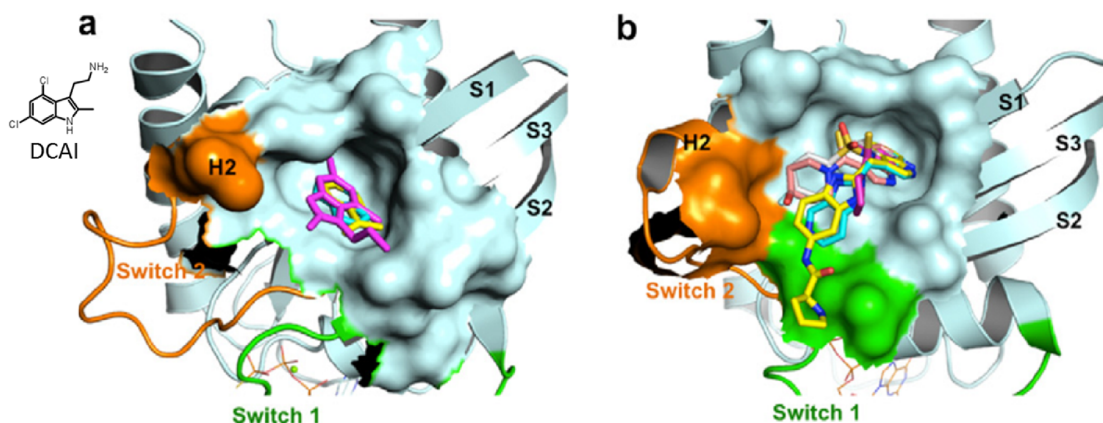


Figure 25. Ras ligand binding revealed in co-crystal structures. (This figure is adapted from Wang et al. [69]) (A) Overlay of ligand-bound K-Ras GTP γ S crystal structures determined by Maurer et al. Magenta: 4,6-dichloro-2-methyl-3-aminoethyl-indole (DCAI); cyan: benzimidazole; yellow: benzamidine. (B) Overlay of our ligand-bound K-Ras GDP crystal structures. Cyan:4; magenta:2; pink:5; white:6; yellow:13.

The binding sites for the Genentech compounds (DCAI, benzimidazole, and benzamidine) are restricted in the primary pocket. In contrast, our indole derivatives extended into a secondary binding cleft towards switch I region (site 1), which is adjacent to the Ras-effectors binding interface. If our inhibitors bind to the GTP-bound K-Ras in a similar fashion, they may be used to block the downstream effectors of Ras, such as Raf and PI3K. We attempted to determine the co-crystal structure of K-Ras-GTP with indole-based inhibitors, but did not succeed.

Interestingly, Genentech obtained a co-crystal structure of GTP-bound K-Ras with ligand bound. An overlay of three ligand-bound structures of GTP γ S (guanosine 5'-O-[gamma-thio] triphosphate, a non-hydrolyzable GTP analog)-bound K-Ras is depicted in Figure 13A. By comparing the GDP and GTP γ S -bound K-Ras crystal structures, we found that the primary binding pocket, which accommodates the indole moiety, is very similar between these two forms. More dramatic changes can be observed at the secondary binding cleft, mainly because of the movement of switch I. Specifically, the sidechain of Glu-37 of GTP γ S-bound K-Ras rotates

towards the secondary binding cleft and partially blocks this cleft. This observation is supported by the fact that most of our hits for GDP-bound K-Ras bind to GTP-bound K-Ras with lower binding affinities.

Surprisingly, DCAI does not clash directly with SOS, but still inhibits SOS-mediated nucleotide exchange. This suggests that reaching into SOS is not required for disrupting the Ras-SOS interaction. Ligand-induced conformational changes in the switch I and switch II regions may be sufficient to interfere with the Ras-SOS interaction.

Nonetheless, these studies provide the first reported examples of high-resolution ligand-bound Ras structures and reveal clear opportunities for the identification of higher affinity binders. The affinity improvement of the indole analogs demonstrated a nice example of structure-based design. These molecules represent a starting point for obtaining probe molecules that may be useful in elucidating new insights into Ras signaling and for discovering K-Ras inhibitors for the treatment of cancer. However, a significant amount of effort will be needed to achieve this goal.

Materials and Methods

Cloning, expression, and purification

The gene encoding the GTPase domain (residues 1-169) of oncogenic mutant K-Ras (G12D) was synthesized with codon optimization for *E. coli* overexpression. A C118S mutation was introduced to increase the stability of the protein during the NMR experiments and is present in all of the K-Ras proteins described here [125]. The expression construct was designed to

include the tobacco etch viral protease (TEV) recognition sequence at the 5' end [126]. This construct was inserted into a donor vector (pDONR-221) and transferred by recombinational cloning into the pDEST-HisMBP vector for expressing a fusion protein. The K-Ras protein was expressed in Rosetta 2 (DE3) E.coli strain by induction with 1 mM IPTG at a cell density corresponding to an absorbance of $OD_{600}=1.0$. Isotopically-labeled K-Ras was prepared in M9 minimal media containing 1.0 g/L $^{15}NH_4Cl$. The fusion protein was purified on a Ni-IDA (ProBond from Invitrogen) column. TEV protease was added at a 1:20 molar ratio, and the solution was incubated at 4°C overnight. The reaction mixture was applied to a Ni-NTA column, and the K-Ras protein was collected in the flow through and exchanged into a low salt buffer. Wild-type K-Ras and other K-Ras mutants were expressed and purified in a similar fashion. The catalytic domain of human Sos (residues 564-1049) was inserted into a donor vector (pDONR-221) and transferred by recombinational cloning into the pDEST-544 vector for expressing a His6-tagged fusion protein. The Sos protein was expressed in BL21-CodonPlus-RIL E.coli strain by induction with 0.2 mM IPTG at a cell density of $OD_{600}=1.0$. The protein was expressed at 18°C overnight and then was purified on a Ni-IDA (ProBond from Invitrogen) column. Purified proteins were concentrated with Amicon ultra centrifugal columns (Millipore) and flash frozen in liquid N_2 and stored at -80°C.

Fragment library

Our fragment library was built by acquiring compounds from ChemBridge, ChemDiv, and five other vendors. Compounds were chosen for purchase if they passed criteria related to the commonly used “Rule of Three” (MW ≤ 300 Da, cLogP ≤ 3.0 , no more than 3 hydrogen bond donors) [127], or no more than 4 rotatable bonds. In addition, compounds were purchased that

were known to favor binding to proteins, and compounds were synthesized in the lab to supplement this collection with molecules and ring systems that are not commercially available and/or not known in the chemical literature. All of these compounds were required to pass a filter designed to remove molecules containing reactive intermediates and functional groups that were either considered unstable, overly promiscuous, or known to cause poor solubility or other performance issues in assays.

Fragment-based screen

Compound binding was detected using two-dimensional sensitivity-enhanced $^1\text{H}/^{15}\text{N}$ -HSQC spectra collected on a Bruker DRX500 spectrometer equipped with a cryoprobe and a Bruker Sample Jet sample changer. Each sample contained 50 μM GDP-bound K-Ras (G12D) protein and 12 fragments at a concentration of 650 μM . Positive hits were deconvoluted by testing samples containing the individual ligands. All screening compound plates were generated and data tracked using the sample handling capabilities of the Vanderbilt Institute of Chemical Biology (VICB) High Throughput Screening (HTS) Core facility. Screening data were processed using Bruker TOPSPIN and analyzed by comparing spectra with and without compounds. Dissociation constants were obtained for selected compounds in fast exchange by monitoring the chemical shift changes of resonances as a function of compound concentration using standard fitting software.

Protein Crystallization

GDP-bound K-Ras (G12D/C118S, G12V/C118S or C118S) protein was exchanged into crystallization buffer (20 mM HEPES, 150 mM NaCl pH 8.0) and concentrated to 40 mg/mL.

Protein-ligand complexes were prepared by adding a concentrated DMSO stock solution of the ligand to a final ligand concentration of 10-15 mM. All crystallization experiments were set up using the Mosquito crystallization robot (TTP Labtech, Royston UK) or performed manually using either the sitting or hanging-drop vapor diffusion method at 18 °C. Apo GDP-bound K-Ras (G12D/C118S) crystallized under a condition containing 30% PEG4000, 0.1 M Tris-HCl pH 8.5, 0.2 M sodium acetate or Li₂SO₄. The K-Ras(C118S)/**2** complex was crystallized from 30% PEG8000, 0.2 M sodium acetate, 0.1 M MES pH 6.5. The K-Ras(G12V/C118S)/**5** complex was crystallized from 32% PEG1500 and 0.7% 1-butanol. Complexes containing compounds **4**, **6** and **13** crystallized from 25% PEG1500, 0.1 M MMT pH 4. Single crystals were obtained after multiple rounds of microseeding. Crystals containing compounds **4**, **6** and **13** were cryo-protected with 10% ethylene glycol for low temperature data collection.

X-ray Data Collection, Structure Solution, and Refinement

X-ray diffraction data were collected at 100K in the oscillation mode on single flash-cooled crystals using a Bruker-NoniusMicrostar rotating anode X-ray generator equipped with a Proteum PT 135 CCD area detector. The instrument is located in the Biomolecular Crystallography Facility in the Vanderbilt University Center for Structural Biology. Data were processed with HKL-2000, and structures were determined by molecular replacement using the coordinates of H-Ras G-domain (residues 1-166; PDB Entry 1AGP). The program package CCP4 [128] and Phenix [129] were employed for phasing and refinement, and model fitting was performed with COOT [130]. The refined models were validated with PROCHECK and Phenix.

Nucleotide Exchange Assay

Purified, recombinant GDP-bound K-Ras is added to a mixture of SOS and BODIPY-GTP. Bound GDP is exchanged for BODIPY-GTP, resulting in an increase in fluorescence with time. The reaction was performed as an association-dissociation experiment in which BODIPY-GTP first associates with K-Ras followed by a dissociation step in which excess unlabeled GTP outcompetes the analog returning fluorescence to baseline. The rate of nucleotide exchange was determined by fitting a single exponential decay function to the dissociation phase of the experiment. Reactions were performed under increasing concentrations of compound in a buffer containing 25 mM Tris (pH 7.5), 50 mM NaCl, 1 mM DTT, and 20 μ M MgCl₂ with final component concentrations of 1 μ M, 1 μ M, 1 μ M, and 200 μ M for Ras, SOS, BODIPY-GTP and unlabeled GTP, respectively.

CHAPTER III

SECOND-SITE SCREENING OF K-RAS IN THE PRESENCE OF A COVALENTLY ATTACHED FIRST-SITE LIGAND

Introduction

In the previous chapter, a fragment-based screen was described using NMR against GDP-bound K-Ras. The hits identified in the screen occupied a hydrophobic pocket between the switch II helix and the central β sheet. We were able to improve the affinity of these compounds using structure-based design and demonstrated that they inhibit SOS-mediated nucleotide exchange of K-Ras. Although these compounds have low affinities due to their small size, the potency of the initial hits could be dramatically improved by linking them to fragments that bind to nearby pockets using the “SAR by NMR” paradigm [116]. Typically, the method used to identify second-site ligands is conducted using a screen carried out in the presence of saturating amounts of the first-site ligand. The second-site ligands can be discovered using multiple methods, such as monitoring chemical shift perturbations of the protein [119], observing intermolecular NOEs (ILNOE) between bound ligands [131] or by attaching a spin-label to the first-site ligand and following the paramagnetic relaxation enhancement of the bound second-site ligands [132]. Once a second-site ligand is found, it can be linked chemically with the nearby first-site ligand to obtain a new ligand with higher affinity.

However, in some cases, the second site screen can be problematic. One of the reasons is that the first-site ligand may not bind tightly enough to saturate the primary binding pocket due

to their weak affinity and poor aqueous solubility. Sometimes, only one “hotspot” is present on the surface of the target protein, and all the hits prefer to bind at that site. In some other cases, the target protein may undergo conformational changes upon ligand binding in the first site pocket and may open up an additional binding pocket that is absent in the native protein structure. Thus, the results of a second-site screen can be difficult or impossible to interpret under such circumstances.

Erlanson and co-workers have reported an approach that takes advantage of the cysteine residues near the pocket followed by a screen for thiol-reactive compounds using mass spectrometry [133]. Inspired by this strategy, we developed an approach that involves the preparation of cysteine mutants of K-Ras that are used to covalently attach a first-site ligand. This approach would enable us to saturate the first-site pocket so that any newly identified hits from the screen would bind to a distinct site. In addition, the modification may lock K-Ras in a state that mimics the conformation when the primary pocket is occupied by our previously identified inhibitors.

(This Chapter is adapted from Sun et al. [121])

Results

Cysteine tethering strategy

We attempted to conduct a second-site screen using conventional methods to further improve the binding affinities of the compounds described in Chapter II. However, we encountered the problem of being unable to find a suitable first-site ligand that could fully saturate the first-site pocket due to its weak binding affinity and poor aqueous solubility. As a result, many of the hits from the second-site screen competed for binding to the first-site pocket, which complicated the interpretation of the data.

Inspired by the “cysteine tethering” strategy pioneered by Erlanson et al. [133], we developed an approach that involved the preparation of cysteine mutants of K-Ras that could be used to covalently attach a first-site ligand to allow us to conduct a second-site screen. To accomplish this, we designed a panel of six cysteine mutants (Figure 26), targeting the region surrounding the primary binding site. Each mutant K-Ras protein was expressed and purified. The $^1\text{H}/^{15}\text{N}$ HMQC (Heteronuclear Multiple Quantum Coherence) spectra of the proteins showed that all of the mutants were folded correctly. Purified proteins were then mixed with thiol-reactive compounds to covalently modify the protein.

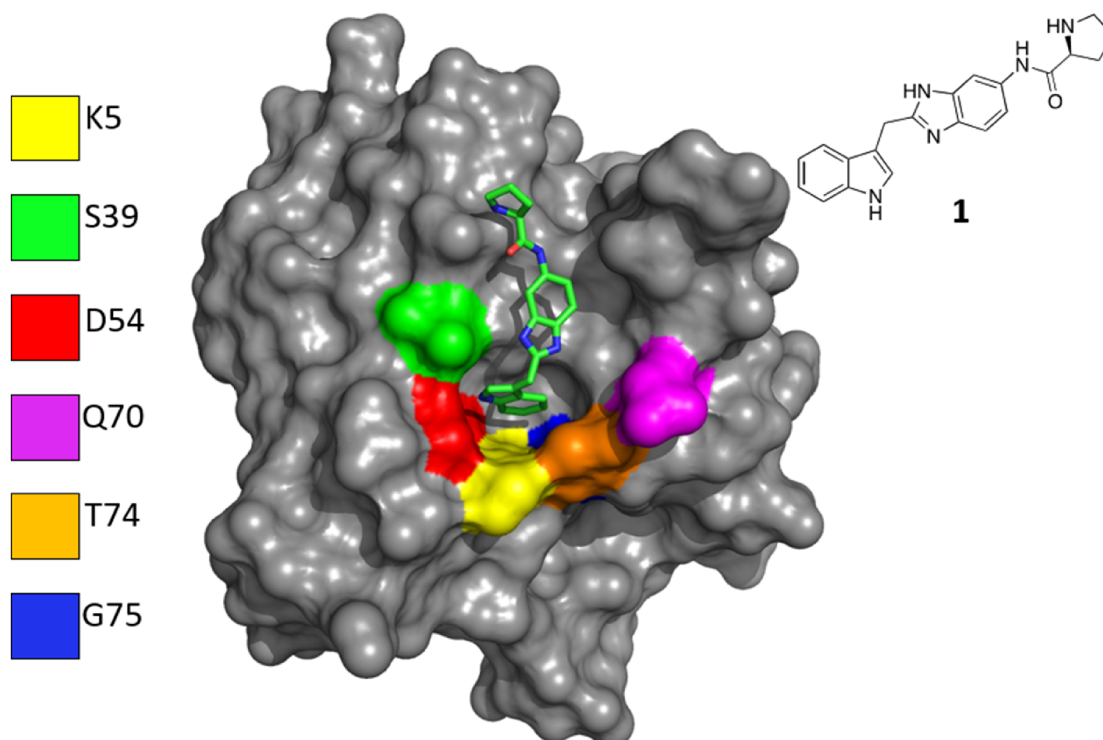


Figure 26. Six residues around the primary binding pocket were mutated to cysteine. A previously identified K-Ras inhibitor (**1**) is depicted as a stick figure to indicate the location of the primary binding pocket

Since a large number of our screening hits contain an indole, we started with an indole-containing compound (compound **2**, Figure 27). This compound was allowed to react with the cysteine mutants, and mass spectrometry was used to confirm that the reaction was complete. Next, we obtained crystal structures of tethered mutant proteins to determine where the attached indole was bound. For the T74C mutant, the indole moiety was found to point out of the pocket (Figure 27a), while in the S39C mutant, the indole moiety occupies the pocket, but it does not bind in the same conformation as the original ligand and is unable to form a hydrogen bond with Asp-54 (Figure 27b). Interestingly, the Q70C mutant attached to **2** was also not suitable for screening since the indole moiety binds in a pocket of a neighboring protein molecule in the unit cell, and induces the formation of a crystallographic dimer (Figure 27c). Full occupancy of the

first site pocket should block binding of compound **1**. However, when we added compound **1**, we observed chemical shift changes of the residues near the primary binding pocket in the HMQC spectra, indicating that the primary pocket was not fully blocked.

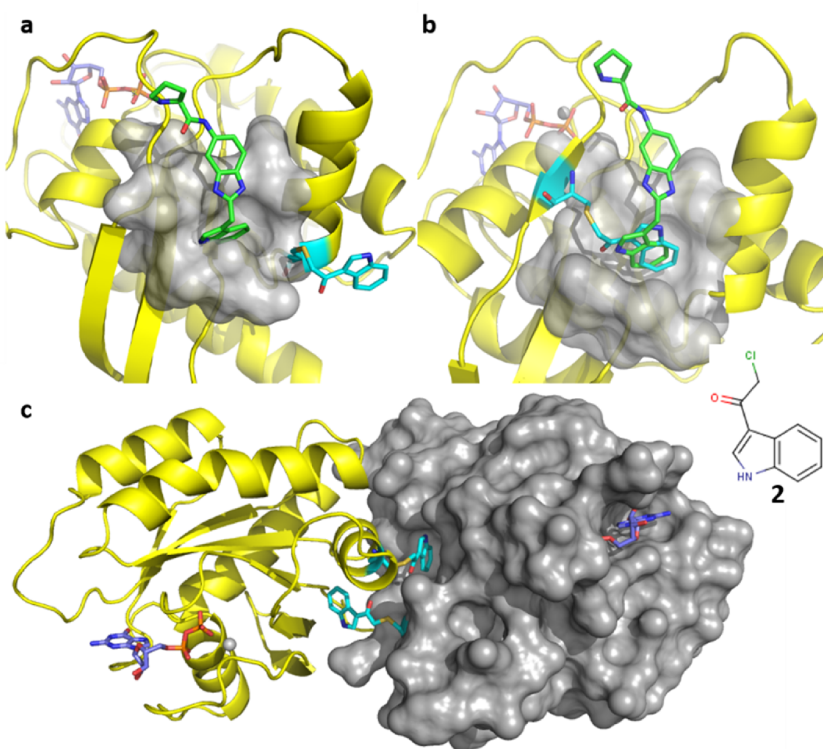


Figure 27. Crystal structures of K-Ras mutants covalently attached to a thiol-reactive probe. Crystal structures of various K-Ras mutants are covalently attached to compound **2** (cyan). (a) In mutant T74C, the covalently attached compound **2** is pointing towards the solvent. (b) In the mutant S39C, the linked compound is sitting inside of the primary pocket, but the NH group of the indole is pointing in the opposite direction compared to compound **1** (green). (c) The modified Q70C mutant crystallized as a dimer with the indole portion of the compound occupying the pocket of a neighboring molecule. (PDB entry 4PZY) None of these modifications blocks the probe compound **1** from binding to the first-site.

After these initial failures, we prepared a small library of 32 thiol-reactive compounds (Figure 28) to identify the desired combination of cysteine mutants and thiol-reactive compounds. Each compound was reacted with each of the cysteine mutants, and the reaction was

monitored using mass spectrometry and NMR. To test whether the covalently attached molecule could be displaced from the primary site, the probe compound **1** was added, and $^1\text{H}/^{15}\text{N}$ HMQC spectra were recorded. The overall workflow is depicted in Figure 29.

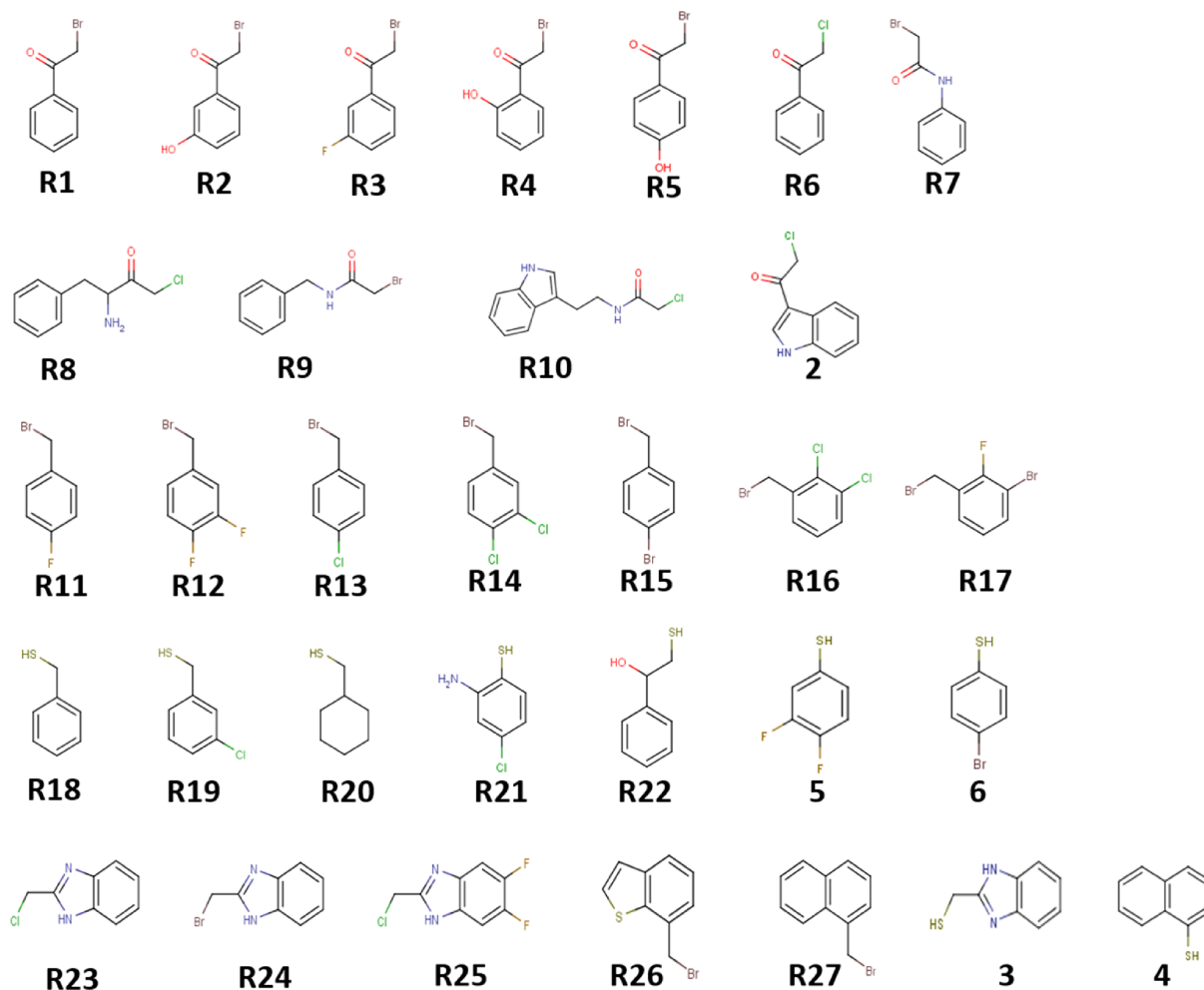


Figure 28. The thiol-reactive compounds used to identify the preferred mutant/compound combination for the second site screen.

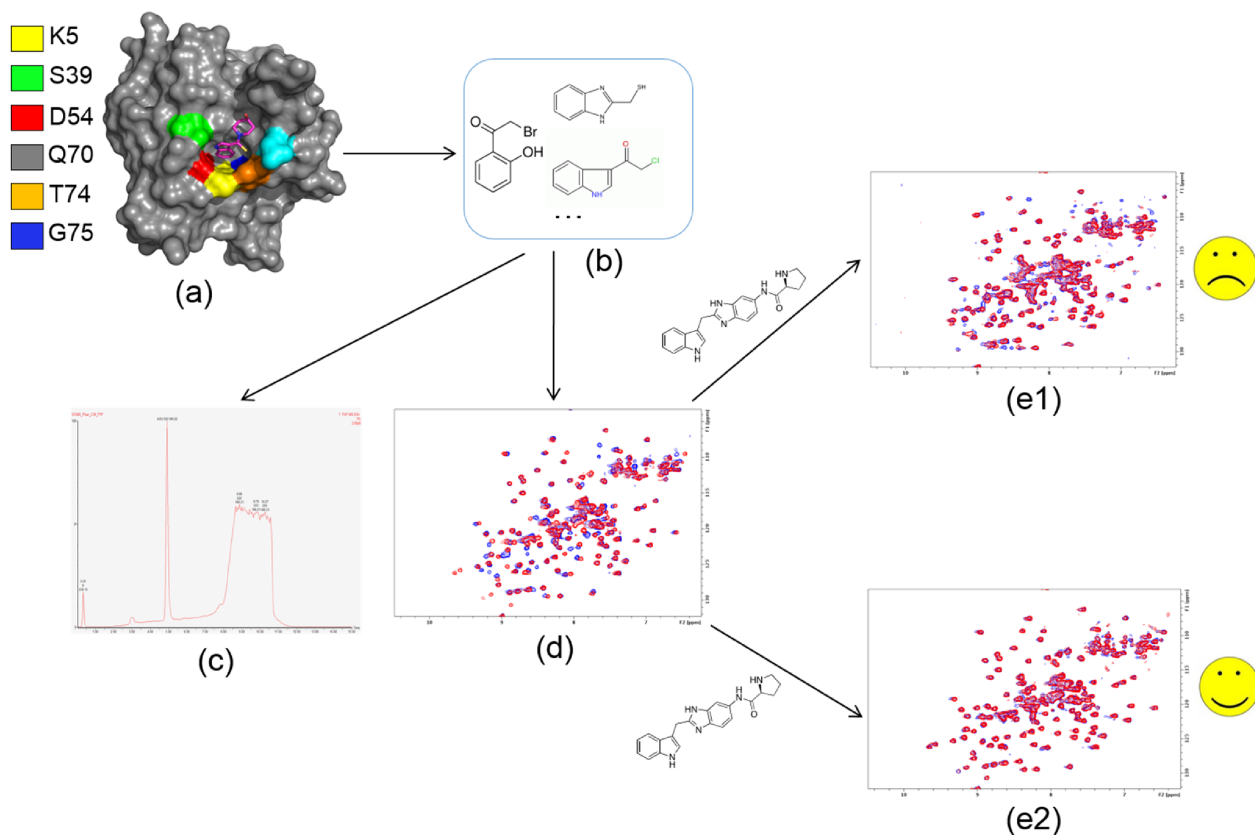


Figure 29. Strategy to identify thiol-reactive compound that blocks the first-site binding pocket. (a) six residues around the first-site binding pocket were mutated to cysteine, and each K-Ras mutant was expressed and purified individually. (b) Each mutant was mixed with a small library of thiol-reactive compounds. (c) Reactions were confirmed by mass spectrometry analysis. (d) The reacted protein was examined by comparing the ^{15}N HSQC upon addition of the thiol-reactive compounds. The HSQC spectrum of the unreacted protein is shown in blue, reacted protein is shown in red. (e) The reacted protein was further validated using an indole-containing probe compound. (1) Additional changes on the HSQC when adding the probe compound indicate that the primary pocket is not blocked (e1). No additional changes would indicate that the primary binding pocket is fully blocked. (e2)

Using this approach, we were able to identify four suitable mutant/compound combinations in which the primary pocket was fully occupied and saturated (Figure 30). As confirmed by NMR, no further chemical shift changes were observed upon the addition of compound **1**. Superposition of the structure of K-Ras S39C/benzimidazolethiomethane (**3**) covalent complex with that of an indole-containing compound **1**, showed a perfect overlap

between the indole and benzimidazole (Figure 30a). The latter blocks the pocket without interfering with potential nearby binding sites. Thus, we chose the modified protein K-Ras S39C/3 to be used in our second-site screen.

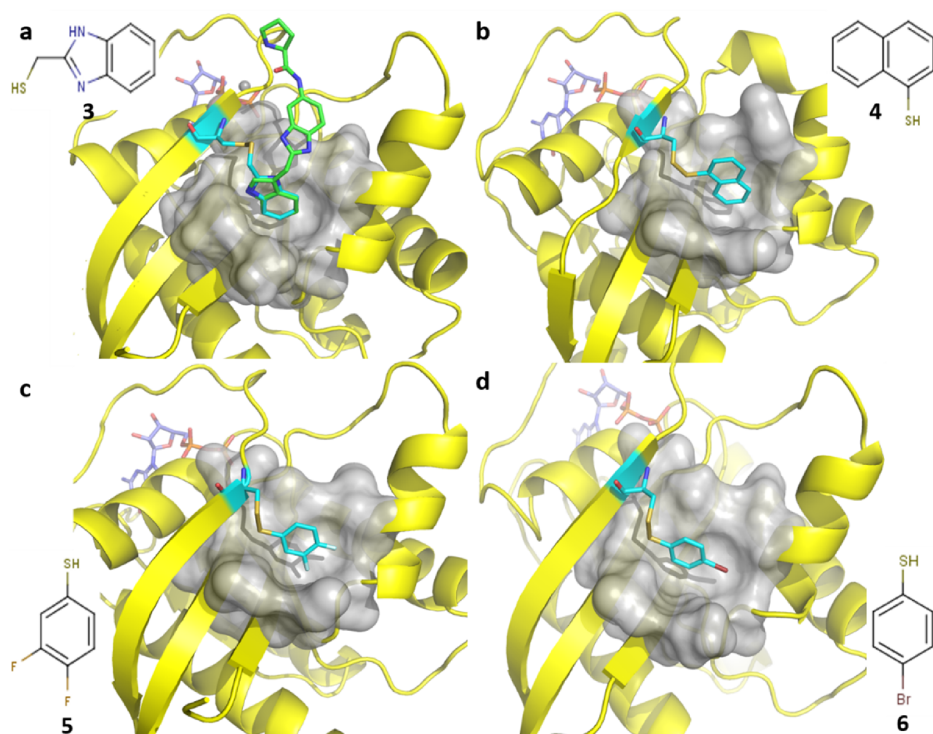


Figure 30. Crystal structures of GDP-bound K-Ras S39C that was reacted with thiol-reactive compounds. Ribbon and molecular surface representations of the crystal structures of GDP-bound K-Ras S39C that was reacted with thiol-reactive compounds (cyan) a) **3**, (PDB 4PZZ) b) **4**, (PDB 4Q01) c) **5**, (PDB 4Q02) and d) **6**. (PDB 4Q03) All these compounds completely block the pocket and prevent the probe compound from interacting with the protein. Among them, compound **3** perfectly overlays with the probe compound **1** (green).

Fragment Screening for the Second-site Ligand

Unlike the initial first-site screen, which yielded over 140 hits, only 36 hits were identified in a second-site screen from a library containing ~13,000 compounds. Table 2 showed a list of examples of the hits. They bind to both modified and native K-Ras protein with affinities ranging from 0.3-3 mM.

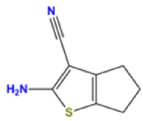
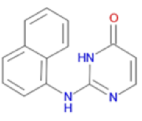
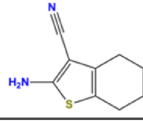
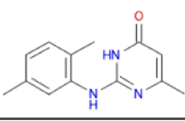
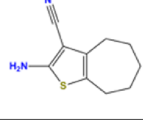
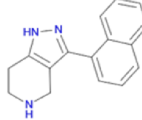
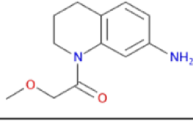
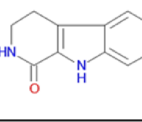
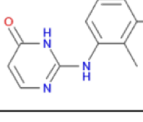
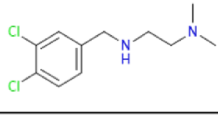
Compound	K_d (μM)	LE	Compound	K_d (μM)	LE
N1 	1080	0.38	N6 	350	0.27
N2 	746	0.36	N7 	174	0.31
N3 	364	0.37	N8 	1400	0.21
N4 	1700	0.24	N9 	2800	0.26
N5 	1500	0.25	N10 	1430	0.27

Table 2. Examples of the hit identified from the second-site screen.

Crystal structures of the second-site ligands bound to a new pocket

To determine the location of the second-site ligands, we co-crystallized the modified S39C mutant of K-Ras with several second-site ligands. Surprisingly, crystal structures of the protein/ligand complexes revealed that the second-site hits bind in a distinct pocket near the guanine nucleotide. This site was highlighted as site 3 previously in chapter I. Therefore, the newly identified ligands are referred as S3 ligands. As shown in Figure 31, this binding pocket is formed by Val-9, Phe-78 and Val-103, as well as the hydrophilic residues Glu-63 and Asp-69. It is created by the rotation of Met-72 and Arg-68 along with movement of the Switch II helix. Tyr-71 rotates towards the solvent and forms a stacking interaction with the covalently linked benzimidazole, which opens up a new pocket located between Switch II and helix 3.

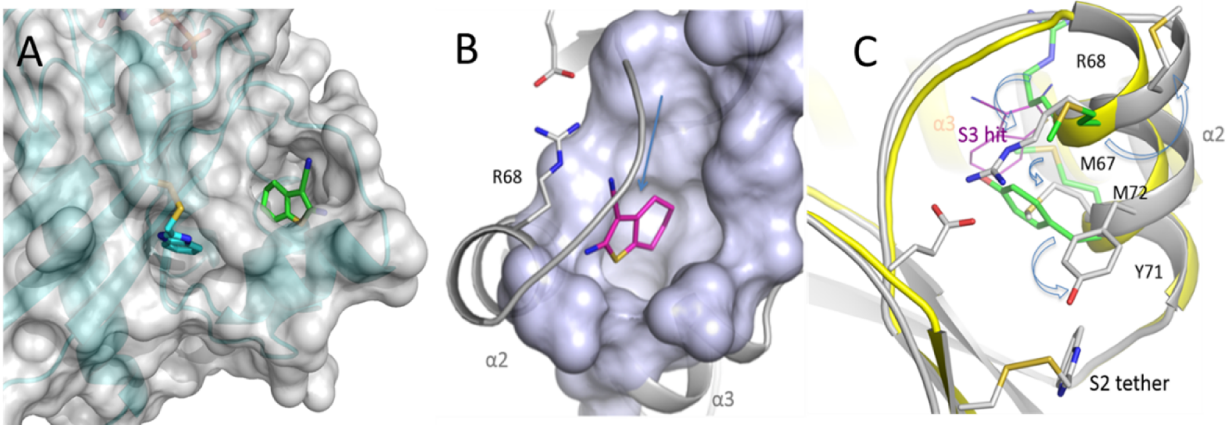


Figure 31. Crystal structures revealed small-molecules bind at the S3 pocket of K-Ras. (A) The relative position between the covalently-linked first-site ligand (cyan) and the second-site ligand (green). A few flexible residues on switch II have been removed from the structure. (B) The second-site ligand **N2** (magenta, arrow) binds in a pocket under a flexible loop of the switch II. (C) The $\alpha 2$ helix (yellow) moved away (grey) from the protein center upon covalently attaches the first-site ligand to Cys-39. Three residues, Arg-68, Met-67 and Y71 (green) rotate towards the first-site ligand, create space for the S3 ligand (magenta) to bind.

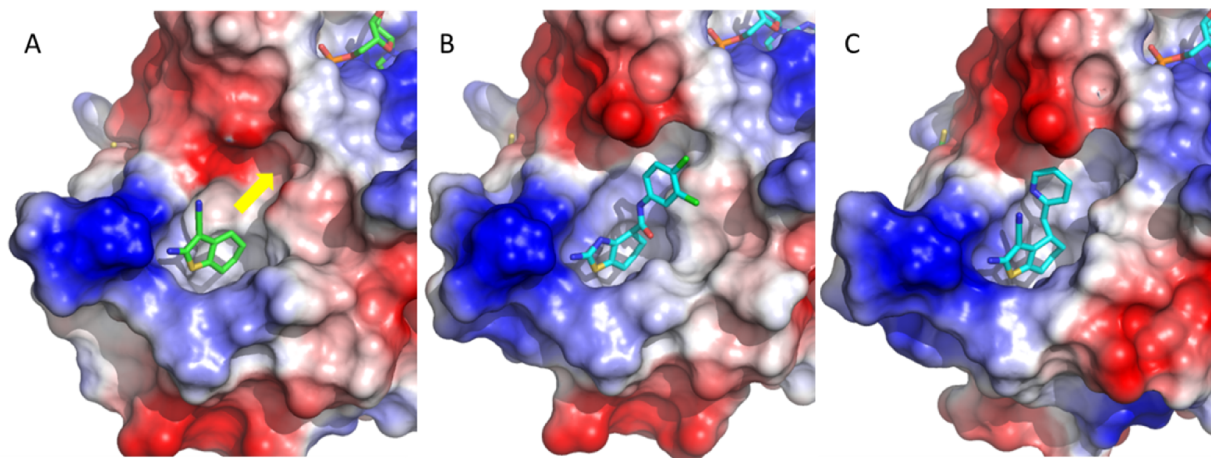


Figure 32. Crystal structures of optimized analogs bind in the S3 pocket. A hit **N2** (A) from the second-site screen is being optimized for binding to the S3 pocket. An aromatic moiety, pyridine (B) or Di-Cl-benzene (C) were attached to compound **N2** at 4' position via peptide (B) or methylene (C) linker.

From the crystal structures, we noticed a binding pocket not occupied by the S3 ligand (Figure 32A, yellow arrow). By linking an aromatic moiety at the 4' position of the compound

N2, we obtained compound VU0516466 (Figure 32B) and VU0516979 (Figure 32C), both compounds extended into nearby binding pocket and showed better affinity to the protein.

Discussion and Conclusion

In this chapter, I described a useful approach for identifying small molecules that bind to a protein at a second-site that differs from the primary binding pocket. The method solves the problem of the need to saturate the first-site pocket, which is a major issue when conducting a second-site screen.

The basic idea of covalent tethering that has been previously described is to screen for thiol-reactive compounds that covalently bind to a cysteine using mass spectrometry [133]. This strategy was also used in the second-site screen. In this approach, an extender with thiol-reactive warhead was added to first-site ligands to catch the reactive fragments that bind nearby [134].

Our method differs from these previously described tethering approaches using mass spectrometry in several ways. A major advantage of our method is that it does not require a large library of reactive compounds. Any conventional compound library can be used in our method once the modified protein target is prepared. In the absence of covalent constraints, the second-site ligands identified in our approach are more likely to preserve natural binding poses. Oftentimes the second-site pockets are not readily observable from the static crystal structures. Attaching a compound covalently to the first-site pocket, will mimic a tightly bound first-site ligand and may induce conformational changes that open up additional binding pockets. However, this goes two-ways: The hits identified under such condition may preferably bind to

the modified protein and show weaker affinities to the native protein target. Indeed, the S3 binding pocket on Ras is stabilized upon covalently saturating the first-site pocket. Therefore, the S3 ligands bind to the native K-Ras protein with lower affinities, and the crystal structure of native K-Ras complexed to S3 ligands was never obtained.

The bottleneck of our method is to be able to identify the ideal combination between a cysteine mutated protein and a cysteine-reactive compound. The covalently attached compounds must have the correct orientation and linker length to fully saturate the first-site pocket. For K-Ras, thiol-based compounds were generally more successful than alkyl-halides because the disulfide bond provides more flexibility to correctly position the hydrophobic portion of the compounds in the pocket. In our experience, the best way to find an optimum covalently attached first-site ligand is to screen a small library of well-designed thiol-reactive compounds in combination with several cysteine mutant proteins. Once a suitable combination of mutant/compound is found, the modified protein can be used to screen for second-site ligands using conventional methods.

Several possible limitations must be considered. At the beginning, we attempted to simply mutate the residues inside of the primary binding pocket to cysteine or other amino acids with bulky sidechains to block the pocket. However, that usually results in significant changes on the shape of the entire binding area, as well as some distant regions. Especially for the residues at the bottom of the pocket, the mutations and covalent modifications may induce significant conformational changes on the protein, which may cause unfavorable artifacts in the screening or even destabilization of the protein. In our case, the G75C mutation on the protein destabilized the entire switch II region. (Figure 33) In the crystal structure of K-Ras G75C, the entire switch II is invisible.

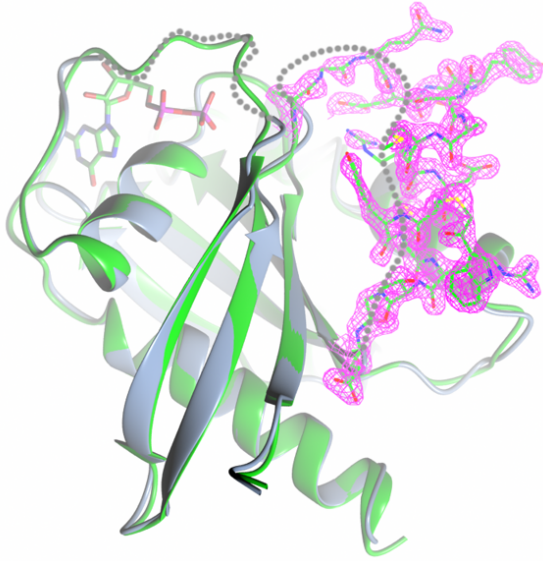


Figure 33. Crystal structure of K-Ras G75C showed a disordered switch II. Green: Ribbon diagram of GDP-bound K-Ras switch II residues (60-75) in stick models superimposed with the electron density map of the modified Q70C mutant. Blue: K-Ras G75C mutant, where the entire switch II region including the modified cysteine was not observed in the structure. The missing parts of that model are represented by the dotted lines.

In addition, the covalent modifications may induce distal changes on the protein.

Furthermore, the newly identified “second-site” ligands can be far from the first-site ligands, making them difficult to link. Unfortunately, this was the case for us with K-Ras. The newly identified S3 binding pocket is not close to the first-site pocket. This new binding pocket is quite far from the first-site. Using computational modeling, we attempted to find a route to link the first and second-site ligands together. As shown in Figure 10, we found that the switch II helix is blocking the direct route from the first-site to the second-site ligands. In order to link them together, the linker would have to bypass or penetrate the loop of switch II. Connecting ligands from the S2 to S3 pockets would require a very long (>15 Å) flexible linker, which is not practical.

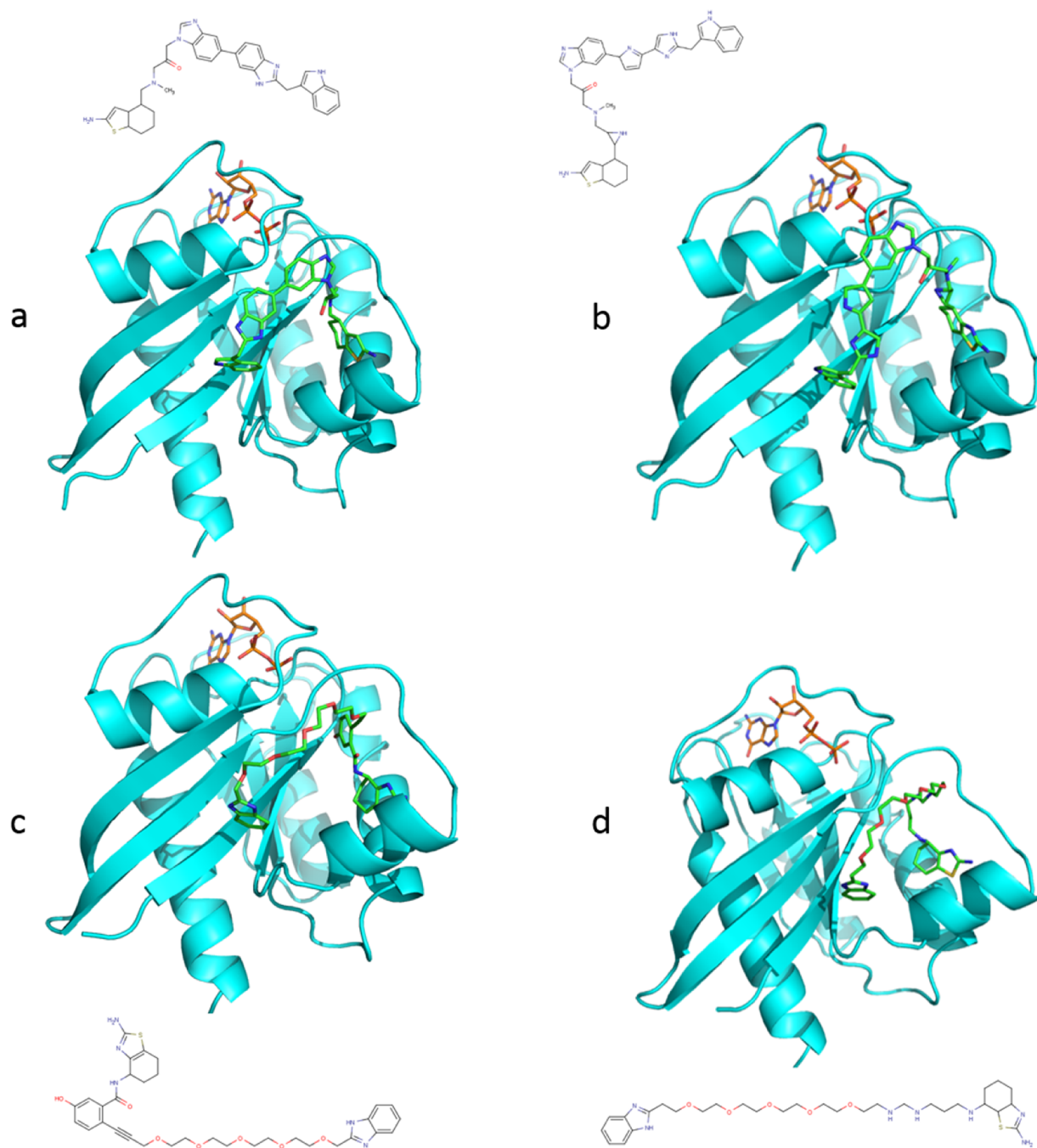


Figure 34. Molecular modeling to determine how to connect the first-site ligands and the second-site ligands. Both rigid (c, d) and flexible (a, b) protein models were used to generate docking templates. Modeling indicates that a long linker is required to connect the first-site and second-site ligands. Unfortunately, this linker will have to pass through under the switch II loop.

Opportunities to specifically target K-Ras G12C

In the chapter I, I list two examples for targeting the K-Ras G12C mutant using irreversible inhibitors [86-88]. One of these irreversible inhibitors, **S6**, binds to the same pocket as our S3 ligands (site 3) [88]. This suggests that our S3 ligands could possibly be used to discover irreversible inhibitors against the G12C mutant of Ras.

A major challenge for irreversible inhibitors is to develop specificity against the target of interest [90]. Nonspecific protein labeling by reactive groups usually causes low efficacy and high toxicity *in vivo*. To gain specificity, the inhibitors will need to bind tightly to the target in the absence of the electrophile. An overlay of cysteine-reactive compound **S6** and our S3 ligands is shown in Figure 35A. Compared to the cysteine-reactive compound **S6**, our S3 ligands bind deeper and make more hydrophobic interactions with the surrounding residues, which suggests that we may be able to utilize the S3 ligands to discover better inhibitors to target G12C mutant of K-Ras. Figure 35B depicts a possible route to reach Cys-12. Based on the volume and hydrophobic enclosure of this pocket, we expect a substantial improvement in potency and selectivity compared to the previously reported irreversible inhibitors.

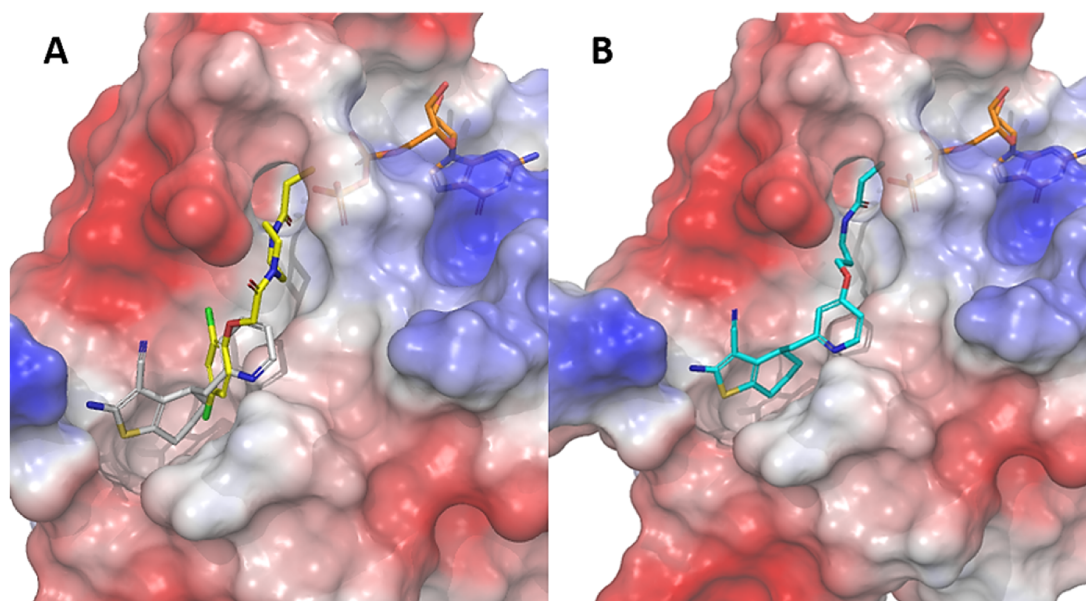


Figure 35. Covalently attach S3 ligands to Cys-12. (A) Overlay of the covalent inhibitor **S6** (yellow) with one of our S3 ligands VU0516979 (grey). (B) A linker (cyan) is designed to connect the compound VU0516979 to Cys-12.

Although the G12C mutant is the most prevalent K-Ras mutation in lung cancers, it only represents a small percentage for other cancers [135]. It would be advantageous if we optimized our S3 ligands to lead compounds with high binding affinities without having to covalently attach it to a cysteine so that it can be used for wild-type and other Ras mutants. From all the hits from our second-site screen, we have only obtained crystal structures for the amino-cyano-thiophene series. Using NMR chemical shift perturbation experiment, we found that some screening hits from other chemical series are also affecting the residues near the S3 site. These compounds have different chemical scaffolds and distinct SAR, and are likely to bind differently than the amino-cyano-thiophenes, suggesting that there might be opportunities for linking and merging. Therefore, in the future we plan on determining the high-resolution structure of these compounds when bound to Ras.

Materials and Methods

Cloning, expression and purification of K-Ras protein

All K-Ras proteins described here contain the G12V oncogenic mutation and C118S mutation for thio-reaction selectivity. The DNA construct, cloning, expression, and purification procedures were described in the previous chapter. Each of the 6 mutations (K5C, S39C, D54C, Q70C, T74C, G75C) was introduced by site-directed mutagenesis using the QuickChange Kit.

Screen for the appropriate combination between mutants and thiol-reacted compounds

Each of the 6 mutant K-Ras protein was expressed in uniformly ^{15}N labeled form. $^1\text{H}/^{15}\text{N}$ SOFAST HMQC [136] spectrum was collected to ensure the mutants were properly folded. The protein was exchanged in a buffer containing 25mM Tris-HCl pH7.0, 150mM NaCl and concentrated to 5 mg/mL. The thiol-reactive compounds were added individually at a concentration of 2-5 mM. The reactions were carried out at 4 °C overnight, and the reaction mixture was applied to a G25 desalting column to remove the excess compound. The modified protein was then subject to mass spectrometry to confirm the covalent modification. In addition, the HMQC spectrum of modified protein was collected. A significant chemical shift changes for the residues near the binding pocket indicates binding of the small molecule. Finally, a probe compound **1** (N-[2-(1H-indol-3-ylmethyl)-1H-benzimidazol-5-yl]-L-prolinamide) was added at a concentration of 2mM. No additional chemical shift changes indicated that the primary pocket is fully blocked.

Fragment screen

The fragment screen of the second site was conducted using the K-Ras S39C mutant linked to compound **3**. The NMR screening procedure was the same as that described in the previous chapter.

Protein Crystallization

GDP-bound K-Ras (G12V/C118S) with a cysteine mutation (K5C, S39C, D54C, Q70C, T74C, G75C) was exchanged into a reaction buffer (20mM Tris, 150mM NaCl pH8) and concentrated to 40 mg/mL. Protein-ligand complexes were prepared by adding a concentrated DMSO stock solution of the ligand to a protein:compound molar ratio of 1:5, incubated at 4 °C on a rocker overnight. The reaction mix was subject to a desalting column to remove excess ligand and exchanged into crystallization buffer (20 mM HEPES pH 7.5, 150 mM NaCl, 5 mM MgCl₂, 2 mM GDP). All crystallization experiments were set up using either the sitting or hanging-drop vapor diffusion method at 18 °C. GDP-bound K-Ras T74C and S39C linked to compound **2** crystallized in 25% PEG3350, 0.1 M Bis-Tris-HCl pH 5.5, The GDP K-Ras Q70C linked to compound **2** crystallized in 30% PEG MME 2000 and 0.1 M KSCN. K-Ras S39C linked to compounds **3** and **6** crystallized from 24% PEG4000, 0.1 M MMT pH 4.0. K-Ras S39C linked to compounds **5** crystallized from 28% PEG4000, 0.1 M sodium acetate, and pH 5.0. K-Ras S39C linked to compounds **4** crystallized from 22% PEG4000, 0.1 M sodium acetate pH 4.5. The co-crystal of **N2** complexed to K-Ras S39C/**3** is obtained from 0.24 M sodium malonate pH 7.0, 22% PEG3350. All crystals were cryoprotected with 10% ethylene glycol addition for low-temperature data collection.

X-ray Data Collection, Structure Solution, and Refinement

X-ray diffraction data were collected at 100K in the oscillation mode on single flash-cooled crystals using a Bruker-Nonius Microstar rotating anode X-ray generator equipped with a Proteum PT135 CCD area detector (Biomolecular Crystallography Facility in the Vanderbilt University Center for Structural Biology), as well as the synchrotron radiation (Beamline 21 LS-CAT, Advanced Photon Source, Argonne National Laboratory). Data were processed with HKL-2000, and the structures were determined by molecular replacement using the coordinates of GDP K-Ras G-domain (residues 1-169; PDB Entry 4EPY) with solvent and ligand molecules stripped off. The program package Phenix was employed for phasing and refinement, and model fitting was performed with COOT. The refined models were validated with Molprobit.

CHAPTER IV

TARGETING RAS SIGNALING WITH NUCLEOTIDE EXCHANGE ACTIVATORS

Introduction

From fragment-based screening of K-Ras as described in Chapter II, we identified over 140 hits. All of these hits, as well as a number of the analogs of these hits were characterized by a nucleotide exchange assay. Although most of these compounds inhibited SOS-mediated nucleotide exchange, a few of them increased SOS-mediated nucleotide exchange. Activating nucleotide exchange is expected to enhance downstream signaling and promote cell proliferation, however, we found that they inhibited downstream signaling of Ras.

In this chapter, the discovery of small molecules will be described that activates SOS-mediated nucleotide exchange of K-Ras, but paradoxically downregulate the downstream pathways of Ras. In addition, structural studies revealed a novel, functionally relevant pocket on the CDC25 domain of SOS near the Ras:SOS interface. Using mix-and-match strategy based on the crystal structures of compounds in multiple series, we have significantly improved the potency of these compounds.

(This Chapter is adapted from Burns et al. [122])

Results

Discovery of activators from the nucleotide exchange assay

From the nucleotide exchange assay, compounds were identified that increase the rate of nucleotide exchange *in vitro*, which was indicated by an increase in the exchange of BODIPY-GDP for unlabeled GTP. (Figure 36)

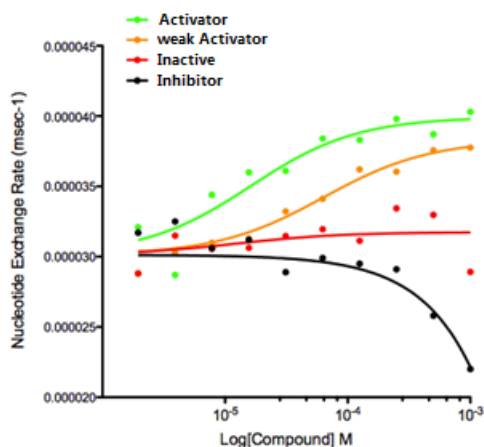


Figure 36. Nucleotide exchange activators were detected. Active molecules were identified in an assay that measures the effect of the fragment hits in the SOS-mediate nucleotide exchange of K-Ras. Molecules that activate (green/orange) and inhibit (black) the nucleotide exchange of K-Ras were found.

One of the series of compounds that activate SOS-mediated nucleotide exchange is represented by compound **1**, a 3-(4-amino-piperidinyl)methyl-indole (API) attached to a glycine.(Figure 37A) However, unlike our previously reported nucleotide exchange inhibitors, the structure–activity relationship of the compounds in this series did not correlate with their direct binding affinity to K-Ras (Table 1). These compounds bind to K-Ras only weakly, (in the millimolar range) but activate the SOS-mediated nucleotide exchange at low micromolar concentrations. We synthesized additional compounds based on the amino-piperidine indole core. The addition of a tryptophan resulted in a more potent compound (**2**), which activated

nucleotide exchange in a concentration- dependent manner (Figure 37B and E). The addition of a methyl or halide group to the 5' position of the indole (compounds **3** or **4**, respectively) produced additional increases in nucleotide exchange activation and lower EC₅₀ values (Table 3).

Compound **4** increased SOS-mediated nucleotide exchange with an EC₅₀ of 14 μM (Figure 37C and E). Replacement of the methylene linker between the indole and piperidine ring with a carbonyl resulted in a complete loss of activity (compound **5**) (Figure 37D and E). This compound served as a useful control in our studies.

Compound	Nucleotide exchange EC ₅₀ (μM)	Relative percent activation*	NMR K _D (μM) to K-RasG12D	FITC-4 competition experiment IC ₅₀ [†]
1	>100	19.4	322	>100
2	>100	48	279	>100
3	25.1	91.8	868	20
4	14	100	1,346	43
5	>100	-5.4	1,283	>100

*Calculated at 100 μM concentration for each compound.

[†]Conducted using 10 μM SOS^{GAT} and 300 nM FITC-4.

Table 3. The Structure-Activity Relationship of activator compounds **1-5**. No correlation was found between the nucleotide exchange activity of these compounds and their binding affinity to the K-Ras.

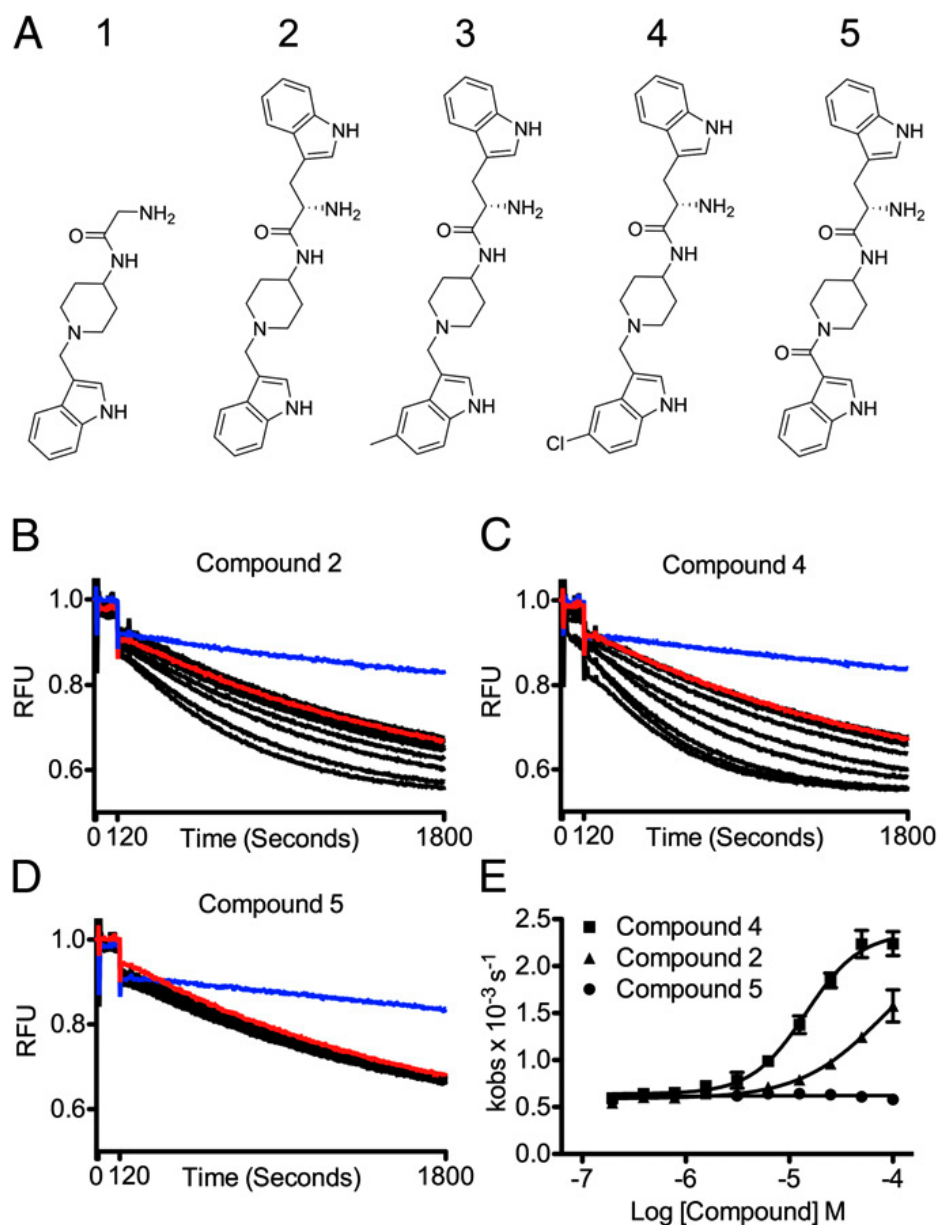


Figure 37. Amino-piperidine indole (API) compounds increase SOS^{cat}-catalyzed nucleotide exchange on Ras. (A) Chemical structures of compounds 1–5. SOS catalyzed nucleotide exchange assays were conducted with increasing concentrations of compounds (B) 2, (C) 4, and (D) 5. Compound was added (at 10 s) to BODIPY-GDP-loaded Ras followed by a second addition of excess GTP ± GEF (at 120 s). Kinetics of nucleotide exchange was monitored as a decrease in relative fluorescence units (RFU) with time. Ras alone (blue) and Ras + SOS^{cat} (red) DMSO-matched controls are shown. Compound was added in a 10-point, two-fold dilution series with a top concentration of 100 μM (black). Experiments shown in B-D were conducted in triplicate. (E) Mean rate was calculated and is plotted ($\pm\text{SD}$) for each compound as a function of concentration.

Using the nucleotide exchange assay as a tool, Michael Burns, a graduate student in our group, screened a library of small molecules from the Vanderbilt University High-throughput screening (HTS) facility. From approximately 100,000 small molecules, he discovered several classes of compounds that acted as activators in the SOS-mediated nucleotide exchange assay. These compounds (Figure 38) are structurally distinct from the amino-piperidine indole series and from each other. By performing a chemical shift perturbation experiment, we found that most of these compounds do not bind to K-Ras at all. Instead, they bind to the catalytic domain of SOS, as indicated by NMR saturation transfer differences (STD) experiment. Thus, the discrepancies between the direct binding to K-Ras and EC_{50} in nucleotide exchange assay remained a major issue. It was, therefore, important to understand how these molecules function at the molecular level.

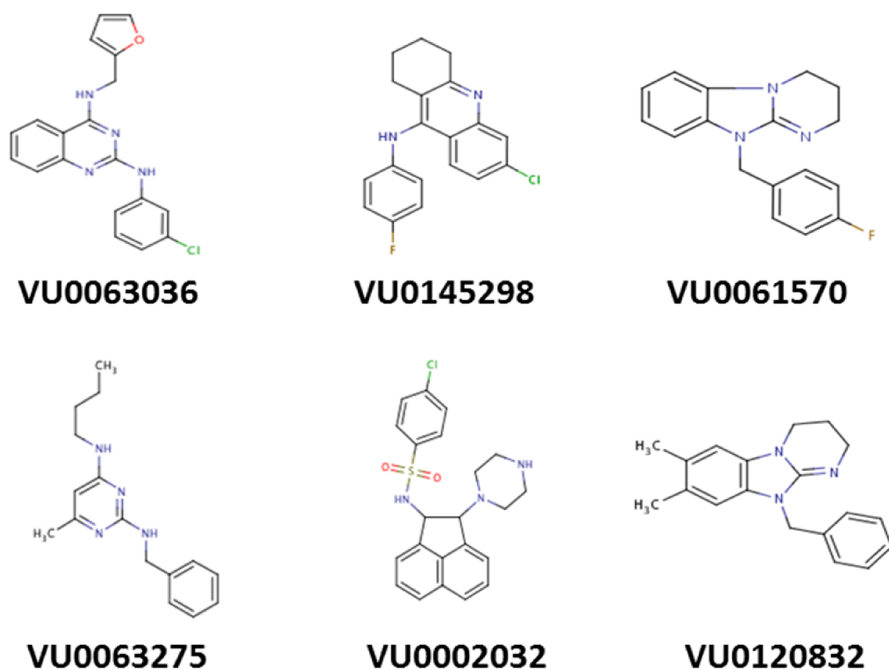


Figure 38. Compounds that activate the SOS-mediated nucleotide exchange of K-Ras were identified from a High-throughput screen.

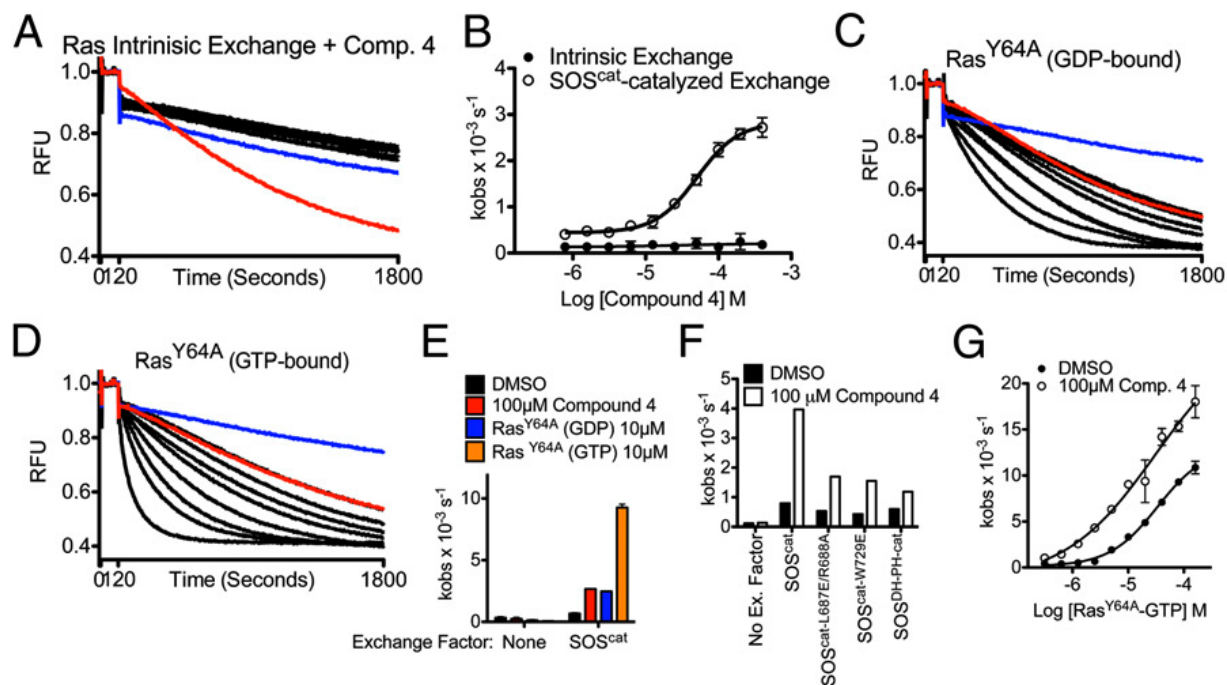


Figure 39. Nucleotide exchange activation by amino-piperidine-indole compounds is SOS-dependent and does not require the allosteric Ras binding site. (A) Intrinsic nucleotide exchange in the presence of compound **4** (10-point, two-fold dilution; 400 μM top concentration). Intrinsic and SOS^{cat}-catalyzed controls are shown in blue and red, respectively. (B) SOS^{cat}-catalyzed and intrinsic nucleotide exchange are displayed as a function of compound concentration ($n = 3 \pm \text{SD}$). Nucleotide exchange with Ras^{Y64A} loaded with GDP and GTP is shown in C and D, respectively (10-point, twofold dilution; 16 μM top concentration). (E) Quantification of SOS^{cat}-catalyzed nucleotide exchange with the indicated activator present ($n = 3 \pm \text{SD}$). (F) Nucleotide exchange in the presence or absence of 100 μM compound **4** catalyzed by SOS^{cat-W729E}, SOS^{cat-L687E/R688A}, or SOS^{DH-PH-cat}. (G) SOS^{cat}-catalyzed nucleotide exchange rates are displayed as a function GTP-loaded Ras^{Y64A} concentration in the presence or absence of 100 μM compound **4**.

A unique feature about SOS compared to other GEFs is the allosteric activation caused by a GTP-bound Ras molecule binding at a cleft between the REM and the CDC25 domains. At first, we thought that the activators may occupy the same pocket and mimic the function of Ras that binds to the allosteric site. To test this hypothesis, we tested K-Ras^{Y64A} in the nucleotide exchange assay to monitor the change in activity. SOS mutants, SOS^{W729E}, SOS^{cat-L687E/R688A}, as well as the longer SOS^{Dbl homology-pleckstrin homology (DH-PH)} mutant, was also used to rule out the allosteric activation effect. Interestingly, as shown in Figure 39, probing allosteric Ras binding

and compound in combination revealed that compound **4** was able to further activate SOS-mediated nucleotide, even in the presence of saturating levels of GTP-bound Ras^{Y64A} (Figure 39G). Compound **4** increases the catalytic activity of SOS^{W729E}, which is a mutant that cannot be activated by GTP-bound Ras^{Y64A}. These data strongly support the hypothesis that these compounds activate nucleotide exchange through a distinct mechanism, which can be elicited regardless of the presence or absence of GTP-Ras bound at the allosteric site.

Crystal structure of activator-bound ternary complexes

The mystery was finally uncovered by the crystal structure of an activator-bound Ras:SOS:Ras ternary complex. This ternary complex was determined using H-Ras [15]. We thought K-Ras would work similarly due to the high homology between H- and K-Ras. We first assembled K-Ras:SOS^{cat} complex by adding them together in the presence of EDTA. Then the ternary complex was obtained by adding an excess amount of GppNHp-bound K-Ras^{Y64A} to the binary complex, followed by size-exclusion chromatography to remove the excess K-Ras^{Y64A}. However, this ternary complex did not produce any crystals. By analyzing the published H-Ras^{WT}:SOS^{cat}:H-Ras^{Y74A} ternary complex (PDB entry: 1NVV), we found that the residues on H-Ras that differ from K-Ras are making critical contacts in the crystal packing. Indeed, switching from K-Ras to H-Ras produced high-quality crystals. By co-crystallizing the ternary complex with the ligands, we were able to obtain ligand-bound structures.

We co-crystallized the H-Ras^{WT}:SOS^{cat}:H-Ras^{Y64A}(GppNHp) ternary complex with the ligands and obtained X-ray structures of multiple compounds bound to the ternary complex (Figure 40). Subsequently, ligand-bound H-Ras^{WT}:SOS^{cat} binary complexes were also crystallized using similar conditions. These crystal structures revealed that the compounds bind

to the Ras:SOS:Ras complex in a hydrophobic pocket that is formed by the CDC25 domain of SOS adjacent to the switch II region of Ras. (Figure 40B) The pocket is formed principally by the α E and α F helices of the SOS catalytic domain, which are connected by a solvent exposed helical turn involving P894 [14]. The amino acid residues that form the rest of the pocket are from the coiled region and helical turn connecting the α D and α E helices of SOS. Some of the residues of SOS that form the pocket (e.g., N879, Y884, and H905) have previously been reported to interact directly with Ras. Notably, R73, located in the switch II region of Ras at the catalytic site of SOS, forms a stacking interaction with Y884 and interacts with the backbone carbonyl of N879 (Figure 40B). Importantly, N879 and Y884 form the anterior wall of the binding pocket (Figure 40B) and provide a direct link from the compound to the switch II region of Ras, which is critical for binding to the catalytic domain of SOS [137]. K-Ras and H-Ras have no residue changes within proximity to the binding pocket, suggesting that the compounds are not likely to be specific for activating one isoform of Ras over another.

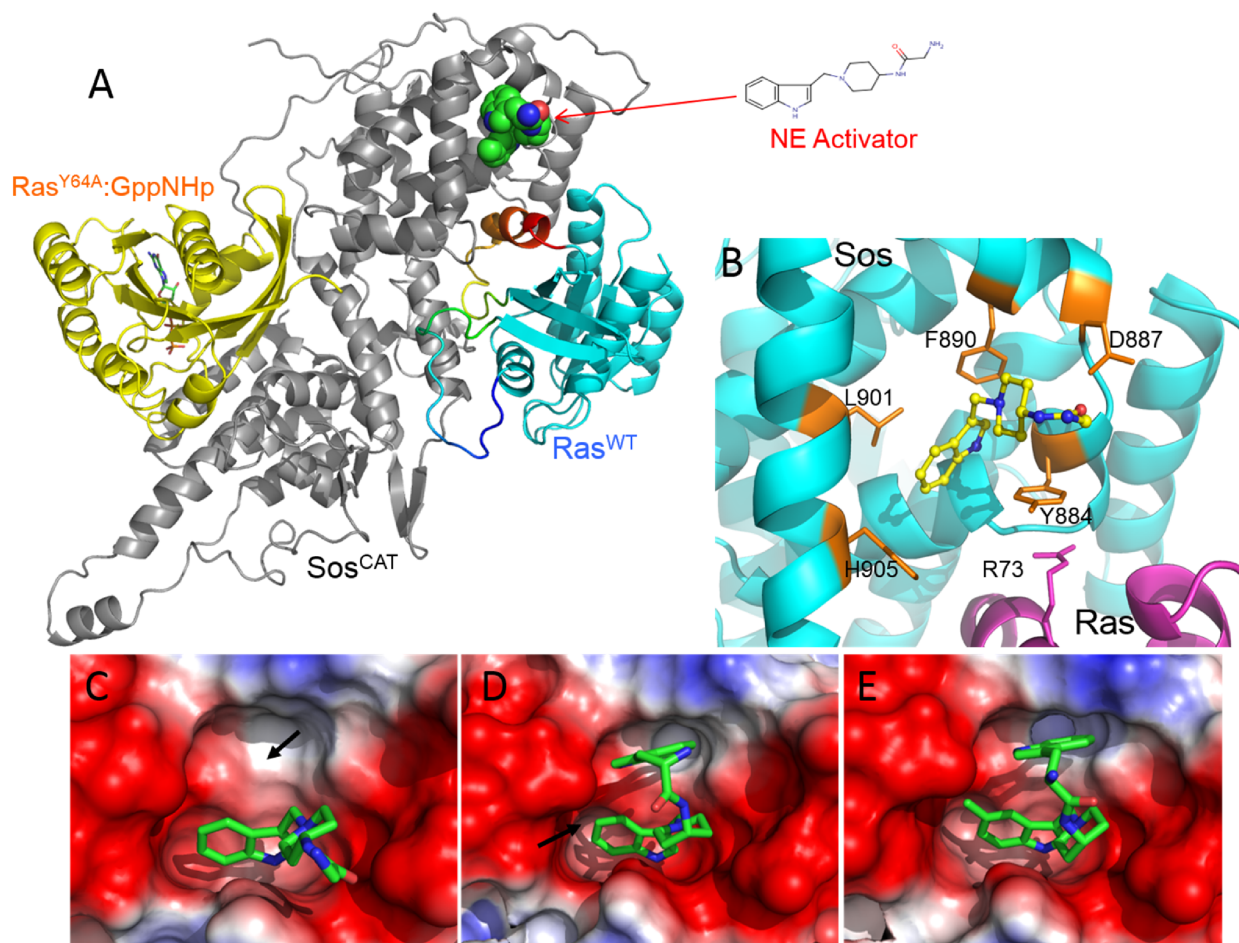


Figure 40. Amino-piperidine indole (API) compounds bind to the HRas^{WT}:SOS^{cat}:HRas^{Y64A} ternary complex. A) The SOS^{cat} (grey) is bound by Ras^{Y64A}-GppNHp (yellow) at the allosteric site and nucleotide-free Ras (cyan; switch regions shown in red and blue) at the catalytic site. The API compound (showed as space-filling model) binds at the CDC25 domain of the SOS^{cat} near the Ras-Sos binding interface. B) The hydrophobic pocket is formed by the CDC25 domain of SOS (cyan) adjacent to the switch II region of Ras (magenta). Critical residues forming the pocket are labeled. C-E) Surface depictions with amino-piperidine indole compounds **1**, **2**, and **3**.

The structure–activity relationships of amino-piperidine indole based compounds can be rationalized from the X-ray co-crystal structures. All compounds bind in a similar fashion, with the core indole occupying the most hydrophobic portion of the pocket (Figure 40C–E). The NH of the indole core forms a hydrogen bond at the bottom of the pocket with the backbone carbonyl of M878; whereas, the amino-piperidine moiety is surface-exposed and rotated towards D887. For compound **1**, the terminal amine is oriented to the solvent (Figure 40C). The tryptophan

moiety of compound **2** folds back and occupies a hydrophobic pocket located at the helical turn formed by P894 (Figure 40D). Compound **1**, which lacks this tryptophan moiety, cannot access this pocket (Figure 40C, arrow). The increased activity of compound **2** could be caused by the additional interactions made by the tryptophan moiety. Methyl-substitution at the 5' position of the core indole (compound **3**) further improved its activity (Table 3). The methyl group points to a space not occupied by the unsubstituted indole of compound **2** (Figure 40D, arrow and E). Compound **4**, a more potent compound (Table 3), was unable to be crystallized because of limited compound solubility. However, it is hypothesized to bind similarly to compound **3**, with the -chloro substitution occupying the same space as the methyl group of **3**. Based on the crystal structures, FITC-conjugated derivatives of compounds **2** and **4** were synthesized. Saturation binding and competition experiments conducted with these probes indicate that improved compounds bind SOS with a higher affinity (Figure 41A and B and Table 3). These crystallographic and biochemical data suggest that the activity of the compounds is determined by their ability to optimally fill the pocket.

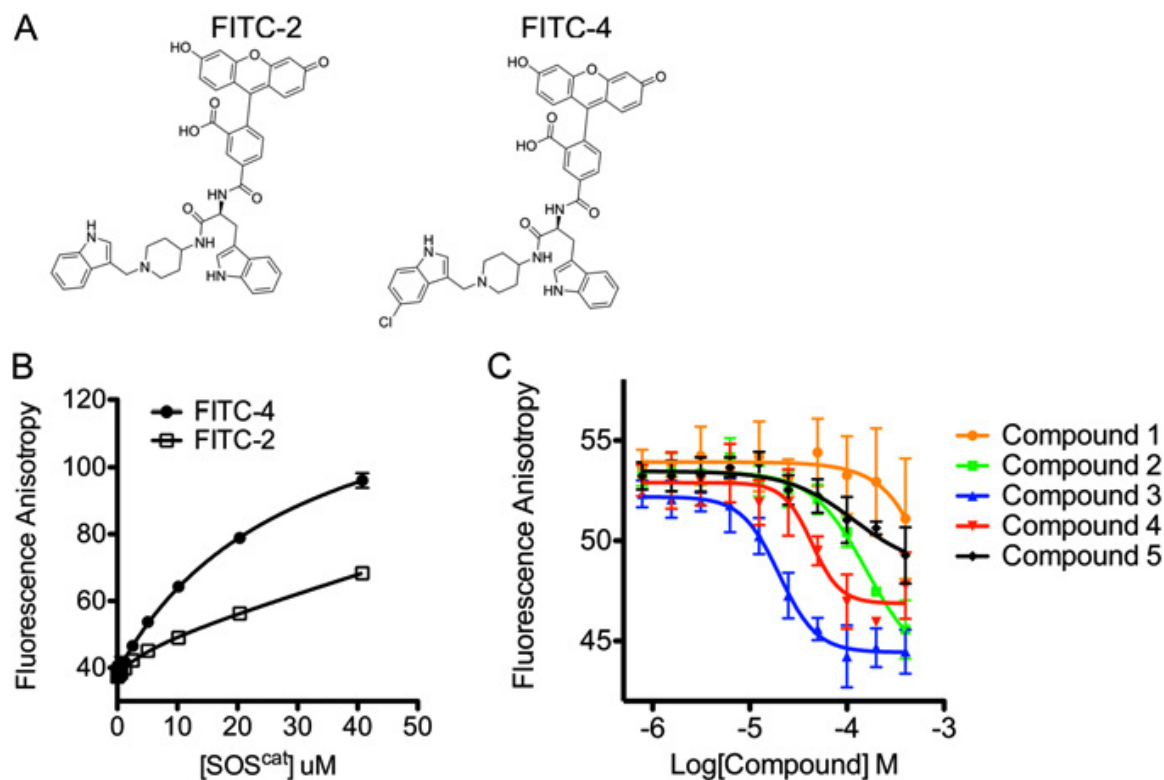


Figure 41. Saturation and competition binding experiments conducted using FITC-conjugated compounds. (A) Chemical structures of compounds FITC-2 and -4. (B) Saturation binding experiments were conducted by titration of increasing amounts of SOS^{cat} to a well containing FITC-2 or -4 (300 nM final concentration; n = 3 ±SD). (C) Increasing concentrations of unlabeled compounds 1-5 were used to outcompete SOS^{cat} (10 µM) binding to FITC-4 (300 nM; n = 3 ± SD).

Functional relevance of the new pocket

Residues in this pocket have been previously identified as being mutated in developmental RASopathy disorders. Two mutations in the cdc25 domain of SOS, E846K and P894R, cause Noonan Syndrome [138]. E846K has been shown to profoundly perturb intracellular signaling and P894R slightly activates nucleotide exchange on Ras compared with WT SOS [139, 140]. Of particular note, P894 forms the helical turn that defines the pocket occupied by the tryptophan moiety of compounds 2 and 3 (Figure 40B), further supporting the hypothesis that the binding pocket occupied by the compounds in the co-crystal structures is important for the activation of Ras by SOS.

To further validate the functional relevance of this pocket, we used the crystal structures to design mutations that would be predicted to perturb compound binding. Nine mutants of SOS^{cat} (D887A, D887E, D887H, D887N, D887V, F890L, L901M, L901K, and H905M) (Figure 40B) were cloned, expressed, and purified. Mutations of F890, L901, and H905 were designed to reduce the space available at the bottom of the hydrophobic pocket, whereas mutations of D887 were used to determine the importance of this residue for binding (Figure 40B). Nucleotide exchange rates were determined for each mutant form of SOS^{cat} from experiments conducted in the presence of DMSO or 100 μ M compound **2** (Figure. 42B). All mutant forms of SOS^{cat} catalyzed nucleotide exchange, confirming the proper folding and function of the mutant proteins. Mutation of F890, L901, and H905 prevented compound-induced activation of nucleotide exchange, suggesting that compound activity is mediated predominantly by hydrophobic interactions in the pocket (Figure 42). In contrast, mutation of D887 did not prevent the ability of compound **2** to activate nucleotide exchange (Fig. 42B and C). These data strongly support the conclusion that this binding pocket is functionally important for the activation of Ras by SOS and responsible for the compound-mediated activation of SOS^{cat}-catalyzed nucleotide exchange.

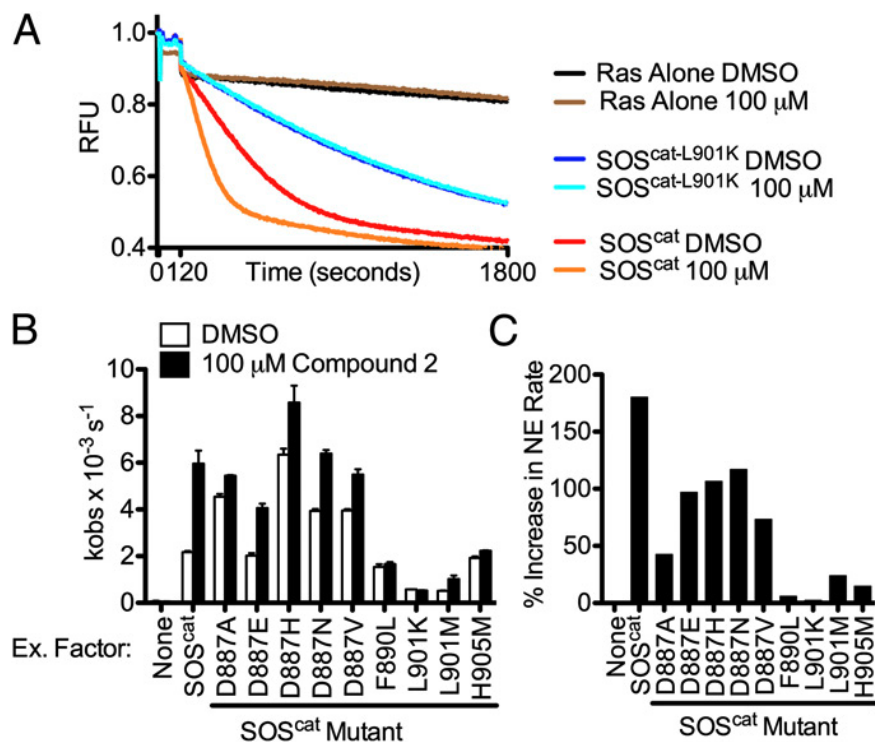


Figure 42. Mutation of the activator binding site on SOS prevents activation of nucleotide exchange by amino-piperidine indole. (A) Nucleotide exchange was conducted with each mutant form of SOS^{cat} in the presence of DMSO or 100 μ M compound 2 as shown for SOS^{cat}-L901K. (B) Nucleotide exchange rates in the presence of DMSO or 100 μ M compound 2 ($n = 3 \pm$ SD). (C) Percent increase in nucleotide exchange rate after the addition of the compound to each mutant.

Co-crystal structures of the different classes of activators

We have also co-crystallized the activators identified from the High-throughput screen. (A complete list of compounds co-crystallized with Ras:SOS:Ras ternary complex, Ras:SOS binary complex and SOS-CDC25 domain is attached in Appendix C) As shown in Figure 43, they also bind to the same pocket as the amino-piperidine indole based compounds. The only significant difference is the conformational change of F890. As indicated in Figure 43H, the sidechain of F890 flipped “up” (red arrow) and opened up a large hydrophobic hole underneath it, allowing the aromatic ring of the ligands to access. As a result, the hydrophobic pocket

previously occupied by the Tryptophan moiety of compound **3** (yellow arrow) is now partially blocked by the sidechain of F890. (Figure 43G, H)

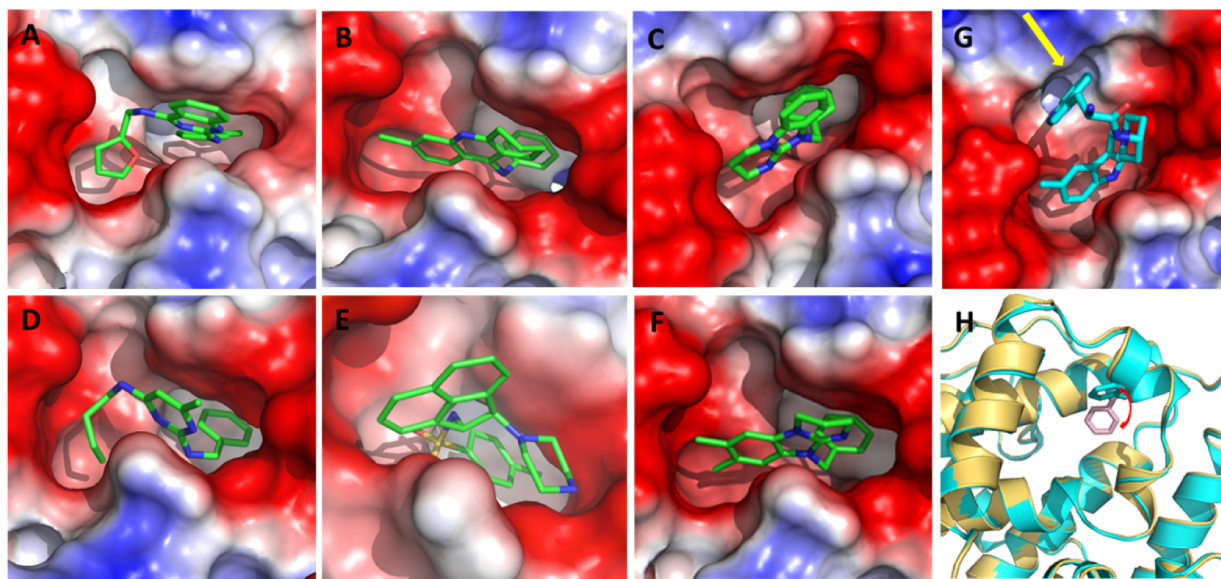


Figure 43. Crystal structures of activators from High-throughput screen when bound to SOS. A) VU0063036, B) VU0145298, C) VU0061570, D) VU0063275, E) VU0002032, F) VU0120832, G) compound **3**, H) the sidechain of F890 flipped from “down” position (purple) to “up” position (cyan) upon binding of VU0063275.

Most of the activators co-crystallized with Ras^{WT}:SOS^{cat}:H-Ras^{Y64A} ternary complex or Ras^{WT}:SOS^{cat} binary complex, with only one exception. The crystal structure of VU0002032 was obtained by co-crystallizing the CDC25 domain of Sos with the compound. Notably, the protein/ligand complex crystallized as a dimer, in which VU0002032 makes critical contacts in the crystal packing. (Figure 44) A unique feature here is that the piperazine group on VU0002032 directly interacts with the acidic side chain of D887. Mutations on D887 significantly reduce the activity of VU0002032 but have no effect on the amino-piperidine indole or other activators identified from HTS.

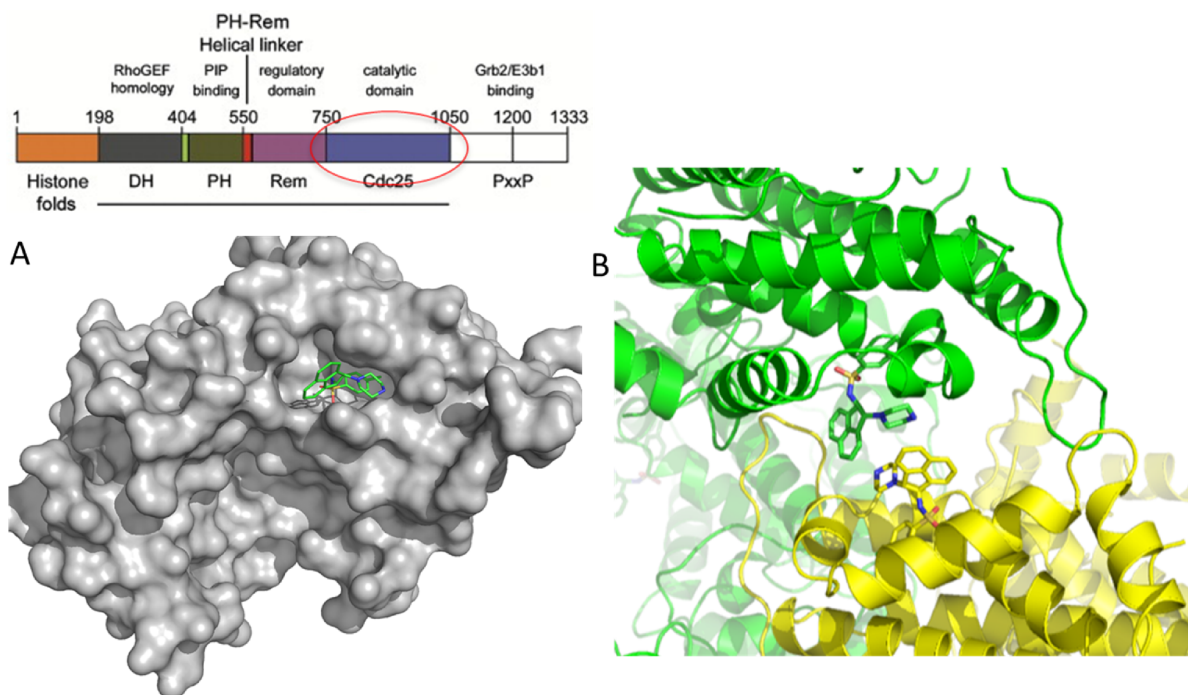


Figure 44. A ligand bound co-crystal structure of SOS-CDC25 domain. (A) The CDC25 domain of SOS was purified and co-crystallized with VU0002032. (B) There are two CDC25 molecules in each asymmetric unit. Two ligands from each asymmetric unit are contacting to each other, making them essential for crystal formation.

Design and Optimization of HTS activators

With the sidechain of F890 “up”, more hydrophobic area is exposed. We believed it would be easier to design high-affinity ligands based on this conformation. Thus, we designed and synthesized analogs based on two series of HTS activators, the quinazolines (VU0063036) and benzimidazoles (VU0120832). As shown in Figure 45A, we created compounds to fill the three hydrophobic areas inside the pocket, labeled as H1, H2 and H3. In addition, we attached basic moieties to the compounds to interact with residues D887 and E902. As exemplified by the analogs made based on the original quinazoline VU0063036. A 3-chlorine, 4-fluorine di-substituted benzene ring optimally fills the H1 pocket and greatly increases the potency of the compound. To occupy the pocket H2, the furan ring on VU0063036 was replaced by a

cyclopropyl group and an alkyl chain was added to reach H3. The improved compound VU0652002 (Figure 45B) had an EC₅₀ of 2.7 μM.

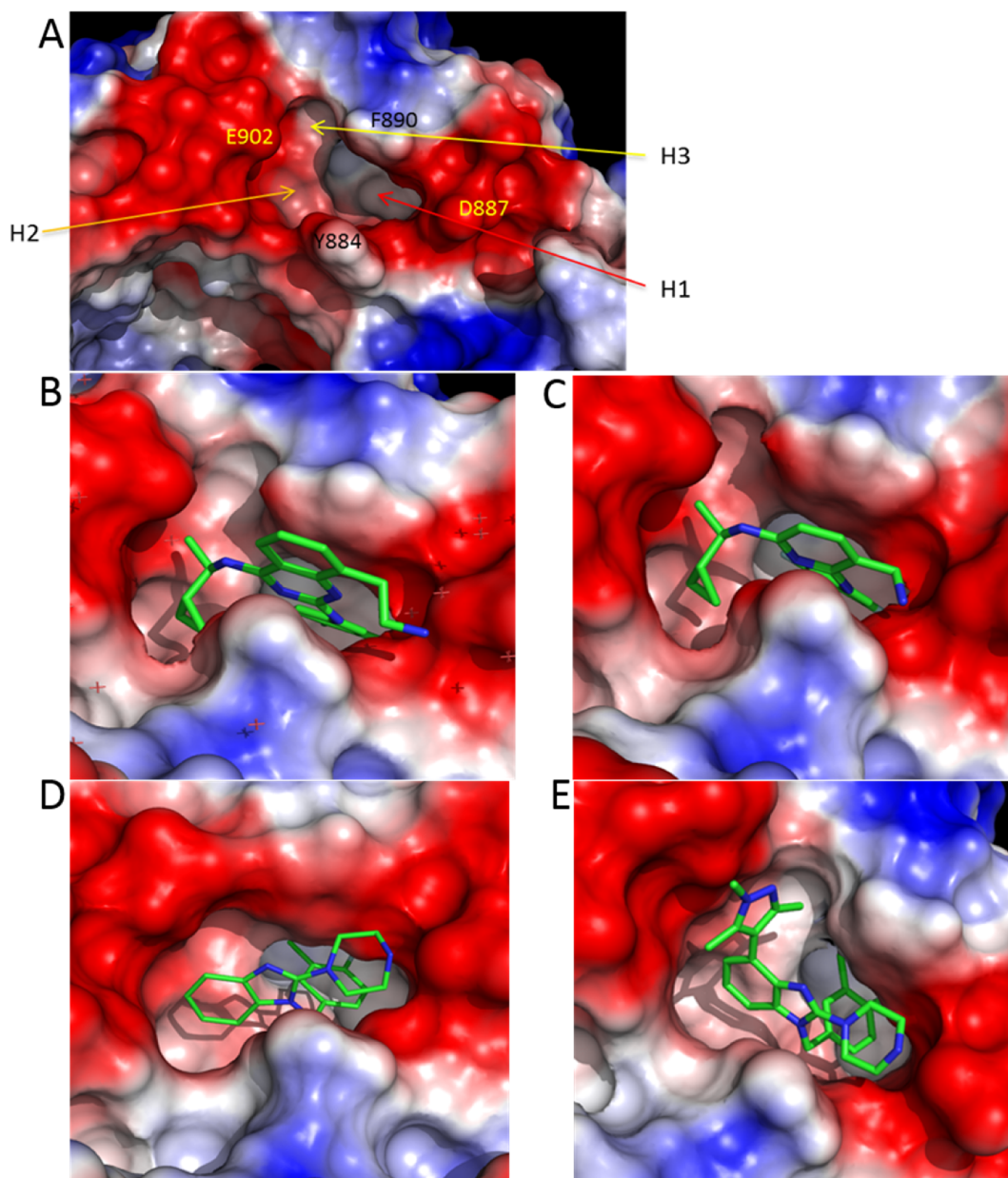


Figure 45. Strategies to design compounds to fill the pocket optimally. A) The binding pocket for the activators with F890 “up”. Three major hydrophobic areas are labeled as H1, H2, H3. Optimized analogs compound VU0652002 (B), VU0657316 (C), VU0549918 (D), VU0651044 (E) binds to the pocket with higher affinity.

For the benzimidazole series, we designed molecules by including the important binding moieties of VU0002032 and VU0120832. As expected, these compounds were more potent. ($EC_{50}=5.4 \mu\text{M}$) (Figure 45D) Additional modifications were made at the 4' position of the benzimidazole core. By adding a 3-methyl-pyrazole group or an alkyl chain with an NH_2 moiety (VU0653057) to reach E902, we were able to further enhance the activity of the compounds. (Figure 45E) The workflow of this mix-and-match strategy is demonstrated in Figure 46.

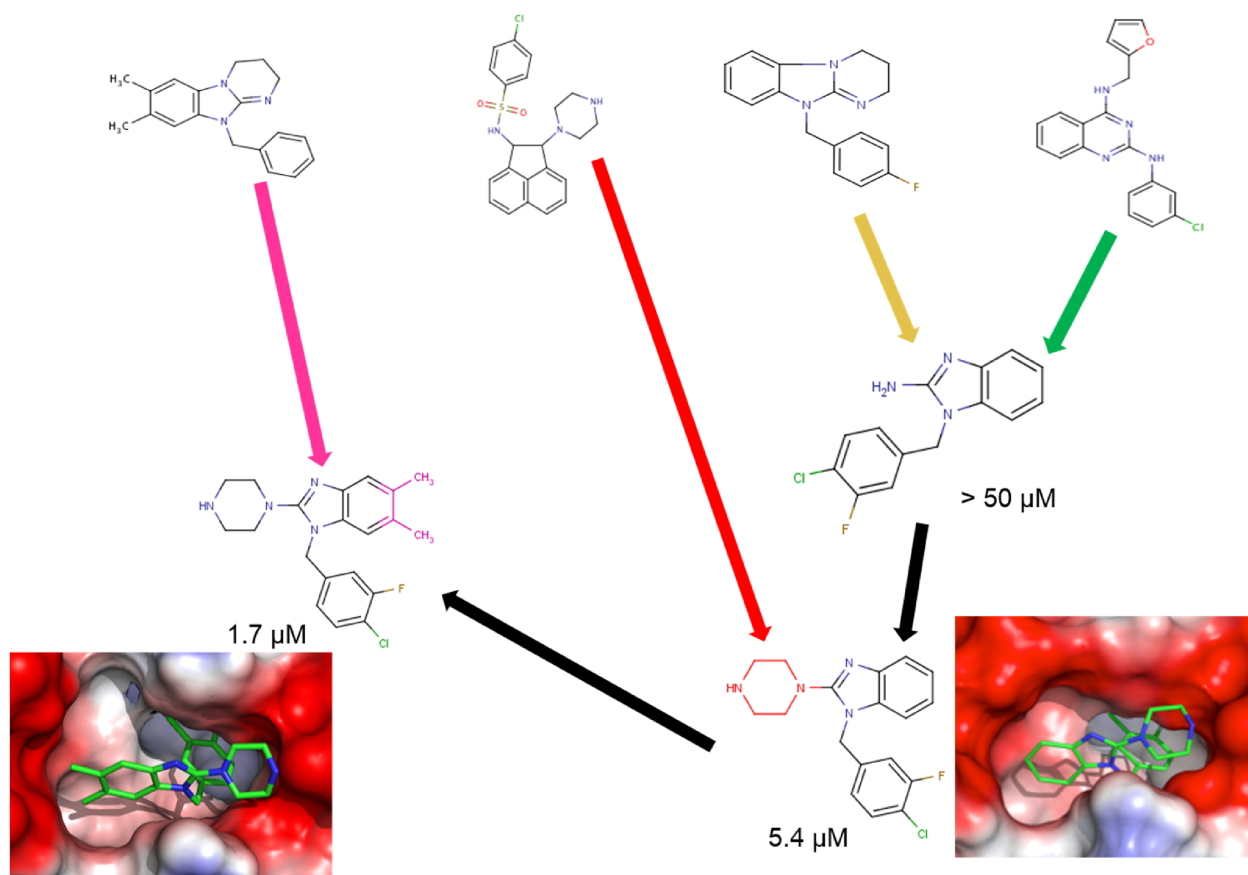


Figure 46. Mix-and-match strategy in designing improved ligands.

Compounds Increase Ras-GTP and Perturb Ras Signaling in Cells

In order to determine if the activators were active in cells, we tested them in different cancer cell lines. First, HeLa cells were treated with FITC-conjugated compound **4** and subsequently washed with PBS. A high intracellular fluorescence signal was observed, confirming that these compounds are suitable for use in cell-based experiments (Figure 47A). HeLa cells were treated for 15 min with DMSO, the inactive compound **5**, or the active compounds **2** and **4** to assess the ability of these compounds to activate endogenous Ras. Ras-GTP levels were determined using a Ras binding domain pull-down assay. No increase in Ras-GTP levels was observed in cells treated with the inactive compound **5**. In contrast, treatment with compound **4** resulted in a threefold increase in Ras-GTP levels (Figure 48A); whereas, compound **2** resulted in a smaller increase, consistent with their relative *in vitro* nucleotide exchange activity (Table 3). Treatment of HeLa cells with 100 μ M compound **4** led to elevated Ras-GTP levels within 5 min that remained elevated for the entirety of a 30-min time course (Figure 48B). These experiments show that the compounds activate nucleotide exchange in the cellular setting containing full-length endogenous SOS and Ras proteins. We determined the effect of compounds **2–5** on Ras-mediated signaling in the MAPK and PI3K pathways. Treatment with compounds **2–4** causes a biphasic response in the MAPK pathway that is characterized by inhibition of extracellular signal regulated kinase (ERK) phosphorylation at high compound concentration followed by a peak of increased ERK phosphorylation as compound concentration decreases (Figure 48C).

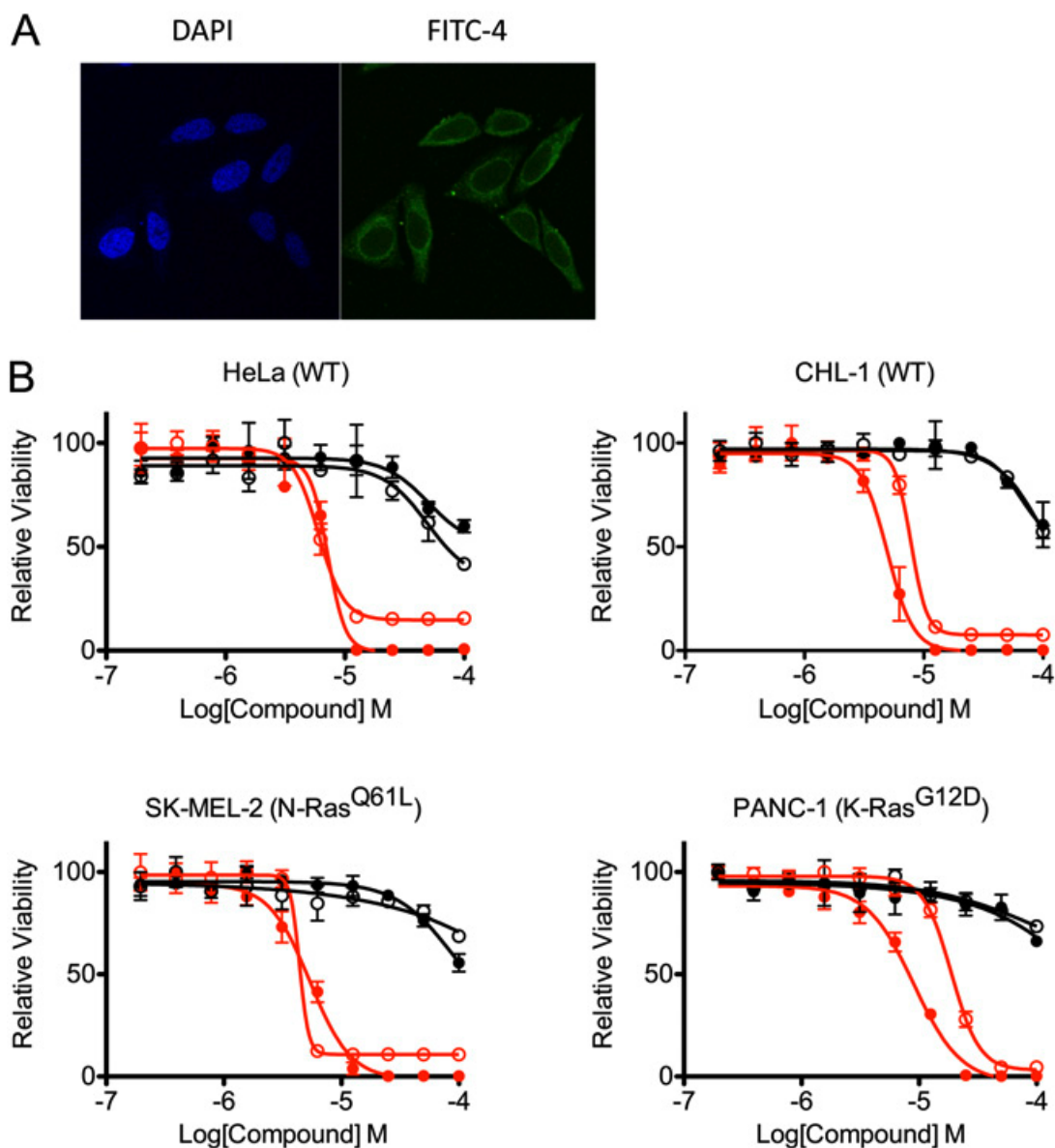


Figure 47. Compounds are cell-permeable and inhibit cell proliferation and anchorage-independent growth. (A) HeLa cells were treated for 30 min with FITC-4, washed 3 times with ice-cold PBS, fixed, mounted, and imaged on a confocal microscope to assess cell permeability. (B) Compounds **4** (red) and **5** (black) were tested for their ability to alter cell proliferation after 3 d (●) or anchorage-independent growth in soft agar after 7 d (○). Data were normalized to DMSO control (n = 3 ±SD). Corresponding IC₅₀ values are presented in Figure 48 F and G.

This signaling pattern is most evident with compounds **3** and **4**. Because of the decreased potency of compound **2**, only the increased ERK phosphorylation is visible in this concentration range. Compounds **2–4** also inhibited PI3K pathway signaling, which was evidenced by a

decrease in phosphorylation of the protein kinase AKT. Importantly, the peak in ERK phosphorylation correlates with the IC_{50} for inhibition of phosphorylation of AKT (Figure 48C), suggesting that the two may be regulated by the same underlying mechanism. As expected, the inactive compound **5** had no effect on ERK or AKT phosphorylation.

The biphasic response in ERK phosphorylation closely resembles the signaling induced by inhibitors of the B-Raf kinase in cells containing WT Raf [141]. To investigate whether they presented the same activation mechanism, we examined the effects of our compounds in melanoma cell lines harboring well-characterized mutations in the Ras pathway. In the context of WT Ras (CHL-1) or N-RasQ61L (SK-MEL-2), the B-Raf inhibitor dabrafenib and compound **4** elicited a biphasic response in both mitogen-activated protein extracellular signal-regulated kinase kinase (MEK) and ERK phosphorylation (Figure 48D). In MALME-3M cancer cells, which harbor a B-Raf^{V600E} mutation, dabrafenib was able to potently inhibit MEK and ERK phosphorylation, which was expected (Figure 48D). Compound **4**, however, had no effect on MEK or ERK phosphorylation, suggesting that this compound acts by a unique mechanism of action at the level of the Ras–SOS interaction, upstream of Raf kinase.

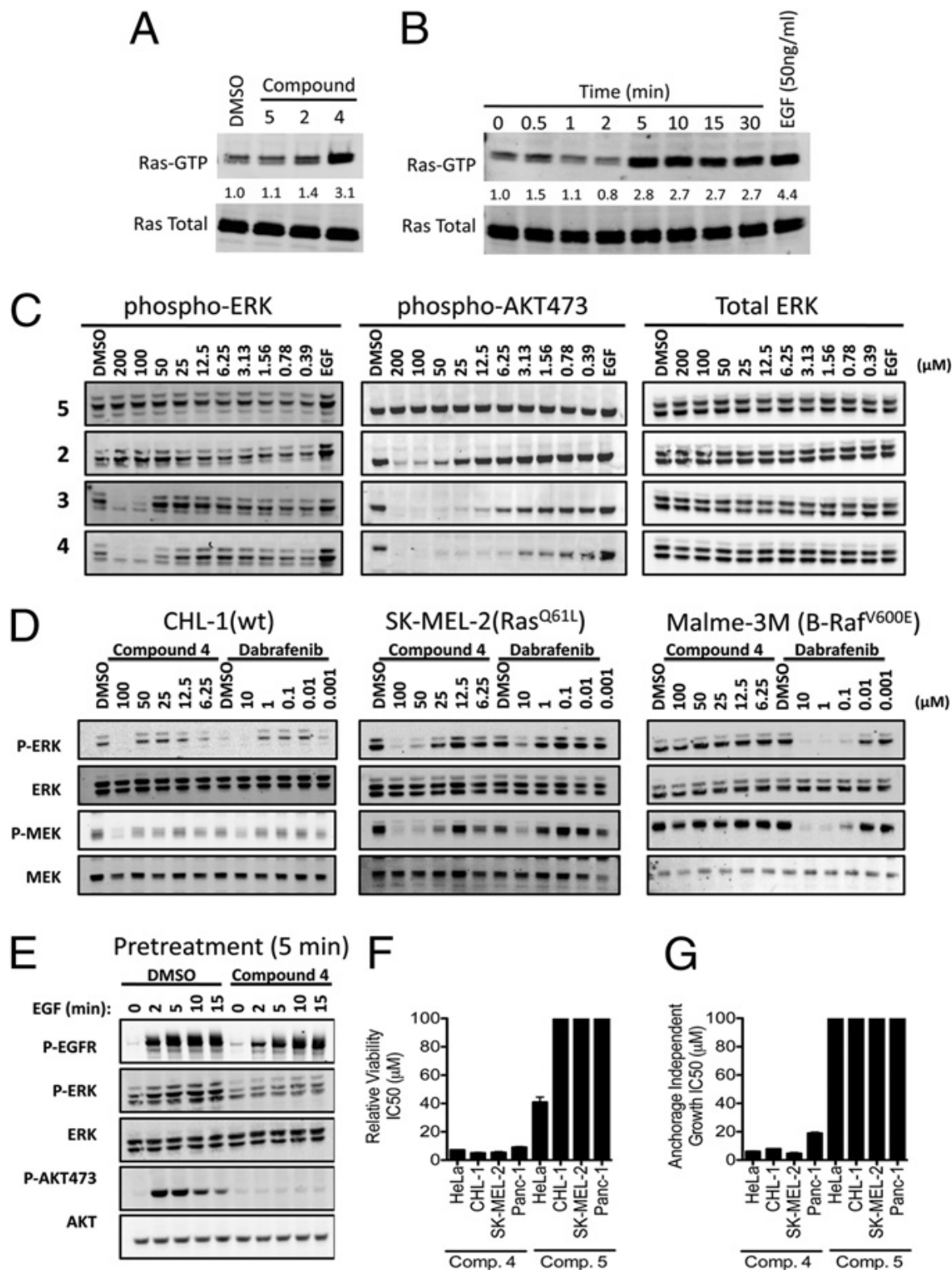


Figure 48. Aminopiperidine indole compounds perturb Ras signaling by acting at the level of the Ras-SOS interaction. (A) Endogenous Ras-GTP levels from HeLa cells treated for 15 min with DMSO or 100 μ M compound 5, 2, or 4. (B) Endogenous Ras-GTP levels from HeLa cells

treated with 100 μ M compound **4** for 0–30 min. (C) HeLa cells treated for 30 min with compounds **2–5** and analyzed by Western blot. EGF (50 ng/mL; 10 min) was used as a positive control. (D) Lysates from CHL-1, SK-MEL-2, and MALME-3M cells treated for 30 min with compound **4** or dabrafenib were analyzed by Western blot. (E) HeLa cells were serum-starved overnight, pretreated for 5 min with DMSO or 100 μ M compound **4**, and stimulated with EGF (50 ng/mL) for 0–15 min. (F) IC₅₀ values for cell proliferation and (G) anchorage-independent growth after treatment with compound **4** or **5**.

To further test the hypothesis that these compounds act at the level of the Ras-SOS interaction, serum-starved HeLa cells were pretreated with DMSO or 100 μ M compound **4** and then stimulated with EGF. Compound **4** prevented EGF-induced activation of MEK and ERK; however, it had no effect on the activation of EGF receptor upstream of Ras, which was shown by an increase in tyrosine 1068 phosphorylation (Figure 48E). These data support the conclusion that the compounds act at the level of the Ras-SOS interaction, downstream of EGF receptor and upstream of Raf, and establish a means to study acute Ras-mediated signaling using an approach that is distinct from other small molecules targeting this pathway. In addition, compounds **4** and **5** were assessed for their ability to affect cell growth and transformation. Consistent with the signaling observed in these cell lines, both WT (HeLa and CHL-1) and mutant (SK-MEL-2 and PANC-1) Ras harboring cancer cells showed a decrease in cell proliferation and anchorage-independent growth after treatment with compound **4** (Figure 48F and G and Figure 47B). In contrast, the inactive compound (**5**) had little or no effect at concentrations up to 100 μ M. This suggests that compounds binding to the Ras:SOS:Ras complex do not enhance cell growth but instead, may represent a mechanism to inhibit cell proliferation and transformation.

Discussion and Conclusion

In summary, small molecules were accidentally discovered that increase the rate of SOS-mediated nucleotide exchange in a GEF-dependent manner. Compounds activate nucleotide exchange regardless of mutation or allosteric activation status, suggesting that activation occurs through a distinct mechanism. Consistent with this hypothesis, the compounds bind to a hydrophobic pocket on the CDC25 domain of SOS, which is adjacent to the switch II region of Ras at the catalytic site of SOS.

Importantly, mutations, both naturally occurred and designed, support the conclusion that this pocket is functionally relevant for regulating the activation of Ras by SOS. This raises an important question: What's the function of this pocket? Are there any natural ligands that bind to this pocket to regulate the nucleotide exchange process? To study the function, we can overexpress a mutant SOS, which doesn't have this pocket, and monitor the outcome. In addition, sequence and structural alignments of the CDC25 domain of SOS1 with other GEF proteins suggest that a similar pocket may exist in other GEFs. Targeting this conserved pocket may represent a unique approach to alter the function of these closely related proteins. In order to search for natural ligands, we can start with a literature search on all the GEFs that have similar pocket. On the other hand, we may use our current activators as template to search for natural ligands that have similar structures. In addition, we can perform a cell-based SOS pull-down experiment, followed by Mass Spectrometry analysis to find out if we can identify any unknown ligands that bind to SOS. By comparing the pull-down products in the presence and absence of the activator molecules, we may be able to identify natural ligands that bind into this pocket. Furthermore, whether the activators affect the membrane localization of SOS, which has been

shown to be important for the activation of Ras, remains to be determined [142].

Based on our *in vitro* biochemical studies, we expected that the treatment of cells with these nucleotide exchange activators would cause an increase in downstream signaling of the MAPK and PI3K pathways. Although, Ras-GTP levels increase after treatment of HeLa cells with the compounds, consistent with the increase in nucleotide exchange activity, we unexpectedly observed a biphasic response in MAPK signaling and inhibition of PI3K signaling.

A similar pattern of biphasic MAPK signaling has been observed in recent studies. B-Raf inhibitors were found to induce a paradoxical activation of MAPK signaling in cells with WT B-Raf, and this effect was intensified by the presence of mutant Ras [141]. In the same setting, compound **4** elicited signaling similar to Raf inhibitor-induced paradoxical activation. However, in contrast to dabrafenib, no effect was seen after treatment with compound **4** in MALME-3M cancer cells, which harbor a V600E mutation in B-Raf. These data suggest that the common biphasic signaling pattern elicited by these two compound classes is brought about through distinct mechanisms. Raf dimerization has been shown to underlie paradoxical activation in the case of B-Raf inhibitors, and although Ras has been implicated in this dimerization event, the biochemical and structural roles of Ras in this process remain to be elucidated [99, 143].

Based on the importance of Ras in Raf inhibitor-induced paradoxical activation and the data presented here, it is tempting to hypothesize that the signaling observed after treatment with compound **4** is regulated at the level of the Ras-Raf interaction. Additional investigation to uncover how these compounds alter other interactions, such as the Ras-Raf interaction, how they affect Ras and SOS localization, and how they influence negative feedback loops governing signal output will be required to fully understand their effects.

In our work, X-ray crystallographic studies provided important information on how the

compounds bind to the protein which was used to rationalize the structure-activity relationships. The observation of additional binding pockets not exploited by the current compounds leads us to believe that additional improvements in activity can be achieved by the design and synthesis of new analogs. Figure 49 demonstrated a few compounds that were designed to better fit the pocket. Compound **Q154**, designed based on the quinazoline series (Figure 49A), fills the H1, H2 and H3 pockets by taking advantage of the structural information from multiples crystal structures. Basic amines were added to interact with D887 and E902, while the ring structure was rigidified to minimize the number of rotatable bonds. The benzimidazole derivative **B211** was also designed by following the same principles. (Figure 49B) Both compounds were predicted by the glide docking program to be more potent analogs.

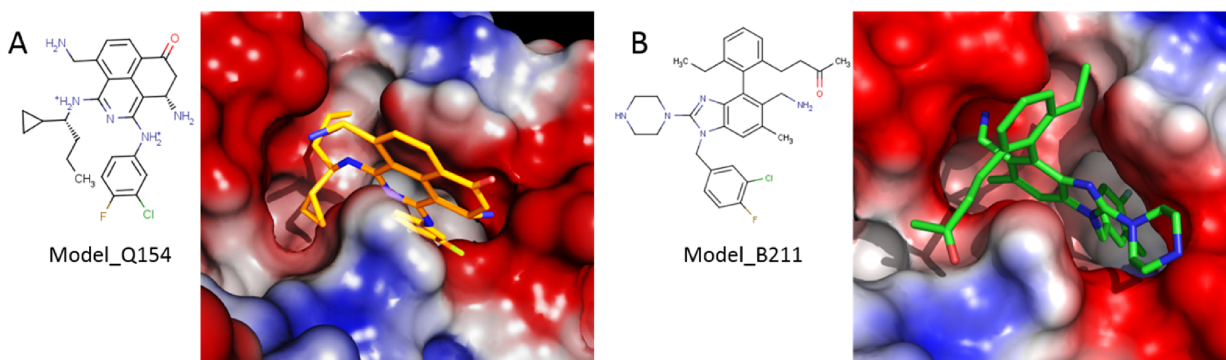


Figure 49. Compounds designed from molecular modeling.

Despite being considered as one of the most validated targets in cancer, the inhibition of oncogenic Ras remains a major challenge. The scientific community has sought unique, functionally active small molecules to provide a path forward for the discovery of Ras-targeted therapeutics [69], and recent work has aimed at validating new strategies to achieve this goal. The identification and characterization of a functionally important small molecule binding site on

the Ras:SOS:Ras complex provides another innovative approach to target Ras signaling. Additional studies on how these compounds work at the molecular level and further investigation of this approach as a way to inhibit Ras function in cells may enable the discovery of therapeutics for the treatment of Ras-driven cancers.

Materials and Methods

Protein Purification

For nucleotide exchange assays, recombinantly expressed K-Ras^{G12D} (referred to as Ras; amino acids 1–169) and human Son of Sevenless 1 [SOS1; a catalytically active form of human SOS1 (SOS^{cat}); amino acids 564–1049 and SOS^{Dbl homology–pleckstrin homology (DH-PH)-cat} (SOS^{DH-PH-cat}); amino acids 197–1049] were purified as described previously [120]. The synthetic gene of K-RasG12D/C118S was cloned into a pDEST-HisMBP vector. The plasmid was transformed into the Rosetta 2 (DE3) *Escherichia coli* strain and expressed, and the His-tagged protein was purified on a Ni-IDA (ProBond; Invitrogen) column. TEV protease was added at a 1:20 molar ratio, and the solution was incubated at 4 °C until cleavage was complete. The reaction mixture was applied to a Ni-NTA column, and the Ras protein was collected in the flow-through. H-Ras was expressed and purified in a similar fashion. Full-length human SOS1 in a Gateway Entry Vector was purchased from Thermo Scientific Open Biosystems. SOS^{cat} and SOS^{DH-PH-cat} were amplified by PCR and cloned with a 5' Tev cleavage site and a 3' stop codon into Gateway Entry Vector pDONR-221. SOS^{cat} was transferred into Gateway expression vector pDEST-17 carrying an N-terminal His6 tag for purification and expressed in BL21- RIL *E. coli* at 18 °C for 7 h

followed by purification on a Ni-IDA column. SOS^{cat} mutants were generated using a Quik-Change method (Agilent) and purified similar to SOS^{cat}. Synthetic murine Ras-GRF1 gene was purchased from GenScript with codon optimization for BL21 bacterial strain and subcloned into pDEST-17 as previously described [144].

For the X-ray crystallographic studies, Ras and SOS^{cat} were cloned and expressed as described above. Ras was further purified using an additional Superdex 75 column. For SOS^{cat}, the terminal His₆ tag was cleaved, the mixture was applied to a Ni-NTA column, and SOS^{cat} protein was collected in the flow-through. Concentrated SOS^{cat} was then applied to an HiTrap Q column (5 mL). H-Ras^{Y64A}(GppNHp) was prepared by first incubating concentrated protein with 10 mM EDTA for 30 min at 37 °C. EDTA was removed by buffer exchange, 2.5 mM GppNHp was added with apyrase (5 μL/mL; Sigma), and the mixture was incubated at 37 °C for 2 h; 5 mM MgCl₂ and an additional 2 mM GppNHp were added, and the H-Ras^{Y64A}(GppNHp) was purified using a Superdex 75 column. The H-Ras^{WT}:SOS^{cat}:H-Ras^{Y64A}(GppNHp) complex was prepared as described previously [15]. H-Ras^{WT} and SOS^{cat} were dialyzed into a buffer containing 25 mM Tris·HCl (pH 7.5), 50 mM NaCl, and 2 mM DTT. The H-Ras:SOS^{cat} binary complex was prepared by adding four-fold excess of H-Ras^{WT} to SOS^{cat} in the presence of EDTA. The mixture was incubated overnight at 4 °C, and the SOS^{cat}:Ras binary complex was purified using a Superdex 200 column. The binary complex was concentrated; a four-fold excess of H-Ras^{Y64A}(GppNHp) was added, and the mixture was incubated at 4 °C for 2 h. The H-Ras^{WT}:SOS^{cat}:H-Ras^{Y64A}(GppNHp) was then purified using a Superdex 200 column. The cdc25 domain of SOS (752-1046) was inserted into a donor vector (pDONR-221) and transferred by recombinational cloning into the pDEST-HisMBP vector for expressing a fusion protein. The His₆-MBP-cdc25 protein was expressed in BL21 (Ril) *E.coli* strain by induction with 0.2 mM

IPTG at a cell density corresponding to the absorbance of $OD_{600}=1.0$. The fusion protein was purified on a Ni-IDA (ProBond from Invitrogen) column. TEV protease was added at a 1:20 molar ratio, and the solution was incubated at 4°C overnight. The reaction mixture was applied to a Ni-NTA column, and the cdc25 protein was collected in the flow-through and concentrated to 35 mg/mL.

Protein Crystallization

H-Ras^{WT}:SOS^{cat}:H-Ras^{Y64A}:GppNHp was exchanged into a buffer containing 25 mM Tris, 50 mM NaCl, and 2 mM DTT (pH 7.5) and concentrated to 25 mg/mL. Protein: ligand complexes were prepared by adding a concentrated DMSO stock solution of the ligand to a final concentration of 2–5 mM. All crystallization experiments were set up using the Mosquito crystallization robot (TTP Labtech) or performed manually using the hanging-drop vapor diffusion method at 4 °C. The apo ternary complex crystallized from 0.1 M sodium acetate and 1.8 M sodium formate (pH 4.5). Crystals appeared within one week. To obtain co-crystal structures of ternary complex with compound **2**, apo crystals were transferred into a reservoir solution containing 20 mM compound **2** and soaked overnight. The ternary complexes containing compounds **1** and **3** crystallized under conditions containing 0.1 M sodium acetate and 2.0 M sodium formate (pH 4.0). The activators from the HTS screen co-crystallized with either H-Ras^{WT}:SOS^{cat}:H-Ras^{Y64A}(GppNHp) ternary complex or H-Ras^{WT}:SOS^{cat} binary complex from a series of conditions containing 1.8-2.2M sodium formate (pH 4.0-4.5) and 0.1 M sodium acetate. The cdc25 domain co-crystallize with VU0002032 in the condition of 0.1 M MgCl₂, 25% PEG 3350, 0.1 M Tris-HCl pH 7.5.

X-Ray Data Collection, Structure Solution, and Refinement

X-ray diffraction data were collected at 100K using synchrotron radiation (beamline 21 LS-CAT; APS). Data were processed with HKL-2000, and structures were determined by molecular replacement using the coordinates of H-Ras^{WT}:SOS^{cat}:H-Ras^{Y64A}(GppNHp) (PDB entry: 1NVV and 1NVX).. The program package CCP4 [128] and Phenix [129] were employed for phasing and refinement, and model fitting was performed with COOT [130]. The refined models were validated with PROCHECK and Phenix.

Nucleotide Exchange Assays

Nucleotide exchange assays were conducted using BODIPY-GDP (Life Technologies) - loaded Ras in a buffer containing 25 mM Tris (pH 7.5), 50 mM NaCl, and 1 mM MgCl₂. Baseline fluorescence was recorded for 10s followed by the addition of compounds or Ras^{Y64A} when specified. A second addition of excess GTP ± SOS^{cat} was performed at 120 s. Nucleotide exchange was monitored as a decrease in fluorescence with time. Final reactions contained 1 μM BODIPY-GDP- loaded Ras, 200 μM unlabeled GTP, and 0.5 μM SOS^{cat} or 1 μM SOS^{cat}. Alternative guanine nucleotide exchange factors and compounds were used as indicated. Changes in fluorescence were monitored using a Hamamatsu FDSS 6000 with readings conducted every 3 s for 30 min. Assays were conducted using 40 μL final volume in a 384-well clear-bottom black Aurora microplate. Raw fluorescence data were fit to a single exponential decay function using XLfit (IDBS) software. Derived rates were plotted as mean ± SD. EC₅₀ values were calculated by plotting derived rates as a function of compound concentration and fit using a four-parameter dose-response curve (XLfit). Relative nucleotide exchange activation

was calculated as the percent activation for each compound at 100 μ M normalized between exchange rates calculated for DMSO or saturating amounts of compound **4**, which served as an internal control. All raw nucleotide exchange traces presented were normalized to the mean fluorescence per well before the addition of the compound and graphed using Prism 5 (Graph Pad Software Inc.). Rates were derived from raw fluorescence data.

Fluorescence Anisotropy Binding Assays

Fluorescence anisotropy assays were performed in a black, 384-well, flat-bottom plate (Greiner Bio-One) using an EnVision plate reader (PerkinElmer) as described previously.[145] [146] For saturation binding experiments, FITC-conjugated compound **2** (FITC-**2**) or FITC-conjugated compound **4** (FITC-**4**) was incubated with increasing amounts of SOS^{cat} in a buffer containing 50 mM NaCl, 25 mM Tris (pH 7.5), and 1 mM MgCl₂. Final wells contained 25 μ L volume with 300 nM FITC-conjugated compound present. Reactions were incubated for 20 min, and anisotropy measurements were taken using an excitation wavelength of 480 nm and an emission wavelength of 535 nm. Data were analyzed using Prism 5 (Graph Pad Software Inc.). Curves were fit, and dissociation constants were determined using a single-site binding model (one-site total binding). For competition experiments, serial dilutions of compounds were added to a well containing 10 μ M SOS^{cat} and 300 nM FITC-**4** (final concentrations) and incubated for 20 min before measurement on the EnVision. Data were analyzed by plotting fluorescence anisotropy values as a function of compound concentration. IC₅₀ values were determined using a four-parameter dose–response (variable slope) equation in Prism 5 (Graph Pad Software Inc.). NMR Compound binding was detected by ¹H/¹⁵N selective optimized-flip-angle short-transient heteronuclear multiple quantum coherence spectra [136]. Each sample contains 50 μ M K-Ras

protein, and dissociation constants were obtained by monitoring the chemical shift changes of resonances as a function of compound concentration.

Cell-Based Assays

HeLa cells, cultured in DMEM supplemented with 10% (vol/vol) FBS, were treated with DMSO control or compound as indicated. Lysates from each sample were analyzed by SDS/PAGE and Western blotting using Immobilon-FL PVDF membranes (Millipore) and scanned on an Odyssey imager (LiCor). Levels of endogenous Ras-GTP were determined using a Ras binding domain pull down assay according to the manufacturer's protocol (Millipore). Antibodies for ERK, phospho- ERK, MEK, phospho-MEK, AKT, phospho-AKT473, and phospho-EGF receptor (Y1068) were obtained from Cell Signaling. Pan-Ras antibody used for Ras-GTP pull-down assays was from Millipore.

CHAPTER V

DISCUSSION AND PERSPECTIVE

Significance

Cancer is one of the leading causes of death worldwide; it accounts for 13% of all deaths. Effective therapy is a critical need for cancer patients. Almost 40 years after the “War On Cancer” was declared, the discovery of anti-cancer drugs remains a highly challenging endeavor due to the heterogeneous nature of the disease [147].

Ras is a key signaling molecule in living cells. Mutations in K-Ras fix the protein in the active state and endow cells with capabilities that represent the hallmarks of cancer [4, 37]. These include the ability to proliferate, evade apoptosis, reprogram cell metabolism, induce angiogenesis, activate invasion and metastasis, and escape immune destruction [5]. Aberrant Ras signaling is involved in 30% of human cancers [34]. Inhibition of Ras activity can revert the malignant phenotype in the animal models. Taken together, Ras represents a well-validated anti-cancer target.

The problem is that Ras proteins themselves have been traditionally considered “undruggable”. We cannot easily find pockets on the protein surface by simply looking at the crystal structure of Ras. Major pharmaceutical companies as well as academic labs have performed a significant amount of work to target Ras. However, no effective treatment against Ras has been identified yet.

Identify small molecule inhibitors bind to K-Ras using fragment-based screen

My work was focused on identifying a way to target Ras. Using fragment-based approaches, I discovered several series of small molecules that bind to Ras. These compounds induce a ligand-binding pocket, which cannot be observed in the ligand-free form of Ras. In the X-ray structures of K-Ras/inhibitor complexes that we obtained, a secondary binding cleft was observed that is electronegative in character and contains two acidic residues, Glu-37 and Asp-38. To bind to this region of the protein, we synthesized amide linked amino acid analogs of indole-benzimidazoles. Improved binding to K-Ras was achieved for several of these analogs. The best compound in this series binds to K-Ras with an affinity of 190 μ M. Furthermore, these compounds inhibit SOS-mediated nucleotide exchange of Ras. These studies provide the first reported examples of high-resolution Ras/small-molecule co-crystal structures and reveal opportunities for discovering ligands with higher affinity.

A method for second-site screen using covalently attached first-site ligand

To further optimize the compounds, I conducted a second-site screen. At first, I encountered a major problem: The first-site binders were too weak to block the first-site pocket. Therefore, the interpretation of the “second-site” hits from a conventional the screen was complicated. To solve this problem, I developed a novel method for second-site screening that utilizes engineered cysteine residues located near the first-site pocket. By covalently linking a thiol-reactive molecule to the cysteine, I successfully placed a benzimidazole moiety into the first-site pocket on K-Ras and fully saturated this pocket. This method can be applied to other targets in which the first-site pocket cannot be fully saturated. Using this method, I identified multiple series of second-site hits. Crystal structures of some of these hits complexed with K-Ras

revealed a distant binding pocket located near the guanine nucleotide. Although the ligands in the new binding pocket are too far from the first-site ligands to be linked together, they are very close to the guanine nucleotides and Mg^{2+} . Inspired by the previous work on the discovery of irreversible inhibitors against K-Ras G12C -the most prevalent K-Ras mutation in lung cancer (found in 7% of all lung cancer patients) [89], we plan to grow the ligands that we identified to covalently attach to Cys-12 in the Ras G12C mutant protein.

Alternative approach for targeting Ras using nucleotide exchange activators

In addition to these studies, we identified compounds that activate the nucleotide exchange at low micromolar concentration, but paradoxically inhibit the downstream signaling of Ras through an unknown mechanism. Co-crystal structures uncovered a novel binding site on SOS near the Ras-SOS binding interface. Guided by the structures, we designed and synthesized compounds with improved activities both in the nucleotide exchange assay and cell-based experiments.

Issues and Challenges

The most critical issue in targeting Ras directly is to obtain high-affinity ligands. Although we have improved our molecules using structure-based design, the best ligands so far are still too weak for extensive testing in cell-based experiments. We have synthesized over 2000 analogs based on the initial hits, including indole, phenol and sulfonamide analogs. However, no substantial improvement in affinity was achieved. The main reason is the lack of deep,

hydrophobic pocket on the surface of Ras protein. Based on the crystal structures, we could not identify any apparent binding site close to the first-site binding pocket. Although we conducted the second-site screen and identified additional hits, the hits obtained in the second-site screen bound to a pocket (S3 site) on the other side of the switch II helix. Linking the first-site and these second-site binders appears to be quite difficult due to the long distance between them. However, one potential use of the second-site hits that bind to the S3 site is to growth these ligands towards the guanine nucleotide to covalently attack Cys-12 in a K-Ras G12C mutant. However, irreversible inhibitors have a lot of limitations, such as low specificity and high toxicity [148]. Also, in the case of Ras, the G12C/G13C mutation only represents a relatively small percentage of all Ras mutations, which limit the application of this approach. A potent, non-covalent inhibitor in this pocket would be more useful. Compared to the first-site pocket, the S3 pocket is deeper and more hydrophobic, and this pocket is adjacent to a secondary binding cleft near the nucleotide binding site, which provides potential space for ligand growing. A recent report of Ral inhibitors further supports the hypothesis that the S3 pocket alone may provide enough binding energy for discovering high-affinity ligands. The Ras-like GTPase Ral is an important driver of tumor growth and metastasis. Using *in silico* screening, Chao et al. identified small molecules that bind to the Ral GTPase and inhibit the function of Ral *in vitro* and *in vivo* [149]. Figure 50 shows a docking model of how the inhibitor **RBC6** binds to Ral GTPase. Interestingly, the predicted binding site of **RBC6** roughly overlaps with the S3 pocket of Ras, suggesting that the S3 pocket is quite conserved among the members of the Ras subfamily and may accommodate high-affinity ligands. The key to discover high-affinity ligands using fragment-based method is to identify compounds that bind differently but close to the S3 pocket so that they can be merged or linked together for higher affinity. Although we have identified multiple chemical series of

compounds from the second-site screen, only amino-cyano-thiophene compounds were successfully co-crystallized. Thus, a major focus of future studies is to obtain co-crystal structures of other chemical series.

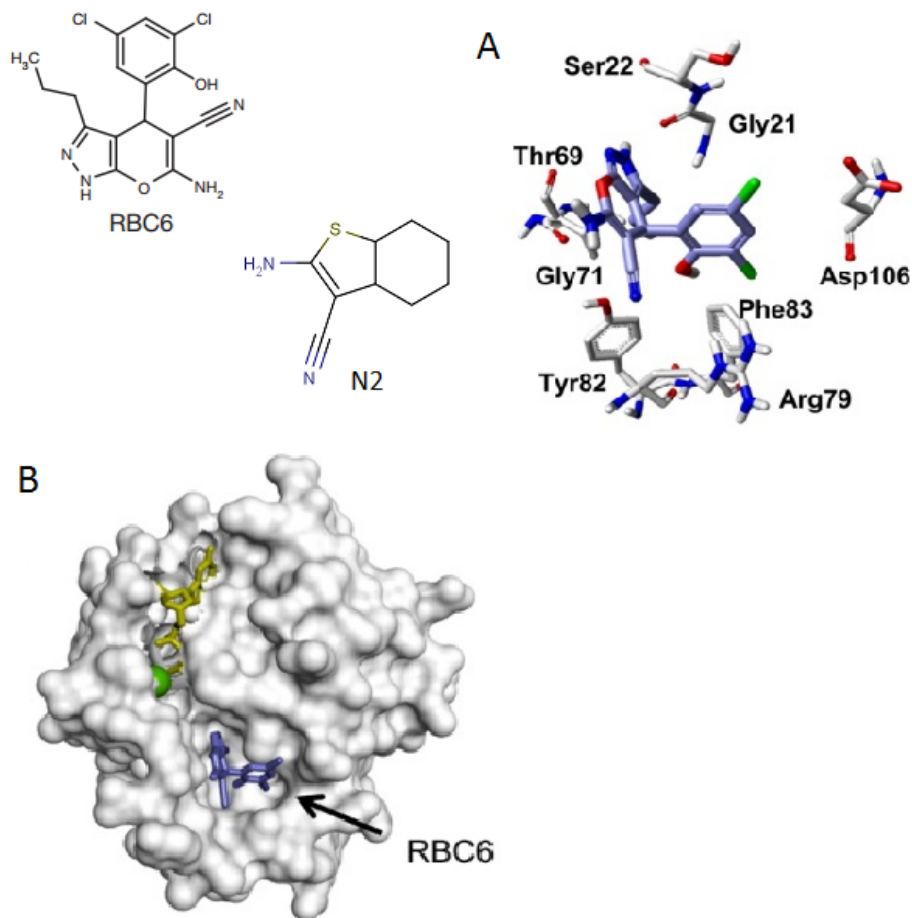


Figure 50. Molecular docking model of inhibitor binding to GDP-bound RalA is shown in stick (A) and surface (B). Notably, compound **RBC6** has some similar feature compared with the K-Ras S3 binder **N2**. (This figure is adapted from Chao et al. [150])

While NMR experiments confirmed that the hits from the second-site pocket bind to the unmodified Ras protein, a co-crystal structure was never obtained without the covalently tethering to Cys-39. This raises the concern that the second-site pocket may be highly dynamic and may only be stabilized by saturating the first-site pocket. In that case, targeting the first-site

and the second-site simultaneously may be necessary. Interestingly, the published crystal structure of K-Ras bound to the irreversible inhibitor **S6** (PDB entry: 4M22) revealed a virtually identical conformation compared to our K-Ras structure with the indole-based K-Ras inhibitors. Therefore, we expect that the irreversible inhibitor **S6** and indole-based K-Ras inhibitors can bind simultaneously. An example of the linking models without covalently attaching to Cys-12 is shown in Figure 51. With only a couple of carbon atoms, we may be able to link them together. This approach may lead to not only significant gains in affinity but also provides a direct path to reach Cys-12 and Mg^{2+} . A rigid linker with the optimal length is required to connect and S3 ligands with other pieces together. The linked compound is expected to lock K-Ras in the inactive state by interfering with GTP binding and inhibit the nucleotide exchange.

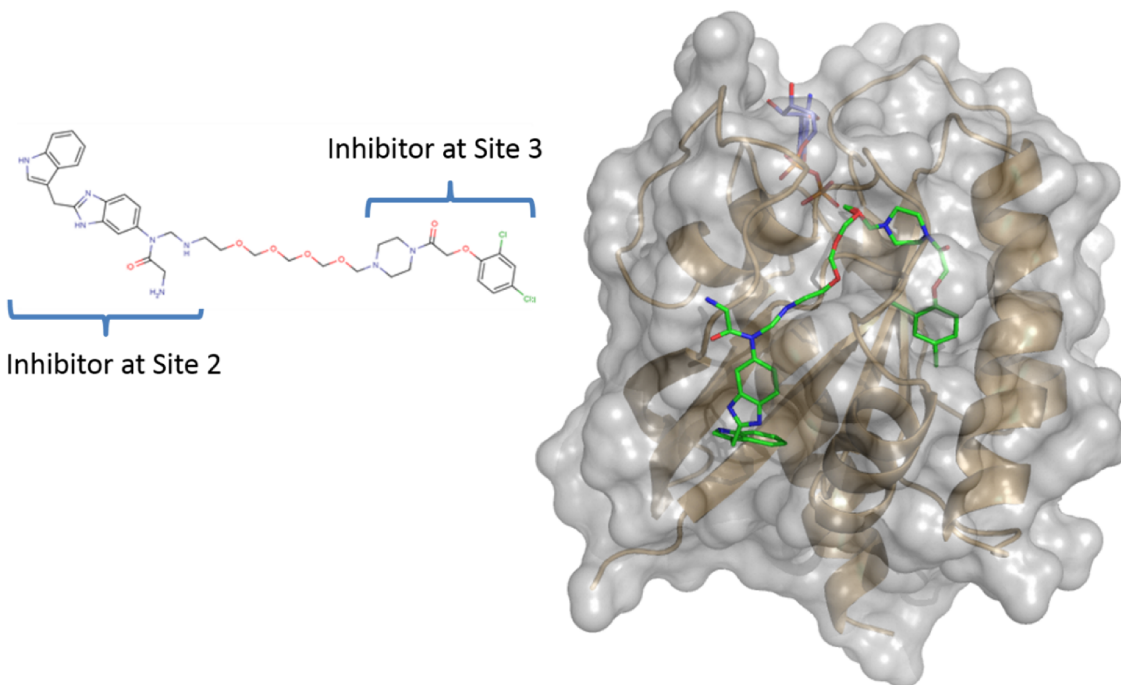


Figure 51. Connecting site 2 and site 3 by modeling. The crystal structure of K-Ras linked to compound **S6** (PDB entry 4M22) and indole compound bound K-Ras structure (PDB entry 4EPY) perfectly overlaps. A flexible linker is designed to connect the indole-based inhibitor at site 2 and the compound **S6** at site 3.

We identified compounds that bind to a novel pocket on SOS near the Ras:SOS binding interface. These compounds activate the SOS-mediated nucleotide exchange but paradoxically inhibit the downstream signaling of Ras and induce cell death. Although the binding affinity of these compounds can be optimized to sub-micromolar affinities, two major issues remain. The first issue is that the mechanism of how the activators enhance the catalytic activity of SOS on nucleotide exchange has not been determined. This mechanism of action may help in the design of more potent compounds, or turn the nucleotide exchange activators into inhibitors. From the crystal structures, SOS-CDC25, SOS:Ras binary complex and Ras:SOS:Ras ternary complex share the same conformation around the binding pocket when bound to a ligand. No structural changes can be observed between ligand-bound and ligand-free structure. All the crystal structures only display static pictures and may not reveal any conformational changes in the solution. A solution-based experiment is needed to solve this problem.

The unknown cellular mechanism behind this paradoxical inhibition is another major problem. A clarified answer would be extremely helpful, especially if we plan to convert the current nucleotide exchange activator into inhibitors. Will a nucleotide exchange inhibitor inhibit downstream Ras signaling in the cell, or activates it?

All the effort discussed above involve interfering with GDP-GTP exchange on Ras. However, the basis of developing GDP-GTP exchange inhibitors is debatable [69, 150]. Oncogenic Ras is locked in its active state and might be less dependent on GEFs for activation [151, 152]. Consequently, inhibition of the Ras-GEF interaction predominantly targets wild-type Ras, which raises the question of whether the inhibition of GEFs represents a promising strategy for the treatment of tumors harboring oncogenic mutant Ras proteins. Although these types of molecules might have little effect on mutant Ras, they can still be beneficial by inhibiting wild-

type Ras function [153]. Mutant and wild-type Ras may have divergent roles in regulating downstream signaling [150]. Growing evidence suggests that, in the presence of mutated Ras, wild-type Ras alleles can show either tumor-suppressive or tumor-promoting activity [153-157]. The diverse roles of wild-type Ras highly depend on the cellular context and the involved Ras isoforms. Hence, a precise understanding of the interplay between the different Ras forms within the signaling network of Ras-dependent cancer cells is essential to elucidate whether selective targeting of mutated Ras is sufficient for therapeutic success.

An alternative approach is to target the Ras-effector interactions. Although small molecules have been reported to target GTP-bound Ras [158-161], these compounds lack potency, and future research needs to explore whether the identified binding pocket can be expanded and filled with chemical matter to yield inhibitors with high affinity. In our experience, a fragment-based screen against GppNHp-bound K-Ras only produced a few weakly bound hits, which indicate that the active form of Ras may be more difficult to target. In addition, the mutation sites on Ras do not overlap with major effector-binding interfaces, suggesting that targeting specific Ras mutants (except G12C, G13C) would be difficult.

Novel approaches

Currently, targeting downstream signaling of Ras is probably the best bet. At least a half-dozen small molecule inhibitors against Raf and more compounds against MEK have been clinically evaluated, and some of them have been approved by the FDA. However, most of them have difficulties against tumors carrying Ras mutations. It is beyond doubt that the central role of

Ras in cancers is irreplaceable and inhibiting Ras may end up being a necessary task that we must accomplish.

Drugging the “undruggable” is an extremely challenging task. Although a few milestones have been reached, we are still far from completing the mission. New approaches may be needed to overcome this difficult problem.

Hybrid Peptide

One approach that may succeed is a hybrid peptide approach using stapled helix peptides containing unnatural amino acids. Stapling can significantly improve the pharmacologic performance of peptides, increasing their binding affinity, proteolytic resistance, and serum half-life while enhancing their ability to penetrate the cell membrane through endocytic vesicle trafficking [162]. Stapled helical peptides are suitable for those targets that lack the deep hydrophobic pockets for small molecule intervention.

Several stapled helical peptides have been reported to bind to Ras. An HBS peptide derived from SOS α H helix (929-944) binds to Ras with an affinity of 28 μ M and inhibited Ras signaling in the cell [83]. However, it still only binds weakly to Ras.

Our lab has recently applied fragment-based screening to aid in the design of more potent stapled helix peptide [163]. We have conducted a fragment screen on RPA70N and identified small molecules that bind to the hotspots on the protein. In the discovery of a stapled peptide inhibitor, we utilized the structure-activity relationship information of these small molecules. Replacing a phenylalanine with an unnatural amino acid containing a 3,4-dichloro substituted phenyl ring was found to bind over 100 fold better to RPA70N compared to the original peptide.

We may apply this strategy on Ras. Figure 52 depicts a model of linking the HBS peptide to one of our inhibitors. The hybrid peptide is expected to have a higher affinity.

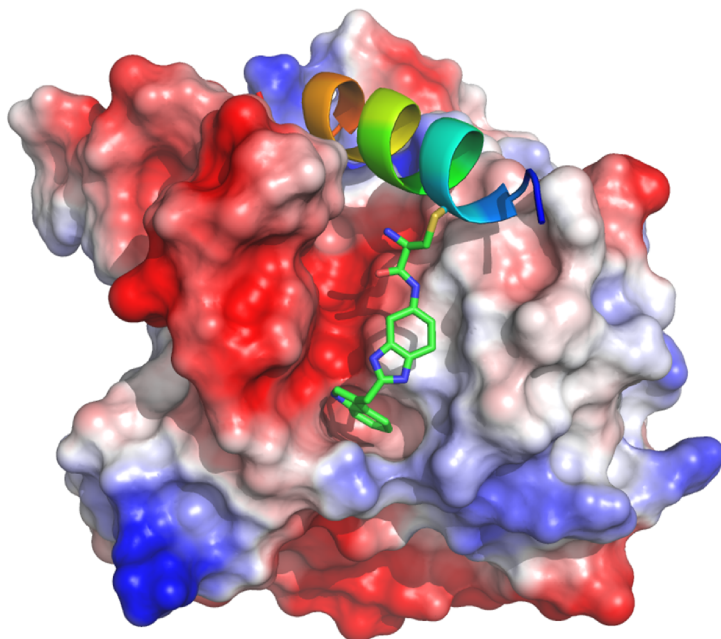


Figure 52. Design a hybrid peptide to inhibit Ras. Modeling showing that an indole-based Ras inhibitor can be linked to HBS peptide easily with a short linker.

Interfacial inhibitor

Another possible approach is to design an interfacial inhibitor [164]. An example of an interfacial GTPase:GEF inhibitor is provided by Brefeldin A, which targets the Arf1:Sec7 domain complex [165] This demonstrates an unconventional way to of inhibiting small G-proteins. (Figure 53A) Arf1 is a small G-protein with ARNO as its cognate GEF. Through an uncompetitive mechanism, small molecule inhibitors either derived from a natural product [166], or from an *in silico* screen [167], trap Arf1-GDP and ARNO into an abortive complex that cannot proceed to the subsequent nucleotide dissociation step. These inhibitors do not show affinity to either Arf1-GDP or ARNO alone, providing an example of an interfacial inhibitor. Given the fact that inhibiting protein–protein interactions is thermodynamically challenging,

stabilizing an abortive complex rather than breaking up a protein–protein interaction might represent a more viable strategy.

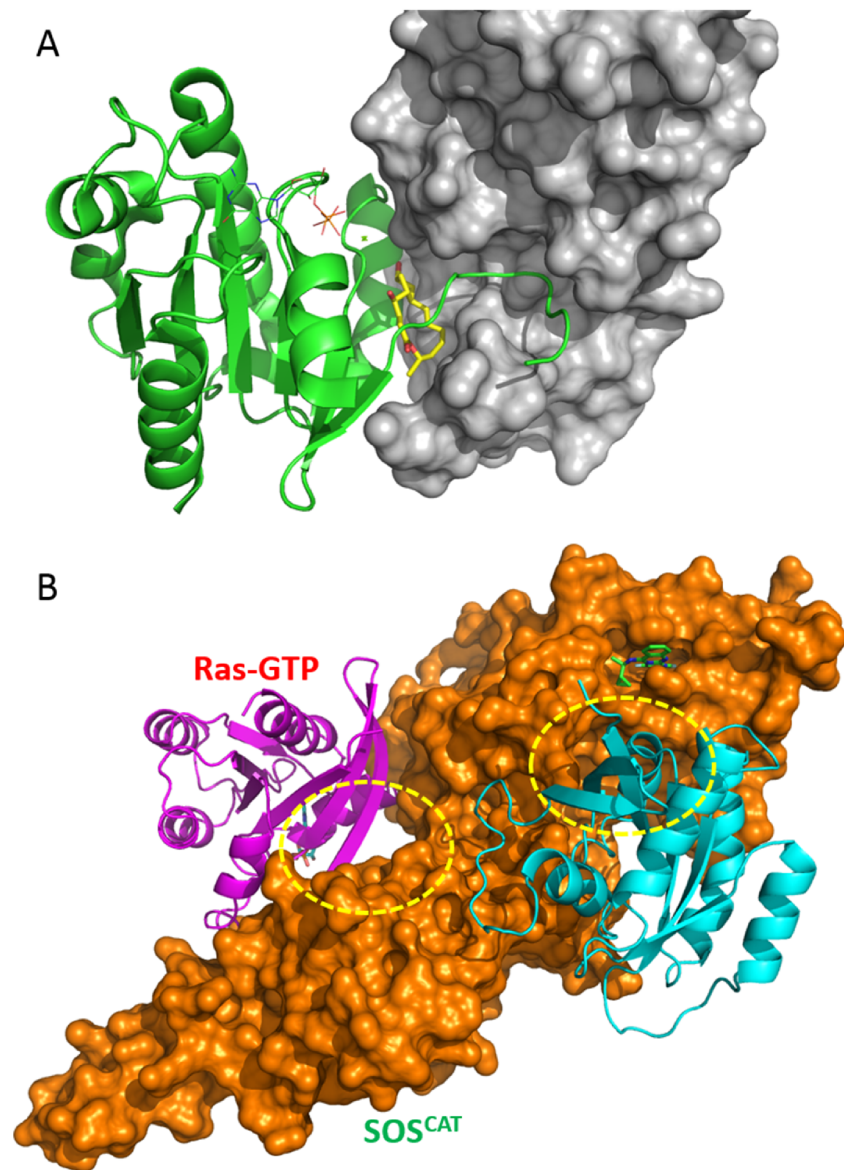


Figure 53. Identify interfacial inhibitors of Ras. (A) Brefeldin A (yellow) sequesters the ARNO/Arf1 complex and inhibits nucleotide exchange. (B) Ras:SOS:Ras ternary complex, potential interfacial binding pockets are marked with yellow circle.

Similarly, an interfacial inhibitor, anchored in this newly identified pocket on SOS, may render Ras incapable of engaging effector proteins by forming a dead end GEF:GTPase complex.

To apply this strategy, a different set of tools may be needed to screen the complex of Ras with its interacting partners, such as SOS, Raf, and PI3K. For an example, we may need to screen for small molecules that bind to the Ras:SOS binding interface. (Figure 53B) Such molecules may stabilize the ternary complex and prevent the turnover of the Ras.

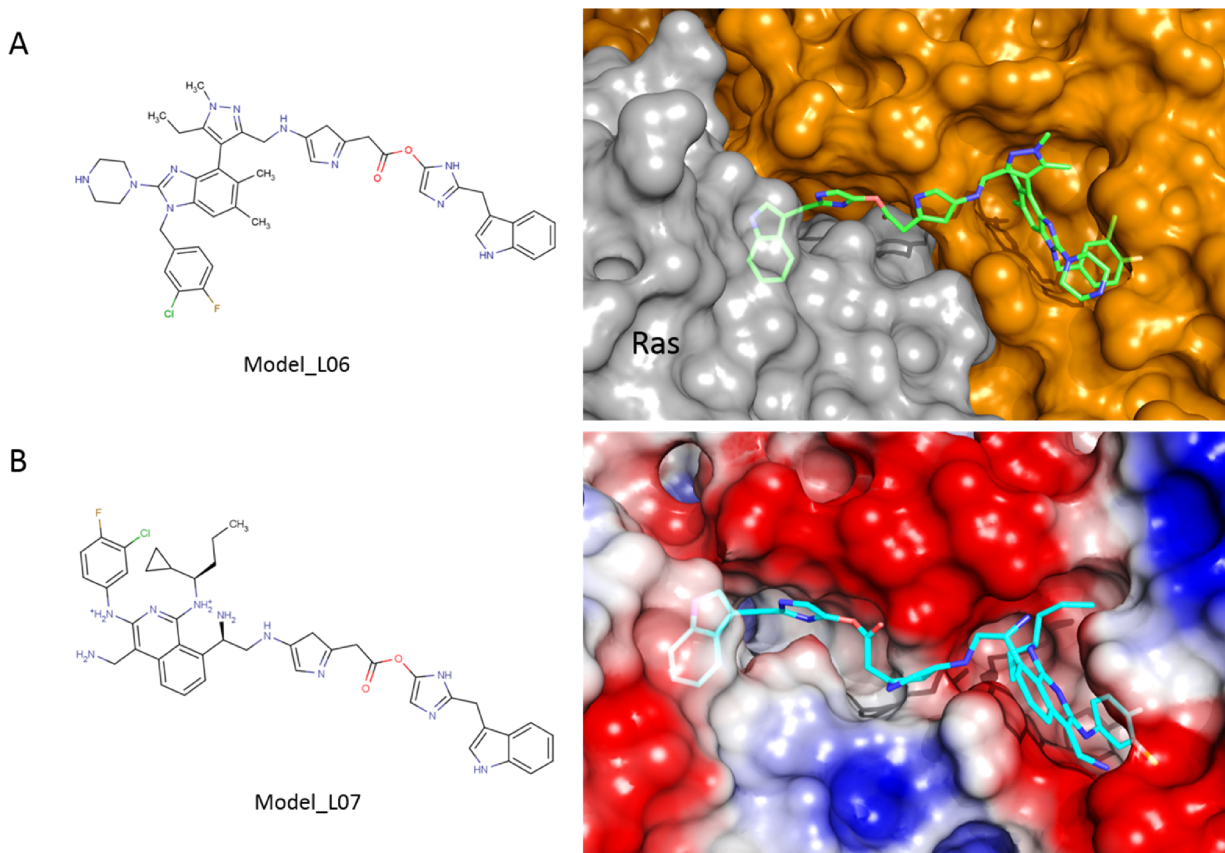


Figure 54. Linking the activators to an indole on Ras with flexible linkers.

A significant amount of modeling work was employed in designing ligands that bind to Ras:SOS complex and inhibit the nucleotide exchange instead of activate it. Nevertheless, due to the paradoxical signaling of pERK and pAKT in response to the activators, it is not clear how Ras downstream signals would respond to interfacial inhibitors. A high affinity tool molecule

can be extremely helpful in studying the mechanism of action. One way to design the inhibitor is to extend the activator molecules into the Ras:SOS interface and block the binding of Ras. However, this can be very difficult to achieve without another fragment that binds to SOS at the binding interface to act as an anchor. Notably, the ligand binding pocket on Ras, which was previously described to be occupied by our indole-based inhibitors, is in the vicinity of the activator pocket. We can use a flexible linker to connect the indole to an optimized activator on SOS. (Figure 54A, B)

Most recently, some encouraging results have been published by a research group from AstraZeneca [168]. They applied fragment soaking method to Ras:SOS binary complex crystals and identified several small molecule binding pockets, including the one previously described in Chapter IV. Most importantly, they found small molecules bind to the “indole pocket” on Ras while also making contacts with SOS. (Figure 55A) The distance between these molecules and the activator pocket on SOS is less 8 Å. (Figure 55B) Using molecular modeling, we can design a linker that is either flexible (Figure 55C) or rigid (Figure 55D) to connect these two pieces together. The linked compounds (**L06**, **L07**, **L21**, **L45**) are expected to have very high binding affinities and presumably “glue” the complex together to create a non-productive complex. Although it appears that these compounds will break the “Lipinski's rule of 5”, with further optimization, they may be useful as tool compounds or potential drug candidates.

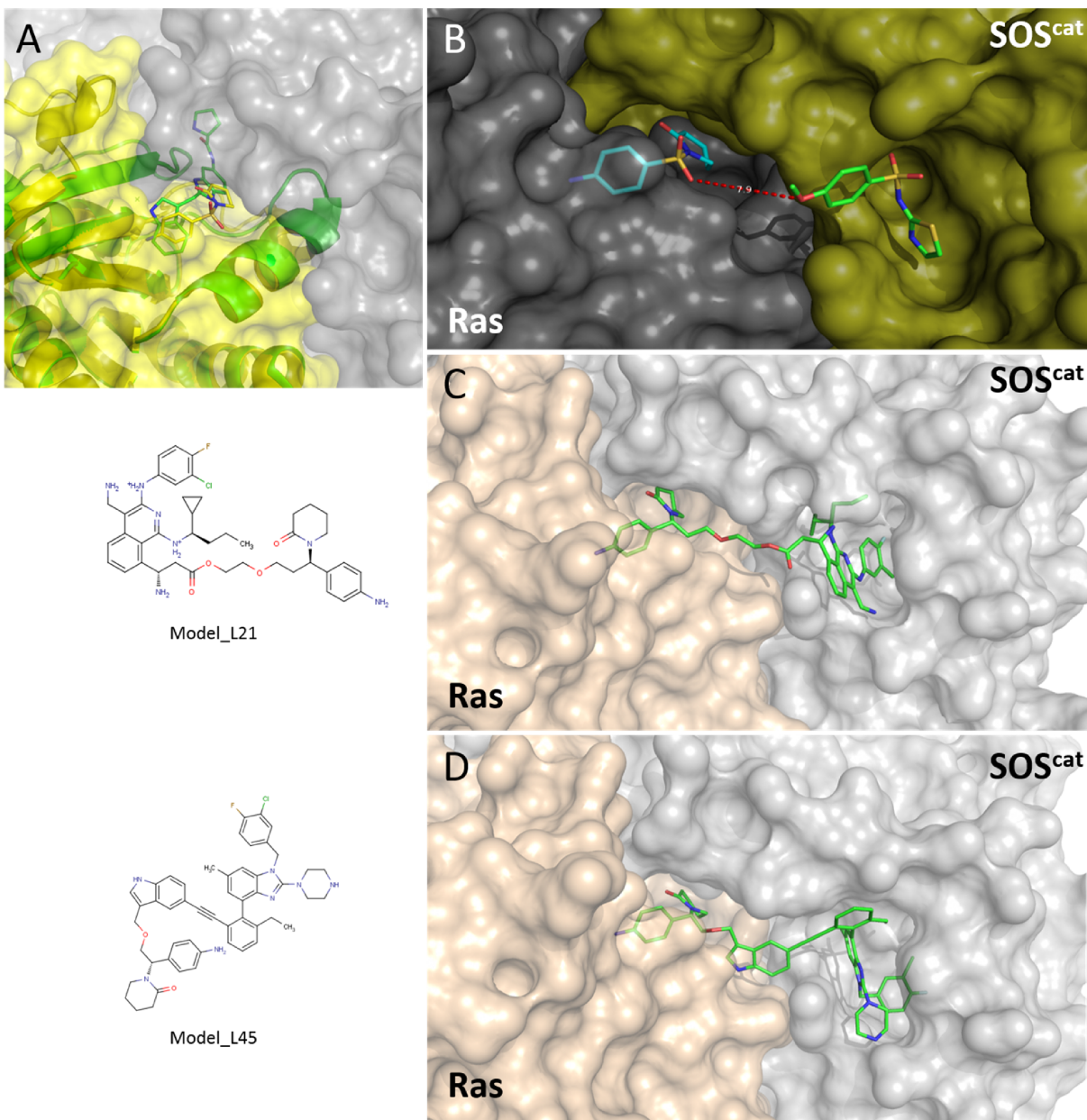


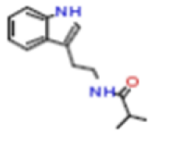
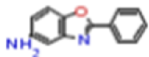
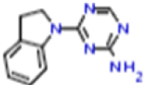
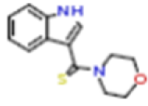
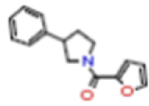
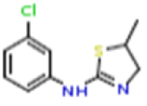
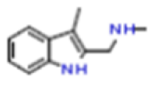
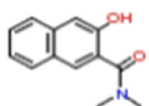
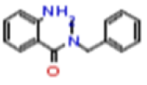
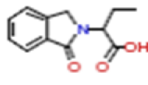
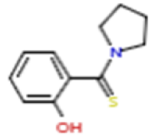
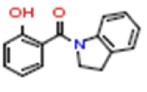
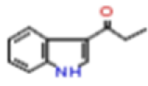
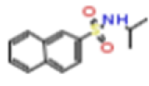
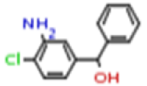
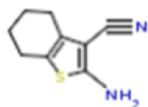
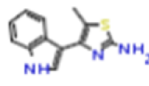
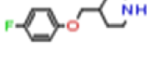
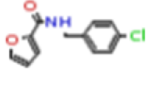
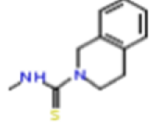
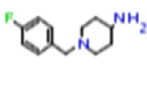
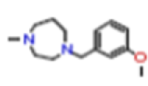
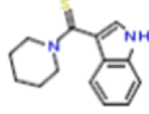
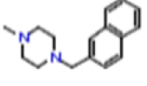
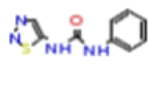
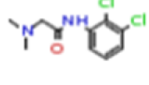
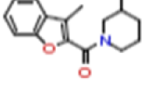
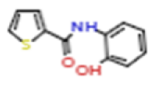
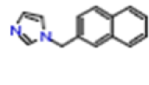
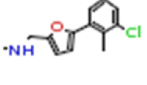
Figure 55. Using molecular modeling to design interfacial inhibitors against Ras:SOS complex. (A) Winter et al. [168] discovered a small molecule (yellow stick model) that binds to the “indole pocket” on Ras while contacting SOS. This molecule occupies the same pocket as one of the indole-based inhibitors (green stick model). A conformational change on Tyr-71 created more space for ligand binding. (B) The distance between these this interfacial pocket and the activator pocket on SOS is about 7.9 Å. These two pieces can be easily linked together (C, D) to produce high-affinity ligands.

Closing

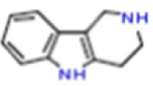
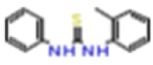
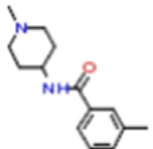
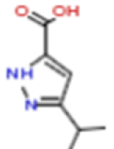
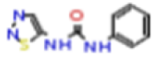
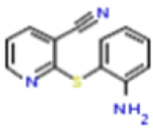
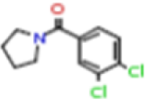
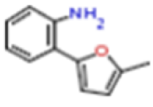
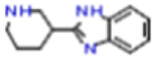
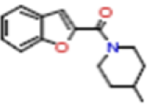
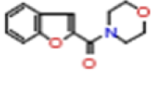
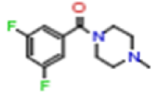
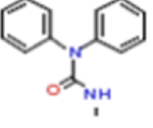
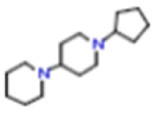
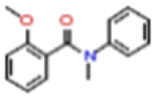
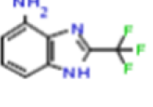
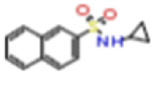
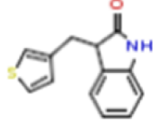
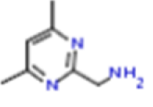
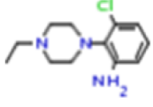
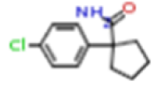
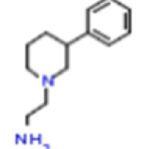
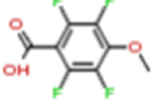
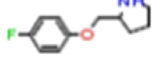
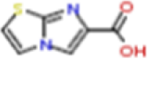
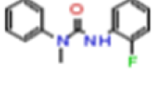
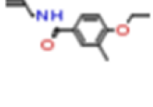
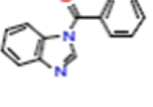
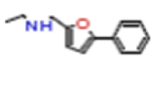
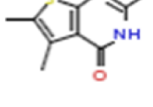
Efficient inhibition of oncogenic Ras signaling has been considered the Holy Grail in cancer therapy. The hunt for effective therapies against Ras has gone on for decades without any effective solution, leading to the notion that Ras is “undruggable”. However, with new knowledge and strategies, we have reached several milestones in this mission, which revived the hope that we may ultimately achieve the goal of drugging the “undruggable” Ras.

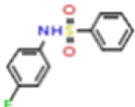
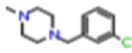
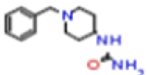
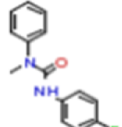
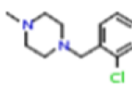
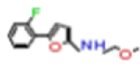
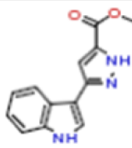
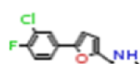
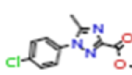
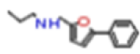
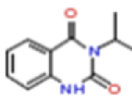
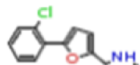
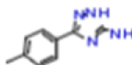
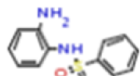
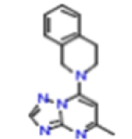
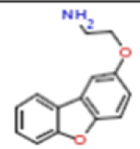
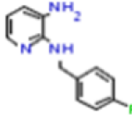
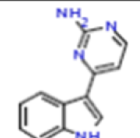
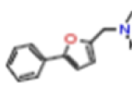
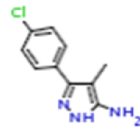
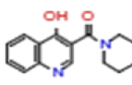
Appendix A. Hits from the fragment screening of GDP-bound K-Ras (G12D).

VU_number	Structures	VU_number	Structures	VU_number	Structures
VU0407796-2		VU0016932-5		VU0085653-2	
VU0079459-2		VU0017737-4		VU0101112-2	
VU0004265-9		VU0019059-2		VU0118450-2	
VU0004545-2		VU0024434-2		VU0118880-2	
VU0006194-3		VU0034402-2		VU0162226-3	
VU0007058-2		VU0049995-2		VU0171882-4	
VU0011509-2		VU0056503-5		VU0180998-4	
VU0012117-2		VU0063428-4		VU0186304-4	
VU0012717-2		VU0075012-2		VU0239533-6	
VU0015906-2		VU0085576-2		VU0240158-2	

VU_number	Structures	VU_number	Structures	VU_number	Structures
VU0272815-2		VU0406590-1		VU0407684-1	
VU0315948-2		VU0406650-1		VU0407741-1	
VU0405937-1		VU0406665-1		VU0408475-1	
VU0405979-1		VU0406713-1		VU0408486-1	
VU0406073-1		VU0406745-1		VU0408573-1	
VU0406148-1		VU0406872-1		VU0408610-1	
VU0406306-1		VU0407016-1		VU0408734-1	
VU0406331-1		VU0407242-1		VU0410542-1	
VU0406390-1		VU0407482-1		VU0410755-1	
VU0406534-1		VU0407586-1		VU0411292-1	

VU_number	Structures	VU_number	Structures	VU_number	Structures
VU0412055-1		VU0416471-1		VU0010710-2	
VU0412157-1		VU0416509-1		VU0016870-2	
VU0412241-1		VU0416709-1		VU0017164-4	
VU0412272-1		VU0417295-1		VU0017169-2	
VU0412466-1		VU0417410-1		VU0018766-2	
VU0412642-1		VU0417630-1		VU0020378-4	
VU0416184-1		VU0417771-1		VU0027168-2	
VU0416204-1		VU0005266-2		VU0067767-2	
VU0416379-1		VU0009224-2		VU0123230-2	
VU0416431-1		VU0009585-2		VU0129090-2	

VU_number	Structures	VU_number	Structures	VU_number	Structures
VU0137813-2		VU0406325-1		VU0408401-1	
VU0156429-4		VU0406390-1		VU0408532-1	
VU0171335-3		VU0406642-1		VU0408537-1	
VU0185082-4		VU0406653-1		VU0408566-1	
VU0209310-4		VU0406696-1		VU0408585-1	
VU0291801-2		VU0407351-1		VU0408612-1	
VU0405900-1		VU0407379-1		VU0408622-1	
VU0405925-1		VU0407380-1		VU0408653-1	
VU0406034-1		VU0407581-1		VU0408678-1	
VU0406215-1		VU0407813-1		VU0408684-1	

VU_number	Structures	VU_number	Structures	VU_number	Structures
VU0410540-1		VU0412529-1		VU0417864-1	
VU0410701-1		VU0412540-1			
VU0411066-1		VU0416211-1			
VU0411304-1		VU0416339-1			
VU0411518-1		VU0416367-1			
VU0411524-1		VU0416502-1			
VU0411732-1		VU0416516-1			
VU0412143-1		VU0416598-1			
VU0412272-1		VU0417057-1			
VU0412329-1		VU0417706-1			

Appendix B. Fragment hits or analogs co-crystallized with GDP-bound K-Ras (WT or G12V).

VU Number	Structure	VU Number	Structure	VU Number	Structure
VU0005345		VU0448430		VU0460002	
VU0019059		VU0448482		VU0460009	
VU0406713		VU0450277		VU0460231	
VU0432387		VU0452072		VU0461458	
VU0433817		VU0452074		VU0466236	
VU0447400		VU0452097			
VU0448179		VU0453633			
VU0448345		VU0459077			

Appendix C. Nucleotide exchange activators co-crystallized with Ras:SOS:Ras ternary complex, Ras:SOS binary complex, or SOS-CDC25 domain.

VU Number	Structure	VU Number	Structure	VU Number	Structure
VU0002032		VU0466175		VU0651044	
VU0019562		VU0467503		VU0651045	
VU0061570		VU0487017		VU0651570	
VU0063036		VU0550068		VU0652002	
VU0063275		VU0604223		VU0656923	
VU0120832		VU0604228		VU0657250	
VU0145298		VU0650187		VU0657313	
VU0453633		VU0650430		VU0657316	
VU0453647		VU0650886		VU0657713	

VU Number	Structure	VU Number	Structure	VU Number	Structure
VU0549906		VU0659518		VU0659183	
VU00549918		VU0659538		VU0657733	
VU0604217		VU0659653		VU0659512	
VU0656927		VU0659660		VU0659565	
VU0657681		VU0659662		VU0659181	
VU0657816		VU0659808			
VU0657840		VU0659815			
VU0659078		VU0660010			
VU0659490		VU0660039			

REFERENCES

1. Schmid, E.F. and D.A. Smith, *Pharmaceutical R&D in the spotlight: why is there still unmet medical need?* Drug Discov Today, 2007. **12**(23-24): p. 998-1006.
2. Burris, H.A., 3rd, *Shortcomings of current therapies for non-small-cell lung cancer: unmet medical needs.* Oncogene, 2009. **28 Suppl 1**: p. S4-13.
3. Knudson, A.G., *Two genetic hits (more or less) to cancer.* Nat Rev Cancer, 2001. **1**(2): p. 157-62.
4. Hanahan, D. and R.A. Weinberg, *The hallmarks of cancer.* Cell, 2000. **100**(1): p. 57-70.
5. Pylayeva-Gupta, Y., E. Grabocka, and D. Bar-Sagi, *RAS oncogenes: weaving a tumorigenic web.* Nat Rev Cancer, 2011. **11**(11): p. 761-74.
6. Ehrhardt, A., et al., *Ras and relatives--job sharing and networking keep an old family together.* Exp Hematol, 2002. **30**(10): p. 1089-106.
7. Milburn, M.V., et al., *Molecular switch for signal transduction: structural differences between active and inactive forms of protooncogenic ras proteins.* Science, 1990. **247**(4945): p. 939-45.
8. Schlichting, I., et al., *Time-resolved X-ray crystallographic study of the conformational change in Ha-Ras p21 protein on GTP hydrolysis.* Nature, 1990. **345**(6273): p. 309-15.
9. Herrmann, C., *Ras-effector interactions: after one decade.* Curr Opin Struct Biol, 2003. **13**(1): p. 122-9.
10. Malumbres, M. and A. Pellicer, *RAS pathways to cell cycle control and cell transformation.* Front Biosci, 1998. **3**: p. d887-912.
11. Ma, J. and M. Karplus, *Molecular switch in signal transduction: reaction paths of the conformational changes in ras p21.* Proc Natl Acad Sci U S A, 1997. **94**(22): p. 11905-10.
12. Trahey, M. and F. McCormick, *A cytoplasmic protein stimulates normal N-ras p21 GTPase, but does not affect oncogenic mutants.* Science, 1987. **238**(4826): p. 542-5.
13. Traut, T.W., *Physiological concentrations of purines and pyrimidines.* Mol Cell Biochem, 1994. **140**(1): p. 1-22.
14. Boriack-Sjodin, P.A., et al., *The structural basis of the activation of Ras by Sos.* Nature, 1998. **394**(6691): p. 337-43.
15. Margarit, S.M., et al., *Structural evidence for feedback activation by Ras.GTP of the Ras-specific nucleotide exchange factor SOS.* Cell, 2003. **112**(5): p. 685-95.
16. Sondermann, H., et al., *Structural analysis of autoinhibition in the Ras activator Son of sevenless.* Cell, 2004. **119**(3): p. 393-405.
17. Scheffzek, K., et al., *The Ras-RasGAP complex: structural basis for GTPase activation and its loss in oncogenic Ras mutants.* Science, 1997. **277**(5324): p. 333-8.
18. Kotting, C., et al., *The GAP arginine finger movement into the catalytic site of Ras increases the activation entropy.* Proc Natl Acad Sci U S A, 2008. **105**(17): p. 6260-5.
19. te Heesen, H., K. Gerwert, and J. Schlitter, *Role of the arginine finger in Ras.RasGAP revealed by QM/MM calculations.* FEBS Lett, 2007. **581**(29): p. 5677-84.
20. Bryant, K.L., et al., *KRAS: feeding pancreatic cancer proliferation.* Trends Biochem Sci, 2014. **39**(2): p. 91-100.

21. Lowy, D.R. and B.M. Willumsen, *Protein modification: new clue to Ras lipid glue*. Nature, 1989. **341**(6241): p. 384-5.
22. Braun, B.S. and K. Shannon, *Targeting Ras in myeloid leukemias*. Clin Cancer Res, 2008. **14**(8): p. 2249-52.
23. Wellbrock, C., M. Karasarides, and R. Marais, *The RAF proteins take centre stage*. Nat Rev Mol Cell Biol, 2004. **5**(11): p. 875-85.
24. Rodriguez-Viciana, P., et al., *Phosphatidylinositol-3-OH kinase as a direct target of Ras*. Nature, 1994. **370**(6490): p. 527-32.
25. Pacold, M.E., et al., *Crystal structure and functional analysis of Ras binding to its effector phosphoinositide 3-kinase gamma*. Cell, 2000. **103**(6): p. 931-43.
26. Vivanco, I. and C.L. Sawyers, *The phosphatidylinositol 3-Kinase AKT pathway in human cancer*. Nat Rev Cancer, 2002. **2**(7): p. 489-501.
27. Lambert, J.M., et al., *Tiam1 mediates Ras activation of Rac by a PI(3)K-independent mechanism*. Nat Cell Biol, 2002. **4**(8): p. 621-5.
28. Malliri, A., et al., *Mice deficient in the Rac activator Tiam1 are resistant to Ras-induced skin tumours*. Nature, 2002. **417**(6891): p. 867-71.
29. Datta, S.R., A. Brunet, and M.E. Greenberg, *Cellular survival: a play in three Akts*. Genes Dev, 1999. **13**(22): p. 2905-27.
30. Khwaja, A., et al., *Matrix adhesion and Ras transformation both activate a phosphoinositide 3-OH kinase and protein kinase B/Akt cellular survival pathway*. EMBO J, 1997. **16**(10): p. 2783-93.
31. DeFeo, D., et al., *Analysis of two divergent rat genomic clones homologous to the transforming gene of Harvey murine sarcoma virus*. Proc Natl Acad Sci U S A, 1981. **78**(6): p. 3328-32.
32. Der, C.J., T.G. Krontiris, and G.M. Cooper, *Transforming genes of human bladder and lung carcinoma cell lines are homologous to the ras genes of Harvey and Kirsten sarcoma viruses*. Proc Natl Acad Sci U S A, 1982. **79**(11): p. 3637-40.
33. Santos, E., et al., *T24 human bladder carcinoma oncogene is an activated form of the normal human homologue of BALB- and Harvey-MSV transforming genes*. Nature, 1982. **298**(5872): p. 343-7.
34. Bos, J.L., *ras oncogenes in human cancer: a review*. Cancer Res, 1989. **49**(17): p. 4682-9.
35. Broach, J.R. and R.J. Deschenes, *The function of ras genes in Saccharomyces cerevisiae*. Adv Cancer Res, 1990. **54**: p. 79-139.
36. Barbacid, M., *ras genes*. Annu Rev Biochem, 1987. **56**: p. 779-827.
37. Hanahan, D. and R.A. Weinberg, *Hallmarks of cancer: the next generation*. Cell, 2011. **144**(5): p. 646-74.
38. Laghi, L., et al., *Common occurrence of multiple K-RAS mutations in pancreatic cancers with associated precursor lesions and in biliary cancers*. Oncogene, 2002. **21**(27): p. 4301-6.
39. Lau, K.S. and K.M. Haigis, *Non-redundancy within the RAS oncogene family: insights into mutational disparities in cancer*. Mol Cells, 2009. **28**(4): p. 315-20.
40. Riely, G.J., J. Marks, and W. Pao, *KRAS mutations in non-small cell lung cancer*. Proc Am Thorac Soc, 2009. **6**(2): p. 201-5.

41. Yen, L.C., et al., *Activating KRAS mutations and overexpression of epidermal growth factor receptor as independent predictors in metastatic colorectal cancer patients treated with cetuximab*. *Ann Surg*, 2010. **251**(2): p. 254-60.
42. Downward, J., *Targeting RAS signalling pathways in cancer therapy*. *Nat Rev Cancer*, 2003. **3**(1): p. 11-22.
43. Bernhard, E.J., et al., *Direct evidence for the contribution of activated N-ras and K-ras oncogenes to increased intrinsic radiation resistance in human tumor cell lines*. *Cancer Res*, 2000. **60**(23): p. 6597-600.
44. Galiana, C., et al., *High frequency of Ki-ras amplification and p53 gene mutations in adenocarcinomas of the human esophagus*. *Mol Carcinog*, 1995. **14**(4): p. 286-93.
45. von Lintig, F.C., et al., *Ras activation in human breast cancer*. *Breast Cancer Res Treat*, 2000. **62**(1): p. 51-62.
46. Cichowski, K. and T. Jacks, *NF1 tumor suppressor gene function: narrowing the GAP*. *Cell*, 2001. **104**(4): p. 593-604.
47. Shannon, K.M., et al., *Loss of the normal NF1 allele from the bone marrow of children with type 1 neurofibromatosis and malignant myeloid disorders*. *N Engl J Med*, 1994. **330**(9): p. 597-601.
48. Side, L., et al., *Homozygous inactivation of the NF1 gene in bone marrow cells from children with neurofibromatosis type 1 and malignant myeloid disorders*. *N Engl J Med*, 1997. **336**(24): p. 1713-20.
49. Ogiso, Y., et al., *trans-Dominant suppressor mutations of the H-ras oncogene*. *Cell Growth Differ*, 1990. **1**(5): p. 217-24.
50. Spencer, J.M., et al., *Activated ras genes occur in human actinic keratoses, premalignant precursors to squamous cell carcinomas*. *Arch Dermatol*, 1995. **131**(7): p. 796-800.
51. Senmaru, N., et al., *Suppression of Erk activation and in vivo growth in esophageal cancer cells by the dominant negative Ras mutant, N116Y*. *Int J Cancer*, 1998. **78**(3): p. 366-71.
52. Shichinohe, T., et al., *Suppression of pancreatic cancer by the dominant negative ras mutant, N116Y*. *J Surg Res*, 1996. **66**(2): p. 125-30.
53. Brummelkamp, T.R., R. Bernards, and R. Agami, *Stable suppression of tumorigenicity by virus-mediated RNA interference*. *Cancer Cell*, 2002. **2**(3): p. 243-7.
54. Fleming, J.B., et al., *Molecular consequences of silencing mutant K-ras in pancreatic cancer cells: justification for K-ras-directed therapy*. *Mol Cancer Res*, 2005. **3**(7): p. 413-23.
55. Aoki, K., S. Ohnami, and T. Yoshida, *Suppression of pancreatic and colon cancer cells by antisense K-ras RNA expression vectors*. *Methods Mol Med*, 2005. **106**: p. 193-204.
56. Bossu, P., et al., *A dominant negative RAS-specific guanine nucleotide exchange factor reverses neoplastic phenotype in K-ras transformed mouse fibroblasts*. *Oncogene*, 2000. **19**(17): p. 2147-54.
57. Chin, L., et al., *Essential role for oncogenic Ras in tumour maintenance*. *Nature*, 1999. **400**(6743): p. 468-72.
58. Podsypanina, K., et al., *Oncogene cooperation in tumor maintenance and tumor recurrence in mouse mammary tumors induced by Myc and mutant Kras*. *Proc Natl Acad Sci U S A*, 2008. **105**(13): p. 5242-7.

59. Arkin, M.R. and J.A. Wells, *Small-molecule inhibitors of protein-protein interactions: progressing towards the dream*. Nat Rev Drug Discov, 2004. **3**(4): p. 301-17.
60. Noonan, T., et al., *Interaction of GTP derivatives with cellular and oncogenic ras-p21 proteins*. J Med Chem, 1991. **34**(4): p. 1302-7.
61. Wolin, R., et al., *Synthesis and evaluation of pyrazolo[3,4-b]quinoline ribofuranosides and their derivatives as inhibitors of oncogenic Ras*. Bioorganic & Medicinal Chemistry Letters, 1996. **6**(2): p. 195-200.
62. Becher, I., et al., *Affinity profiling of the cellular kinome for the nucleotide cofactors ATP, ADP, and GTP*. ACS Chem Biol, 2013. **8**(3): p. 599-607.
63. John, J., et al., *Kinetic and structural analysis of the Mg(2+)-binding site of the guanine nucleotide-binding protein p21H-ras*. J Biol Chem, 1993. **268**(2): p. 923-9.
64. Brenke, R., et al., *Fragment-based identification of druggable 'hot spots' of proteins using Fourier domain correlation techniques*. Bioinformatics, 2009. **25**(5): p. 621-7.
65. Buhrman, G., et al., *Analysis of binding site hot spots on the surface of Ras GTPase*. J Mol Biol, 2011. **413**(4): p. 773-89.
66. Grant, B.J., et al., *Novel allosteric sites on Ras for lead generation*. PLoS One, 2011. **6**(10): p. e25711.
67. te Heesen, H., A.M. Schlitter, and J. Schlitter, *Empirical rules facilitate the search for binding sites on protein surfaces*. J Mol Graph Model, 2007. **25**(5): p. 671-9.
68. Mattos, C. and D. Ringe, *Locating and characterizing binding sites on proteins*. Nat Biotechnol, 1996. **14**(5): p. 595-9.
69. Wang, W., G. Fang, and J. Rudolph, *Ras inhibition via direct Ras binding--is there a path forward?* Bioorg Med Chem Lett, 2012. **22**(18): p. 5766-76.
70. Taveras, A.G., et al., *Ras oncoprotein inhibitors: the discovery of potent, ras nucleotide exchange inhibitors and the structural determination of a drug-protein complex*. Bioorg Med Chem, 1997. **5**(1): p. 125-33.
71. Ganguly, A.K., et al., *Detection and structural characterization of ras oncoprotein-inhibitors complexes by electrospray mass spectrometry*. Bioorg Med Chem, 1997. **5**(5): p. 817-20.
72. Ganguly, A.K., et al., *Interaction of a novel GDP exchange inhibitor with the Ras protein*. Biochemistry, 1998. **37**(45): p. 15631-7.
73. Peri, F., et al., *Design, synthesis and biological evaluation of sugar-derived Ras inhibitors*. Chembiochem, 2005. **6**(10): p. 1839-48.
74. Francesco Peri, C.A., Sonia Colombo, Silvia Mari, Jesús Jiménez-Barbero, Enzo Martegani and Francesco Nicotra, *Sugar-Derived Ras Inhibitors: Group Epitope Mapping by NMR Spectroscopy and Biological Evaluation*. European Journal of Organic Chemistry, 2006. **2006**(16): p. 3707-3720.
75. Muller, C., et al., *Design, synthesis, and biological evaluation of levoglucosenone-derived ras activation inhibitors*. ChemMedChem, 2009. **4**(4): p. 524-8.
76. Airoldi, C., et al., *Glucose-derived Ras pathway inhibitors: evidence of Ras-ligand binding and Ras-GEF (Cdc25) interaction inhibition*. Chembiochem, 2007. **8**(12): p. 1376-9.
77. Palmioli, A., et al., *Selective cytotoxicity of a bicyclic Ras inhibitor in cancer cells expressing K-Ras(G13D)*. Biochem Biophys Res Commun, 2009. **386**(4): p. 593-7.

78. Palmioli, A., et al., *First experimental identification of Ras-inhibitor binding interface using a water-soluble Ras ligand*. *Bioorg Med Chem Lett*, 2009. **19**(15): p. 4217-22.
79. Waldmann, H., et al., *Sulindac-derived Ras pathway inhibitors target the Ras-Raf interaction and downstream effectors in the Ras pathway*. *Angew Chem Int Ed Engl*, 2004. **43**(4): p. 454-8.
80. Spoerner, M., et al., *A novel mechanism for the modulation of the Ras-effector interaction by small molecules*. *Biochem Biophys Res Commun*, 2005. **334**(2): p. 709-13.
81. Rosnizeck, I.C., et al., *Elucidating the Mode of Action of a Typical Ras State 1(T) Inhibitor*. *Biochemistry*, 2014.
82. Rosnizeck, I.C., et al., *Stabilizing a weak binding state for effectors in the human ras protein by cyclen complexes*. *Angew Chem Int Ed Engl*, 2010. **49**(22): p. 3830-3.
83. Patgiri, A., et al., *An orthosteric inhibitor of the Ras-Sos interaction*. *Nat Chem Biol*, 2011. **7**(9): p. 585-7.
84. John, J., et al., *Kinetics of interaction of nucleotides with nucleotide-free H-ras p21*. *Biochemistry*, 1990. **29**(25): p. 6058-65.
85. Brose, M.S., et al., *BRAF and RAS mutations in human lung cancer and melanoma*. *Cancer Res*, 2002. **62**(23): p. 6997-7000.
86. Hunter, J.C., et al., *In situ selectivity profiling and crystal structure of SML-8-73-1, an active site inhibitor of oncogenic K-Ras G12C*. *Proc Natl Acad Sci U S A*, 2014. **111**(24): p. 8895-900.
87. Lim, S.M., et al., *Therapeutic targeting of oncogenic K-Ras by a covalent catalytic site inhibitor*. *Angew Chem Int Ed Engl*, 2014. **53**(1): p. 199-204.
88. Ostrem, J.M., et al., *K-Ras(G12C) inhibitors allosterically control GTP affinity and effector interactions*. *Nature*, 2013. **503**(7477): p. 548-51.
89. Forbes, S.A., et al., *COSMIC: mining complete cancer genomes in the Catalogue of Somatic Mutations in Cancer*. *Nucleic Acids Res*, 2011. **39**(Database issue): p. D945-50.
90. Liu, Q., et al., *Developing irreversible inhibitors of the protein kinase cysteinome*. *Chem Biol*, 2013. **20**(2): p. 146-59.
91. Kolch, W., *Ras/Raf signalling and emerging pharmacotherapeutic targets*. *Expert Opin Pharmacother*, 2002. **3**(6): p. 709-18.
92. Friday, B.B. and A.A. Adjei, *K-ras as a target for cancer therapy*. *Biochim Biophys Acta*, 2005. **1756**(2): p. 127-44.
93. Sridhar, S.S., D. Hedley, and L.L. Siu, *Raf kinase as a target for anticancer therapeutics*. *Mol Cancer Ther*, 2005. **4**(4): p. 677-85.
94. Sebolt-Leopold, J.S., et al., *Blockade of the MAP kinase pathway suppresses growth of colon tumors in vivo*. *Nat Med*, 1999. **5**(7): p. 810-6.
95. Rinehart, J., et al., *Multicenter phase II study of the oral MEK inhibitor, CI-1040, in patients with advanced non-small-cell lung, breast, colon, and pancreatic cancer*. *J Clin Oncol*, 2004. **22**(22): p. 4456-62.
96. Vignot, S., et al., *mTOR-targeted therapy of cancer with rapamycin derivatives*. *Ann Oncol*, 2005. **16**(4): p. 525-37.
97. Gysin, S., et al., *Therapeutic strategies for targeting ras proteins*. *Genes Cancer*, 2011. **2**(3): p. 359-72.

98. Fedorenko, I.V., K.H. Paraiso, and K.S. Smalley, *Acquired and intrinsic BRAF inhibitor resistance in BRAF V600E mutant melanoma*. *Biochem Pharmacol*, 2011. **82**(3): p. 201-9.
99. Heidorn, S.J., et al., *Kinase-dead BRAF and oncogenic RAS cooperate to drive tumor progression through CRAF*. *Cell*, 2010. **140**(2): p. 209-21.
100. Su, F., et al., *RAS mutations in cutaneous squamous-cell carcinomas in patients treated with BRAF inhibitors*. *N Engl J Med*, 2012. **366**(3): p. 207-15.
101. Buday, L., P.H. Warne, and J. Downward, *Downregulation of the Ras activation pathway by MAP kinase phosphorylation of Sos*. *Oncogene*, 1995. **11**(7): p. 1327-31.
102. Porfiri, E. and F. McCormick, *Regulation of epidermal growth factor receptor signaling by phosphorylation of the ras exchange factor hSOS1*. *J Biol Chem*, 1996. **271**(10): p. 5871-7.
103. Rao, S., et al., *Phase III double-blind placebo-controlled study of farnesyl transferase inhibitor R115777 in patients with refractory advanced colorectal cancer*. *J Clin Oncol*, 2004. **22**(19): p. 3950-7.
104. Van Cutsem, E., et al., *Phase III trial of gemcitabine plus tipifarnib compared with gemcitabine plus placebo in advanced pancreatic cancer*. *J Clin Oncol*, 2004. **22**(8): p. 1430-8.
105. Whyte, D.B., et al., *K- and N-Ras are geranylgeranylated in cells treated with farnesyl protein transferase inhibitors*. *J Biol Chem*, 1997. **272**(22): p. 14459-64.
106. Britten, C.D., et al., *A phase I and pharmacological study of the farnesyl protein transferase inhibitor L-778,123 in patients with solid malignancies*. *Clin Cancer Res*, 2001. **7**(12): p. 3894-903.
107. Winter-Vann, A.M., et al., *A small-molecule inhibitor of isoprenylcysteine carboxyl methyltransferase with antitumor activity in cancer cells*. *Proc Natl Acad Sci U S A*, 2005. **102**(12): p. 4336-41.
108. Zimmermann, G., et al., *Small molecule inhibition of the KRAS-PDEdelta interaction impairs oncogenic KRAS signalling*. *Nature*, 2013. **497**(7451): p. 638-42.
109. Chandra, A., et al., *The GDI-like solubilizing factor PDEdelta sustains the spatial organization and signalling of Ras family proteins*. *Nat Cell Biol*, 2012. **14**(2): p. 148-58.
110. Ismail, S.A., et al., *Arl2-GTP and Arl3-GTP regulate a GDI-like transport system for farnesylated cargo*. *Nat Chem Biol*, 2011. **7**(12): p. 942-9.
111. Zhang, H., et al., *Photoreceptor cGMP phosphodiesterase delta subunit (PDEdelta) functions as a prenyl-binding protein*. *J Biol Chem*, 2004. **279**(1): p. 407-13.
112. Humbert, M.C., et al., *ARL13B, PDE6D, and CEP164 form a functional network for INPP5E ciliary targeting*. *Proc Natl Acad Sci U S A*, 2012. **109**(48): p. 19691-6.
113. Zhang, H., et al., *The prenyl-binding protein PrBP/delta: a chaperone participating in intracellular trafficking*. *Vision Res*, 2012. **75**: p. 19-25.
114. Oltsersdorf, T., et al., *An inhibitor of Bcl-2 family proteins induces regression of solid tumours*. *Nature*, 2005. **435**(7042): p. 677-81.
115. Bollag, G., et al., *Clinical efficacy of a RAF inhibitor needs broad target blockade in BRAF-mutant melanoma*. *Nature*, 2010. **467**(7315): p. 596-9.
116. Shuker, S.B., et al., *Discovering high-affinity ligands for proteins: SAR by NMR*. *Science*, 1996. **274**(5292): p. 1531-4.

117. Fink, T., H. Bruggesser, and J.L. Reymond, *Virtual exploration of the small-molecule chemical universe below 160 Daltons*. *Angew Chem Int Ed Engl*, 2005. **44**(10): p. 1504-8.
118. Bohacek, R.S., C. McMartin, and W.C. Guida, *The art and practice of structure-based drug design: a molecular modeling perspective*. *Med Res Rev*, 1996. **16**(1): p. 3-50.
119. Hajduk, P.J., J.R. Huth, and S.W. Fesik, *Druggability indices for protein targets derived from NMR-based screening data*. *J Med Chem*, 2005. **48**(7): p. 2518-25.
120. Sun, Q., et al., *Discovery of small molecules that bind to K-Ras and inhibit Sos-mediated activation*. *Angew Chem Int Ed Engl*, 2012. **51**(25): p. 6140-3.
121. Sun, Q., et al., *A method for the second-site screening of K-Ras in the presence of a covalently attached first-site ligand*. *J Biomol NMR*, 2014.
122. Burns, M.C., et al., *Approach for targeting Ras with small molecules that activate SOS-mediated nucleotide exchange*. *Proc Natl Acad Sci U S A*, 2014. **111**(9): p. 3401-6.
123. Williamson, M.P., *Using chemical shift perturbation to characterise ligand binding*. *Prog Nucl Magn Reson Spectrosc*, 2013. **73**: p. 1-16.
124. Maurer, T., et al., *Small-molecule ligands bind to a distinct pocket in Ras and inhibit SOS-mediated nucleotide exchange activity*. *Proc Natl Acad Sci U S A*, 2012. **109**(14): p. 5299-304.
125. Thapar, R., J.G. Williams, and S.L. Campbell, *NMR characterization of full-length farnesylated and non-farnesylated H-Ras and its implications for Raf activation*. *J Mol Biol*, 2004. **343**(5): p. 1391-408.
126. Nallamsetty, S., et al., *Gateway vectors for the production of combinatorially-tagged His6-MBP fusion proteins in the cytoplasm and periplasm of Escherichia coli*. *Protein Sci*, 2005. **14**(12): p. 2964-71.
127. Congreve, M., et al., *A 'rule of three' for fragment-based lead discovery?* *Drug Discov Today*, 2003. **8**(19): p. 876-7.
128. Collaborative Computational Project, N., *The CCP4 suite: programs for protein crystallography*. *Acta Crystallogr D Biol Crystallogr*, 1994. **50**(Pt 5): p. 760-3.
129. Adams, P.D., et al., *PHENIX: a comprehensive Python-based system for macromolecular structure solution*. *Acta Crystallogr D Biol Crystallogr*, 2010. **66**(Pt 2): p. 213-21.
130. Emsley, P., et al., *Features and development of Coot*. *Acta Crystallogr D Biol Crystallogr*, 2010. **66**(Pt 4): p. 486-501.
131. Li, D., E.F. DeRose, and R.E. London, *The inter-ligand Overhauser effect: a powerful new NMR approach for mapping structural relationships of macromolecular ligands*. *J Biomol NMR*, 1999. **15**(1): p. 71-6.
132. Wolfgang Jahnke, L.B.P., C. Gregory Paris, André Strauss, Gabriele Fendrich, and Carlo M. Nalin, *Second-Site NMR Screening with a Spin-Labeled First Ligand*. *J. Am. Chem. Soc.*, 2000. **122**(30): p. 7394-7395.
133. Erlanson, D.A., J.A. Wells, and A.C. Braisted, *Tethering: fragment-based drug discovery*. *Annu Rev Biophys Biomol Struct*, 2004. **33**: p. 199-223.
134. Erlanson, D.A., et al., *In situ assembly of enzyme inhibitors using extended tethering*. *Nat Biotechnol*, 2003. **21**(3): p. 308-14.
135. Parsons, B.L. and M.B. Myers, *Personalized cancer treatment and the myth of KRAS wild-type colon tumors*. *Discov Med*, 2013. **15**(83): p. 259-67.

136. Schanda, P., E. Kupce, and B. Brutscher, *SOFAST-HMQC experiments for recording two-dimensional heteronuclear correlation spectra of proteins within a few seconds*. J Biomol NMR, 2005. **33**(4): p. 199-211.
137. Hall, B.E., et al., *Structure-based mutagenesis reveals distinct functions for Ras switch 1 and switch 2 in Sos-catalyzed guanine nucleotide exchange*. J Biol Chem, 2001. **276**(29): p. 27629-37.
138. Lepri, F., et al., *SOS1 mutations in Noonan syndrome: molecular spectrum, structural insights on pathogenic effects, and genotype-phenotype correlations*. Hum Mutat, 2011. **32**(7): p. 760-72.
139. Chen, P.C., et al., *Activation of multiple signaling pathways causes developmental defects in mice with a Noonan syndrome-associated Sos1 mutation*. J Clin Invest, 2010. **120**(12): p. 4353-65.
140. Smith, M.J., B.G. Neel, and M. Ikura, *NMR-based functional profiling of RASopathies and oncogenic RAS mutations*. Proc Natl Acad Sci U S A, 2013. **110**(12): p. 4574-9.
141. Poulidakos, P.I., et al., *RAF inhibitors transactivate RAF dimers and ERK signalling in cells with wild-type BRAF*. Nature, 2010. **464**(7287): p. 427-30.
142. Gureasko, J., et al., *Membrane-dependent signal integration by the Ras activator Son of sevenless*. Nat Struct Mol Biol, 2008. **15**(5): p. 452-61.
143. Hatzivassiliou, G., et al., *RAF inhibitors prime wild-type RAF to activate the MAPK pathway and enhance growth*. Nature, 2010. **464**(7287): p. 431-5.
144. Freedman, T.S., et al., *A Ras-induced conformational switch in the Ras activator Son of sevenless*. Proc Natl Acad Sci U S A, 2006. **103**(45): p. 16692-7.
145. Souza-Fagundes, E.M., et al., *A high-throughput fluorescence polarization anisotropy assay for the 70N domain of replication protein A*. Anal Biochem, 2012. **421**(2): p. 742-9.
146. Friberg, A., et al., *Discovery of potent myeloid cell leukemia 1 (Mcl-1) inhibitors using fragment-based methods and structure-based design*. J Med Chem, 2013. **56**(1): p. 15-30.
147. Kamb, A., S. Wee, and C. Lengauer, *Why is cancer drug discovery so difficult?* Nat Rev Drug Discov, 2007. **6**(2): p. 115-20.
148. Johnson, D.S., E. Weerapana, and B.F. Cravatt, *Strategies for discovering and derisking covalent, irreversible enzyme inhibitors*. Future Med Chem, 2010. **2**(6): p. 949-64.
149. Yan, C., et al., *Discovery and characterization of small molecules that target the GTPase Ral*. Nature, 2014. **515**(7527): p. 443-7.
150. Stephen, A.G., et al., *Dragging ras back in the ring*. Cancer Cell, 2014. **25**(3): p. 272-81.
151. Feig, L.A. and G.M. Cooper, *Inhibition of NIH 3T3 cell proliferation by a mutant ras protein with preferential affinity for GDP*. Mol Cell Biol, 1988. **8**(8): p. 3235-43.
152. Quilliam, L.A., et al., *Identification of residues critical for Ras(17N) growth-inhibitory phenotype and for Ras interaction with guanine nucleotide exchange factors*. Mol Cell Biol, 1994. **14**(2): p. 1113-21.
153. Young, A., D. Lou, and F. McCormick, *Oncogenic and wild-type Ras play divergent roles in the regulation of mitogen-activated protein kinase signaling*. Cancer Discov, 2013. **3**(1): p. 112-23.
154. Bentley, C., et al., *A requirement for wild-type Ras isoforms in mutant KRas-driven signalling and transformation*. Biochem J, 2013. **452**(2): p. 313-20.

155. To, M.D., et al., *Interactions between wild-type and mutant Ras genes in lung and skin carcinogenesis*. *Oncogene*, 2013. **32**(34): p. 4028-33.
156. Grabocka, E., et al., *Wild-type H- and N-Ras promote mutant K-Ras-driven tumorigenesis by modulating the DNA damage response*. *Cancer Cell*, 2014. **25**(2): p. 243-56.
157. Luo, F., et al., *Wild-type K-ras has a tumour suppressor effect on carcinogen-induced murine colorectal adenoma formation*. *Int J Exp Pathol*, 2014. **95**(1): p. 8-15.
158. Spoerner, M., et al., *Dynamic properties of the Ras switch I region and its importance for binding to effectors*. *Proc Natl Acad Sci U S A*, 2001. **98**(9): p. 4944-9.
159. Spoerner, M., A. Wittinghofer, and H.R. Kalbitzer, *Perturbation of the conformational equilibria in Ras by selective mutations as studied by 31P NMR spectroscopy*. *FEBS Lett*, 2004. **578**(3): p. 305-10.
160. Liao, J., et al., *Two conformational states of Ras GTPase exhibit differential GTP-binding kinetics*. *Biochem Biophys Res Commun*, 2008. **369**(2): p. 327-32.
161. Shima, F., et al., *In silico discovery of small-molecule Ras inhibitors that display antitumor activity by blocking the Ras-effector interaction*. *Proc Natl Acad Sci U S A*, 2013. **110**(20): p. 8182-7.
162. Verdine, G.L. and G.J. Hilinski, *Stapled peptides for intracellular drug targets*. *Methods Enzymol*, 2012. **503**: p. 3-33.
163. Frank, A.O., et al., *Discovery of a potent stapled helix peptide that binds to the 70N domain of replication protein A*. *J Med Chem*, 2014. **57**(6): p. 2455-61.
164. Pommier, Y. and C. Marchand, *Interfacial inhibitors: targeting macromolecular complexes*. *Nat Rev Drug Discov*, 2012. **11**(1): p. 25-36.
165. Mossessova, E., R.A. Corpina, and J. Goldberg, *Crystal structure of ARF1*Sec7 complexed with Brefeldin A and its implications for the guanine nucleotide exchange mechanism*. *Mol Cell*, 2003. **12**(6): p. 1403-11.
166. Renault, L., B. Guibert, and J. Cherfils, *Structural snapshots of the mechanism and inhibition of a guanine nucleotide exchange factor*. *Nature*, 2003. **426**(6966): p. 525-30.
167. Viaud, J., et al., *Structure-based discovery of an inhibitor of Arf activation by Sec7 domains through targeting of protein-protein complexes*. *Proc Natl Acad Sci U S A*, 2007. **104**(25): p. 10370-5.
168. Winter, J.J., et al., *Small Molecule Binding Sites on the Ras:SOS Complex Can Be Exploited for Inhibition of Ras Activation*. *J Med Chem*, 2015. **58**(5): p. 2265-74.